THE AMERICAN MINERALOGIST

JOURNAL OF THE MINERALOGICAL SOCIETY OF AMERICA

Vol. 42 SEPTEMBER–OCTOBER, 1957 Nos. 9 and 10

DOLORESITE, A NEW VANADIUM OXIDE MINERAL FROM THE COLORADO PLATEAU*

T. W. STERN, L. R. STIEFF, H. T. EVANS, JR., AND A. M. SHERWOOD, *U. S. Geological Survey, Washington 25, D. C.*

ABSTRACT

Doloresite, $H_8V_6O_{16}$ or $3V_2O_4 \cdot 4H_2O$, named for the Dolores River in southwestern Colorado, has been identified from 11 mines on the Colorado Plateau. Very fine fragments under oil immersion are reddish brown to yellow red in transmitted light with a mean index of refraction of about 1.90. The mineral has parallel extinction and exhibits weak absorption. In polished section doloresite is gray, variable in color along the elongation of the crystals, and shows selective absorption in plane polarized light. Under crossed nicols doloresite appears strongly anisotropic. Lamellar twinning, twin plane (100), is almost universal on a submicroscopic scale. The unit cell is monoclinic, space group $C2/m$ with $a = 19.64$ Å, $b = 2.99$ Å, $c = 4.83$ Å, $\beta = 103°55'$, and one formula per cell. The measured specific gravity is 3.27 to 3.33, and calculated specific gravity is 3.41.

OCCURRENCE

Doloresite, $3V_2O_4 \cdot 4H_2O$, named for the Dolores River, a major stream of the Colorado Plateau, was first collected by L. B. Riley, L. R. Stieff, and T. W. Stern in 1951 at the La Sal No. 2 mine at the head of Lumsden Canyon about 3½ air miles southwest of Gateway, Mesa County, Colo. At the La Sal No. 2 mine, doloresite occurs intimately associated with coffinite, $U(SiO_4)_{1-x}(OH)_{4x}$ (Stieff, Stern, and Sherwood, 1956), and carbonaceous matter. In this mine these minerals have formed several black concretionary masses about 1 foot by 2½ feet in cross section. The core of these masses contains large amounts of uranium and vanadium. Doloresite is found in the central part of these masses. The sandstone immediately adjacent to this heavily mineralized area contains small amounts of tyuyamunite.

Additional specimens have been collected by A. D. Weeks, M. E. Thompson, R. G. Coleman, T. W. Stern, and L. R. Stieff from the following mines: Corvusite, Matchless, Arrowhead, Black Mama, and Lumsden No. 2 in Mesa County, Colo.; Golden Cycle, J. J., and Peanut in Montrose County, Colo.; Mi Vida in San Juan County, Utah; and

---

* Publication authorized by the Director, U. S. Geological Survey.

Monument No. 2 in Apache County, Ariz. All of the Colorado mines listed above are in the Salt Wash sandstone member of the Morrison formation (Upper Jurassic). The Mi Vida mine is in the Chinle formation (Upper Triassic), and the Monument No. 2 mine is in the Shinarump member, the basal member of the Chinle formation. The mineral also occurs in sec. 33, T. 12 N., R. 9 E., Valencia County, N. Mex. in the Todilto limestone (Upper Jurassic). Doloresite is found in relatively unoxidized vanadium-uranium ores and is associated with coffinite, uraninite, clausthalite, montroseite, paramontroseite, and other vanadium oxides.

PHYSICAL AND CHEMICAL PROPERTIES

Doloresite is nearly black, with submetallic luster and greenish black streak. The material normally shows a dark bronzy tarnish. Many specimens of doloresite form radiating groups in bands or veinlets, locally penetrating mineralized wood. Exposed bands show botryoidal surfaces.

In polished section doloresite is gray, variable along the elongation of the crystals, and shows selective absorption in plane polarized light. Under crossed nicols doloresite appears strongly anisotropic. Paramontroseite is commonly present as remnant slivers scattered throughout the doloresite mass in varying amounts (Fig. 1). The mode of occurrence of the paramontroseite indicates that the doloresite has formed as a secondary replacement of a primary mass of montroseite.

Doloresite is fine grained and opaque except for very small fragments, which under an oil immersion objective are nonopqaue. The optical properties could not be determined in detail, but the mean index of refraction is about 1.90. The grains show a fibrous cleavage with parallel extinction and are reddish yellow in very thin flakes. No distinct interference figure could be observed, presumably because of the lamellar submicroscopic twinning that was observed in the x-ray study.

The specific gravity of two doloresite samples from La Sal No. 2 mine determined by means of the Berman balance, ranges from 3.27 to 3.33. The specific gravity of doloresite calculated from the unit cell and proposed chemical formula is 3.41.

Microchemical reactions of doloresite have been determined on small fragments. The mineral is slowly soluble in 1:1 HCl, yielding a green solution. A blue solution is produced by 1:1 HNO_3. No reaction is observed with 1:1 NH_4OH, but the mineral is slightly soluble in 40 per cent KOH. No reaction was observed with either 20 per cent KCN or 20 per cent $FeCl_2$.

It is apparent from the optical observations described above, and also the x-ray studies, that doloresite is almost always mixed with other vanadium oxide minerals. The most common impurity is montroseite or paramontroseite (Evans and Mrose, 1955) or both. *X*-ray powder patterns made on numerous samples always show admixed paramontroseite (montroseite transforms rapidly to paramontroseite in air) in proportions varying from predominant to subordinate. Other unidentified phases are also present in some samples. The chemical analysis, specific-gravity determinations, and optical characteristics must be interpreted with due allowance made for the prevalence of admixed impurities.

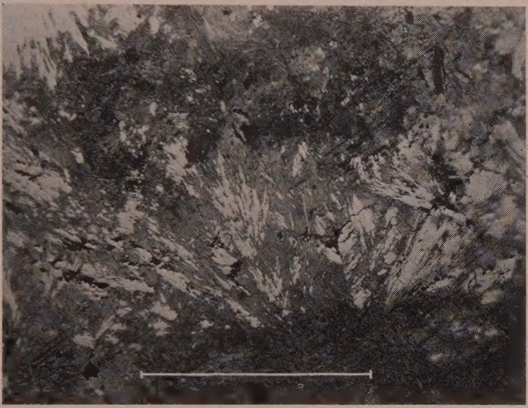

FIG. 1. Photomicrograph of polished section of specimen from the Mi Vida mine, San Juan County, Utah, showing doloresite (gray) replacing paramontroseite (white). Bar indicates 0.1 mm. Photograph courtesy of R. G. Coleman, U. S. Geological Survey.

Only one specimen has been found, obtained from Monument No. 2 mine in Apache County, Ariz., that contains a small seam of doloresite that is relatively pure. This material is in chocolate-brown, bladed masses showing satinlike cleavage surfaces. The metallic luster characteristic of the common impure doloresite is absent. The *x*-ray powder pattern shows only traces of the strong paramontroseite lines. Fragments of this material were used for single-crystal *x*-ray studies, but unfortunately there was insufficient material for any chemical tests.

Chemical analysis

Two samples of doloresite from La Sal No. 2 mine were analyzed quantitatively in the following manner. A part of the sample was dissolved in H_2SO_4 in a covered platinum crucible and titrated with $K_2Cr_2O_7$. In this treatment, V_2O_3 is oxidized to V_2O_4 and FeO to Fe_2O_3. A second part was dissolved in H_2SO_4 and titrated with $KMnO_4$. By this titration V_2O_3 and V_2O_4 are oxidized to V_2O_5 and FeO to Fe_2O_3. A third and fourth portion of the sample were used to determine total V and Fe separately. From these data, the proportions of V_2O_3, V_2O_4, and FeO were calculated. The analyses are given in table 1.

As explained above, these analyses must be interpreted as a mixture of doloresite with montroseite ($V_2O_3 \cdot H_2O$), paramontroseite (V_2O_4), and other impurities. The SiO_2, MgO, Al_2O_3, UO_3, As_2O_3, and Pb can be subtracted as mineral impurities extraneous to the vanadium oxides, but at least part of the FeO is probably present as a result of solid solution in the original montroseite (Weeks, Cisney, and Sherwood, 1953). Analysis no. 2 can be accounted for on a hypothetical basis in terms of 53 per cent doloresite, 44 per cent paramontroseite, and 3 per cent montroseite, assuming that the latter two minerals contain 10 mole per cent Fe replacing V.

TABLE 1.—CHEMICAL ANALYSES OF DOLORESITE
A. M. Sherwood, analyst

Constituent	1	2	3	4
V_2O_4	68.53	78.00	86.7	86.8
V_2O_3	10.30	1.89	2.1	2.2
FeO	3.53	3.83	4.2	4.0
SiO_2	2.04	.30		
MgO	1.12	3.98		
Al_2O_3	2.46	1.33		
UO_2	1.34			
		3.88		
UO_3	3.47			
As_2O_3	.73	.30		
H_2O-	.48	.37		
H_2O+	4.72	6.33	7.0	7.0
Pb	.08	.07		
Total	98.80	100.28	100.0	100.0

1. Sample 1 from La Sal No. 2 mine, Mesa County, Colo. Specific gravity 3.27.
2. Sample 2 from La Sal No. 2 mine. Specific gravity 3.33.
3. Analysis of column 2 with V_2O_4, V_2O_3, FeO, and H_2O recalculated to 100 per cent.
4. Theoretical composition for a mixture of 53 per cent doloresite ($3V_2O_4 \cdot 4H_2O$), 44 per cent paramontroseite (V_2O_4) and 3 per cent montroseite ($V_2O_3 \cdot H_2O$), with 10 mole per cent FeO in solid solution in the paramontroseite and montroseite.

X-RAY CRYSTALLOGRAPHY

Early attempts to obtain single-crystal patterns of doloresite were unsuccessful because of the extremely poor quality of the crystal fragments and the oriented admixture of paramontroseite. Specimens from the Monument No. 2 mine mentioned above gave relatively clean Buerger precession photographs, with only traces of a paramontroseite pattern, although the doloresite pattern was still somewhat diffuse. The patterns conformed to a body-centered orthorhombic lattice, but the lattice constants derived on this basis could not be made to account adequately for the powder pattern. Also, the most diligent efforts to find an orthorhombic crystal structure for doloresite were fruitless. The key to the crystallography of doloresite was finally provided by *x*-ray studies on a new vanadium oxide mineral from Carlile, Wyoming, which proved to be monoclinic with the space group $C2/m$, $a=19.64$ Å, $b=2.99$ Å, $c=4.83$ Å and $\beta=103°55'$. The close relationship between this crystal and doloresite can be appreciated if the above monoclinic cell is transformed to a setting for which the space group would be written $I2/m$, and which is strongly pseudo-orthorhombic in dimensions with $\beta'=90°18'$. In fact, it was found that the orthorhombic intensity distribution found for doloresite from Monument No. 2 mine could be reconciled with the monoclinic patterns of the mineral from Carlile by taking account of the superposition of spots that would arise by twinning the monoclinic lattice on (100) as the twin plane. Finally, the monoclinic lattice was found to give a satisfactory explanation of the powder pattern, as shown in Table 2.

The crystal structure of the monoclinic crystal was readily determined. The unit cell contains one formula and the unit-cell volume of the Carlile crystal and of doloresite is just sufficient to accommodate 16 oxygen atoms with a specific volume of 17.2 Å^3 per atom. This value of the specific volume is entirely consistent with that found for other vanadium oxides; for example, 17.2 Å^3 for montroseite, $V_2O_3 \cdot H_2O$ (Evans and Block, 1953) and 17.1 Å^3 for duttonite, $V_2O_4 \cdot 2H_2O$ (Evans and Mrose, personal communication). The crystal-structure analysis of the Carlile crystal indicates the presence of 6 vanadium atoms, but the number of hydrogen atoms, in the absence of a chemical analysis, must be determined by an indirect method. Thus, the unit-cell content of the Carlile mineral, and consequently of doloresite, is established as $H_nV_6O_{16}$. The crystal structure will not permit n to be greater than 10, and if the oxidation state of vanadium is not greater than 4, n cannot be less than 8. The chemical analyses strongly indicate that doloresite is essentially an oxide of quadrivalent vanadium, and therefore the ideal formula $H_8V_6O_{16}$, or $3V_2O_4 \cdot 4H_2O$, is proposed for this mineral.

It has not yet been established with certainty whether the Carlile mineral is doloresite ($H_8V_6O_{16}$) or a more reduced phase ($H_{10}V_6O_{16}$). In the absence of any possibility of chemical analysis of the Carlile mineral,

TABLE 2.—X-RAY POWDER DATA FOR DOLORESITE FROM MONUMENT NO. 2 MINE, APACHE COUNTY, ARIZ.

Indexed on monoclinic unit cell; space group $C2/m$,
$a=19.64$ Å, $b=2.99$ Å, $c=4.83$ Å, $\beta=103°55'$
CuKα radiation; camera diameter 114.6 mm; *d*(obs.) cutoff at 12 Å

hkl	*d*(calc.) (Å)	*d*(obs.) (Å)	*I*	*hkl*	*d*(calc.) (Å)	*d*(obs.) (Å)	*I*
200	9.52			112	1.804		
400	4.76			512	1.799	1.799	21
001	4.69	4.70	100	711	1.740		
$\bar{2}01$	4.68			911	1.735	1.732	9
201	3.85			602	1.700		
$\bar{4}01$	3.83	3.83	50	$\overline{10}.0.2$	1.690	1.692	6
600	3.17	3.16	42	312	1.688		
401	3.00	2.98	15	712	1.682		
110	2.95			10.0.1	1.632		
$\bar{6}01$	2.95	2.93	6	$\overline{12}.0.1$	1.626		
$\bar{1}11$	2.54			$\bar{2}03$	1.605		
021	2.52			$\bar{4}03$	1.604	1.604	2
111	2.458			12.0.0	1.586	1.584	3
$\bar{3}11$	2.454	2.45	50	003	1.563		
$\bar{2}02$	2.415			$\bar{6}03$	1.558		
800	2.380			512	1.549		
601	2.376			$\bar{9}12$	1.542		
$\bar{8}01$	2.364			911	1.526		
002	2.344			803	1.522		
$\bar{4}02$	2.338			$\overline{11}.1.1$	1.522	1.518	4
311	2.245	2.23	3	802	1.499		
$\bar{5}11$	2.185			020	1.495	1.490	15
202	2.159	2.153	3	$\overline{12}.0.2$	1.491		
$\bar{6}02$	2.148			203	1.486	1.485	11
511	1.987	1.985	5	220	1.477		
$\bar{7}11$	1.981			420	1.426		
801	1.942			$\bar{2}21$	1.424		
$\overline{10}.9.1$	1.933	1.933	25	$\bar{3}13$	1.418	1.417	4
402	1.927			712	1.408		
802	1.916			12.0.1	1.404		
10.0.0	1.903	1.901	2	$\bar{1}13$	1.403		
$\bar{1}12$	1.871			$\bar{5}13$	1.401		
312	1.869	1.864	7	$\overline{11}.1.2$	1.401	1.400	4
						1.385	2
						1.344	5
						1.293	5
						1.224	2

the final decision rests on the detailed refinement of its crystal structure. The detailed description of the crystal-structure analysis of doloresite and of the vanadium oxides from Carlile will be given in another paper.

SUMMARY

A new vanadium oxide mineral from the Colorado Plateau is described and named doloresite after the Dolores River in Colorado. The mineral is very widespread in slightly oxidized vanadium ores and, because of the complexity of the V_2O_4-V_2O_5 hydrate weathering system, is almost always intimately mixed with other oxide minerals, especially paramontroseite, which it replaces. When pure, the mineral is dark brown, massive with radiating botryoidal structure and a fibrous, flaky cleavage. When mixed with paramontroseite it is opaque with a submetallic luster, taking on a dark bronzy tarnish. Optically it is nonopaque, reddish yellow with a mean refractive index near 1.90; in polished section it appears gray and strongly anisotropic. Single crystal x-ray study shows that doloresite is monoclinic with space group $C2/m$, $a=19.64$ Å, $b=2.99$ Å, $c=4.83$ Å, $\beta=103°55'$. Lamellar twinning is practically universal on a submicroscopic scale, with twin plane (100). Crystal structure and chemical evidence indicate that the formula is $H_8V_6O_{16}$ or $3V_2O_4 \cdot 4H_2O$. The mineral is best identified by its x-ray powder pattern.

This work is part of the program conducted by the U. S. Geological Survey on behalf of the Divisions of Research and of Raw Materials of the U. S. Atomic Energy Commission.

REFERENCES

EVANS, H. T., JR., AND BLOCK, STANLEY (1953), The crystal structure of montroseite, a vanadium member of the diaspore group: *Am. Mineral.*, **38**, 1242–1250.

EVANS, H. T., JR., AND MROSE, M. E. (1955), A crystal chemical study of montroseite and paramontroseite: *Am. Mineral.*, **40**, 861–875.

STIEFF, L. R., STERN, T. W., AND SHERWOOD, A. M. (1956), Coffinite, a uranous silicate with hydroxyl substitution: a new mineral: *Am. Mineral.*, **41**, 675–688.

WEEKS, A. D., CISNEY, E. A., AND SHERWOOD, A. M. (1953), Montroseite, a new vanadium oxide from the Colorado Plateau: *Am. Mineral.*, **38**, 1235–1241.

Manuscript received March 12, 1957.

THE AMERICAN MINERALOGIST, VOL. 42, SEPTEMBER-OCTOBER 1957

THE CRYSTAL STRUCTURE OF URANOPHANE $[Ca(H_3O)_2](UO_2)_2(SiO_4)_2 \cdot 3H_2O$

DEANE K. SMITH, JR.,* JOHN W. GRUNER, AND WILLIAM N. LIPSCOMB,
University of Minnesota, Minneapolis, Minnesota.

ABSTRACT

Zero level Weissenberg photographs about the *b*-axis and 0*kl* precession photographs have produced a compatible crystal structure for uranophane. The cell constants are $a=15.97$ Å, $b=7.07$ Å, $c=6.68$ Å, and $\beta=97.3°$ with twice the formula $Ca(H_3O)_2(UO_2)_2(SiO_4)_2 \cdot 3H_2O$ per unit cell. The space group is $C_2^2-P2_1$, although excluding the calcium and water molecules, the symmetry is that of $C_{2h}^5-P2_1/a$.

The structure consists of sheets parallel to (100) with the formula $[(UO_2)_2(SiO_4)_2]^{-4}$. Linking the sheets together are the calcium and water molecules. Seven oxygens surround the uranium, two of which form the linear uranyl ion with the U—O distance 1.91 Å. The other five oxygens, all in SiO_4 tetrahedra, are in a plane normal to the axis of the uranyl ion. Five water or hydronium ions and three oxygens in the sheet surround the calcium ion giving it a total coordination of eight.

INTRODUCTION

Uranophane is one of the earliest known uranium minerals. It was first described by Websky (1853) from Kupferberg, Silesia, and since then has been identified in nearly all major and most of the minor uranium deposits in the world. It is a mineral of secondary origin, usually resulting on alteration of uraninite or coffinite. Recent finds of uranophane in the western United States have been described in compilations by the United States Geological Survey and the Atomic Energy Commission.

The earliest chemical analysis reported was done on uranophane from its type locality by Grundman (Websky 1859). Gorman and Nuffield (1955) list eleven analyses which are quite consistent except in the calcium content. Impurities are minor except for some traces of iron. The content of the unit cell was established by Billet (1936) who determined a set of cell constants on the basis of rotation photographs and the assumption that the cell was orthorhombic. His cell volume and cell constants were near enough to the present values that the cell contents are not changed. The formula could not be determined with any reliability until the structure was known. On the basis of balancing charges Weeks and Thompson (1954) considered the formula as an Si_2O_7 structure type; Frondel (1955) considers it to be an Si_2O_6 chain structure on account of the fibrous habit. The present investigation shows the structure to consist of independent tetrahedra and requires some assumption with respect to the form of the H_2O.

---

* Present address: Research Associate, Portland Cement Association Fellowship, National Bureau of Standards, Washington 25, D.C.

Physical and Optical Properties

Uranophane when well crystallized is always fibrous with its elongation in the direction of the *b* axis. Usually these fibers consist of several crystals in parallel growth. A cluster of single crystals rarely is found. The present investigation was made on crystals found in a vug in uraninite from the Chinkolobwe deposits in the Belgian Congo, Africa. A check on the space group of uranophane was made on capillary crystals from a cavity in Todilto limestone near Grants, New Mexico.

The uranophane crystals from Chinkolobwe show only a few simple forms. The crystals range from very minute sizes to about two millimeters long with a cross section 0.1 by 0.2 mm. The prism zone consists of (001) and (100) with (100) being dominant, and the crystals are terminated by a hemi-bipyramid *hkl* of low indices. Perfect cleavage parallel to (100) exists. Phantom outlines in some of the larger crystals indicate that the crystal grew rapidly along [010] and much less rapidly along directions normal to this axis. Some twinning is evident with (001) as the twin plane. One *h*0*l* Weissenberg photograph verified this twinning as all 00*l* reflections coincided and the remaining reflections were doubled and formed a mirror image about 00*l*.

Where uranophane occurs as radiating fibers, it is yellow and has a vitreous luster, but more commonly it occurs as massive crusts which are pale yellow to yellow-orange and have a waxy luster. The yellow-orange color probably indicates presence of iron. Fluorescence is not present in all uranophanes and may be quenched by impurities such as iron. Where fluorescence is present, it is weak yellow-green that is characteristic of several other uranium minerals.

Optical properties of the Chinkolobwe uranophane were checked for comparison with other uranophanes previously described in the literature. The results are comparable as shown in Table 1, which in part is reproduced from Gorman and Nuffield (1955). The larger crystals probably account for the more intense pleochroic formula. Fig. 1 shows the optical orientation as related to the crystal forms. Inclination of the optic plane with (001) is distinct enough to require monoclinic symmetry. An incomplete determination on the optics of the Grants, New Mexico uranophane yielded similar indices.

Other Uranyl Structures

In the literature may be found several uranyl compounds whose structures have been determined. Among these compounds only three are

TABLE 1. THE OPTICAL PROPERTIES OF URANOPHANE

	Larsen, Hess and Schaller (1926)	Gorman and Nuffield (1955)	Katanga (1956)
α	1.642–1.645	1.642	1.641
β	1.665–1.667	1.666	1.665
γ	1.667–1.672	1.668	1.667
Sign	Negative	Negative	Negative
Dispersion	Strong $r<v$	Marked	Strong $r<v$
2V	32–45°	Small	37°
Optic orient.	Z|| elongation	Z|| elongation	Z|| elongation $Y\wedge C=10°$
Pleochroic formula			
X	Nearly colorless	Nearly colorless	Canary yellow
Y	Pale canary yellow	Nearly colorless	Pale canary yellow
Z	Canary yellow	Pale yellow	Canary yellow

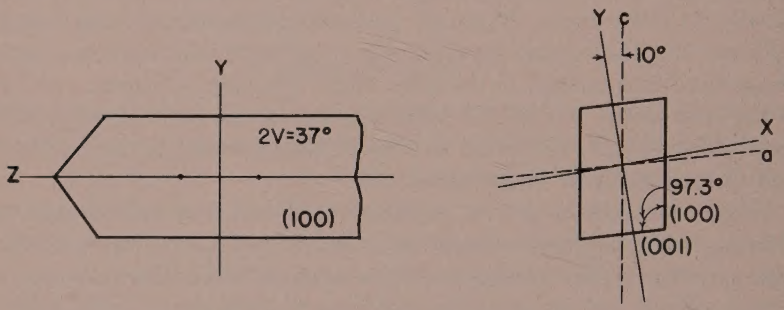

FIG. 1. The optical orientation of uranophane.

minerals, autunite, carnotite, and rutherfordine. Beintema (1938) published the structure of autunite and meta-autunite. The structure of anhydrous synthetic carnotite was solved by Sundberg and Sillen (1949), but subsequently has been shown to be in error by Appleman (1956). The structure of rutherfordine was reported by Clark and Christ (1956).

Striking similarities in the uranium coordination pattern may be seen among the uranyl structures. The uranyl ion is always well defined with the U—O distance near 1.90 Å. All the other atoms bonded to the uranium lie either in a plane normal to the uranyl axis or in a puckered ring of six atoms which approximates a plane. The latter configuration is found in the uranyl compounds $(UO_2)F_2$ (Zachariasen 1948), $Rb(UO_2)(NO_3)_3$ (Dieke and Duncan 1949), and the isomorphous compounds $Ca(UO_2)O_2$ and $Sr(UO_2)O_2$ (Zachariasen 1948), all of which have a total coordination of eight. Uranophane, johannite reported by Appleman (1956), and the structure of carnotite as corrected by Appleman (1956), have a seven-fold coordination with five in the plane. Autunite and meta-autunite have a total coordination of six with four in the plane, and liebigite as determined by Appleman (1956) and rutherfordine are examples of an eight-fold configuration with six in the plane. Thus the uranyl ion may be expected to have four, five, or six atoms around its axis.

Also evident in many of the uranyl minerals that show cleavage are distinct structural sheets. In the autunite group, for example, the sheet has the formula $[(UO_2)_2(PO_4)_2]^{-2}$. A similar sheet with the formula $[(UO_2)_2(SiO_4)_2]^{-4}$ is found in uranophane which also shows a perfect cleavage.

Preliminary Preparation of Intensity Data

Because of the prismatic nature of the crystal, Weissenberg photographs around the *b* axis were easily obtained; the precession method was used for all zones normal to *h*0*l*. Zero level Weissenberg photographs were taken with both copper and molybdenum radiation. Copper gave relatively stronger reflections for a given exposure time than did molybdenum, but because of the longer wave length, $K\alpha = 1.5418$ Å, reflections with $\sin^2\theta/\lambda^2$ greater than 0.4175 Å^{-2} were not included in the sphere of reflection. Therefore, molybdenum with a wave length $K\alpha = 0.711$ Å was used, primarily to lessen the absorption effects, but also to obtain reflections not possible with copper, and reflections with $\sin^2\theta/\lambda^2$ up to 1.5 Å^{-2} were observed.

Intensity photographs used in this structure determination include zero level Weissenberg photographs of the *h*0*l* zone taken with copper radiation, zero level photographs of the same zone using molybdenum radiation, and 30° precession photographs of the 0*kl* zone also using molybdenum. The *h*0*l* copper and molybdenum films were combined by an appropriate weighting procedure to give the composite set of intensities used. Intensity scales were made from the same crystal by exposing one strong spot for varying lengths of time, increasing this time by approximately 10 per cent for each successive exposure. Because each of the above sets differed physically, a different intensity scale was made for each set of photographs. In addition to the above photographs, upper level Weissenberg photographs about the *b* axis up to the ninth level and sets of 30° precession photographs of the *hk*0, *hkh*, and $\bar{h}kh$ zones were taken using molybdenum radiation. These photographs have not yet been analyzed.

The intensities were estimated visually and were corrected for the Lorentz and polarization effects by the method of Cochran (1948) for Weissenberg films and the values given by Waser (1951) for 30° precession photographs. The temperature factor of 0.35 Å^2 was obtained from a Wilson plot of $ln\ \Sigma f^2/|F|^2$ vs. $\sin^2 \theta/\lambda^2$. Scaling of the structure factors was done after determining the uranium positions from the Patterson projection along the *b* axis, and this scale was only slightly modified after the remainder of the structure was determined. Scattering factor curves were obtained from the values in the Internationale Tabellen.

No correction for absorption was made. Two crystals near 0.020 by 0.014 mm. in cross-section were used for all the photographs. These crystals are very close to the optimum size $1/\mu = 0.020$ mm. for molybdenum and not too far from the optimum 0.008 mm. for copper. This assumption is in part justifiable although corrections would unquestionably give a better set of intensities.

CELL CONSTANTS AND SPACE GROUP

The cell dimensions as determined from the above photographs and rotation photographs about the *b* and *c* axes are as follows:

$$a = 15.97\text{ Å}$$
$$b = 7.07\text{ Å}$$
$$c = 6.68\text{ Å}$$
$$\beta = 97.3°$$

The volume of the unit cell is 747 Å^3, and it contains two formula weights of uranophane, therefore, four uranium atoms. The calculated density is 3.89 gm./cm.^{3} which is in good agreement with the measured density, 3.83 gm./cm.^{3} (Gorman and Nuffield 1955).

Absence of $0k0$ reflections when k is odd is the only systematic extinction observed and results in the ambiguous space group $C_2^2 - P2_1$ or $C_{2h}^2 - P2_1/m$. These results disagree with the space group $C_{2h}^5 - P2_1/a$ reported by Gorman and Nuffield (1955), however, weak reflections in the $h0l$ zone when h is odd eliminate the *a* glide plane. A preliminary set of Weissenberg photographs from a uranophane crystal 0.14×0.06 mm. in cross-section showed 98 of the possible 133 $h0l$ reflections with h odd; this crystal unfortunately was too large for reliable intensities. Several crystals from Chinkolobwe and some additional ones from the Todilto Limestone near Grants, New Mexico were checked for these latter reflections, and all of the crystals showed them.

Because the crystals show nearly the symmetry of $P2_1/a$, some of the atoms and especially the uranium atoms must be close to or in $P2_1/a$ general positions, $\pm(x,y,z)$, $(\frac{1}{2}+x,\ \frac{1}{2}-y,z)$. A mirror plane is possible only if $y=\frac{1}{4}$ which would put the uranium atoms on the mirror plane. If $y=\frac{1}{4}$, the $0k0$ reflections would show a normal decline which is not the case. The (060) and (080) reflections have about the same intensity and

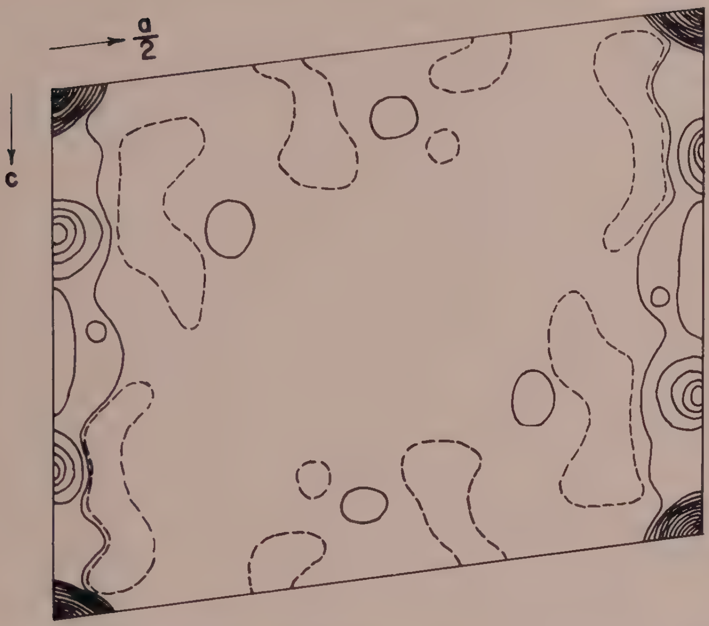

FIG. 2. Projection of Patterson function along *b* axis. Contours are equally spaced; dashed contour is zero.

are very much weaker than (020) and (040). Thus the space group had to be $C_2^2-P2_1$, and the structure determination has verified this assumption.

THE STRUCTURE

The structure determination is based primarily on the *h*0*l* zone for two reasons, first, because it is the only zone which has a center of symmetry, and second, because the Weissenberg photographs, which were easily obtained about the fiber or *b* axis, gave a large number of reflections. In this zone 303 reflections with *h* even and 38 reflections with *h* odd were observed, but only the reflections with *h* even were used in the major part of this structure determination.

A Patterson projection along the *b* axis, shown in Fig. 2, gives a peak at $x=\frac{1}{2}$, $z=0$ with a height very nearly equal to the peak at the origin. Thus for every vector that lies within an atom there must be a second vector with an equal weight from one atom to a second atom $a/2$ away. For the space group $P2_1/a$ this latter fact would be strictly true. However, there is a slight difference in peak heights, and this difference is due to the effect of the atoms violating the $P2_1/a$ symmetry. The mathematics of the Patterson function of the *h*0*l* zone are such that all even *h* intensity values will add at the point $x=\frac{1}{2}$, $z=0$ and all odd h values will subtract. Thus the difference in peak heights is due to the effect of the odd h values, and these values, then, are the contributions of the few atoms in the structure which do not have $P2_1/a$ symmetry and, therefore, no $a/2$ translation. This assumption has proved to be true, and the odd h structure factors are only the contributions of the calcium and water molecules within the limits of error.

From the Patterson projection along the b axis, the location of the uranium atoms was determined. A few trials with slight shifts of the uranium coordinates resulted in the best agreement between the calculated uranium structure factors and the observed ones, and this position has not been changed during the later stages of the determination. After the uranium atoms were located, a difference Fourier series was calculated subtracting out the uranium contributions and is shown in Fig. 3. Superimposed on the electron density map is a projection of the final structure. This electron density map was calculated using the $h0l$ values with h even only, so any atoms violating the space group $P2_1/a$ will appear as twice as many peaks with half the expected height. For ex-

TABLE 2. ATOMIC COORDINATES IN FRACTIONS OF THE UNIT CELL*

Element	x	y	z
U	.256	.787	.138
U	.756	.713	.138
Si	.282	.287	.335
Si	.782	.213	.335
$O_U(1)$	.374	.787	.138
$O_U(1)$	.874	.713	.138
$O_U(2)$	.136	.787	.129
$O_U(2)$	.636	.713	.129
$O_{Si}(1)$	.257	.477	.197
$O_{Si}(1)$	.757	.403	.197
$O_{Si}(2)$	.257	.097	.197
$O_{Si}(2)$	.757	.023	.197
$O_{Si}(3)$	.231	.287	.533
$O_{Si}(3)$	.731	.213	.533
$O_{Si}(4)$	.381	.287	.433
$O_{Si}(4)$	.881	.213	.433
Ca	.019	.750	.271
H_2O	.179		.646
H_2O	.317		.542
H_2O	.264		.771
H_2O	.243		.030
H_2O	.280		.133

* Uranium positions are accurate to ±.002; the other values are accurate to ±.02. H_2O positions are still tentative; some of these positions may not be water molecules.

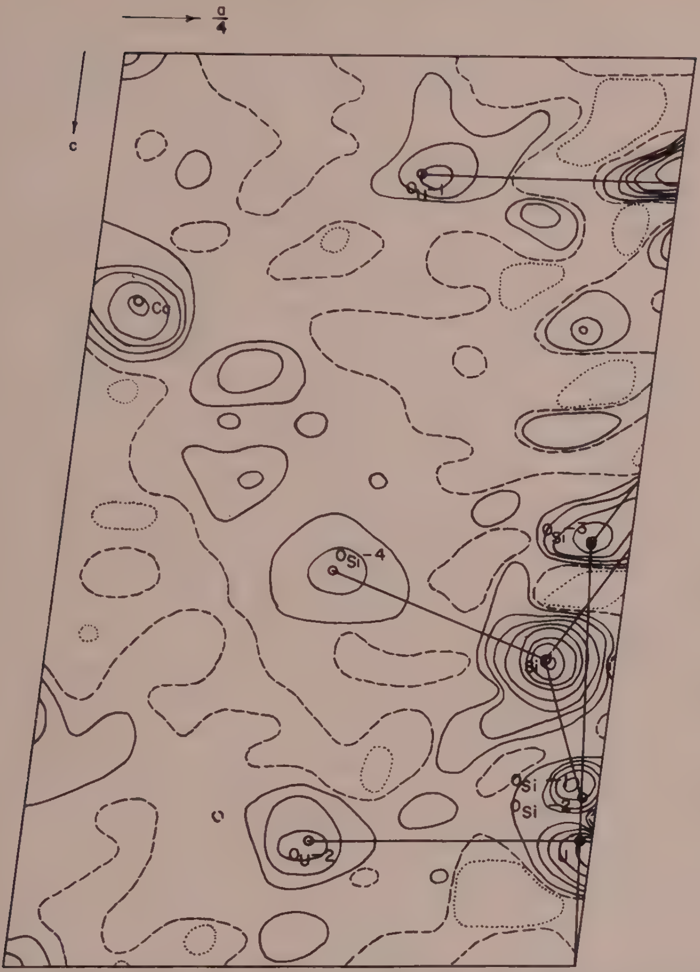

FIG. 3. Electron density with uranium removed, projected along *b* axis. A projection of the structure is superimposed. Zero contour is dotted; other contours at approximately 2 (dashed), 3, 4, 5, 6, etc. electrons/Å^2.

ample, the calcium peak is repeated four times and has a height of about two-thirds the height of the silicon peak. Only two of these peaks, related by a 2_1 axis, represent the calcium atoms in the general 2-fold positions of space group $P2_1$, the other two would be subtracted out and added to the two calcium peaks if all the odd h values were included. Which pair of peaks is chosen to represent the calcium atoms is arbitrary, but once set, the water peaks, which will also appear as four peaks with one-half the expected height, must be chosen correspondingly.

From the perfect (100) cleavage, a structural sheet may be expected parallel to this cleavage. A concentration of electron density around $x=\frac{1}{4}$ in Fig. 3 represents the expected sheet. As in some previous uranyl structure determinations, the uranyl ion may be expected to lie with its axis nearly normal to the sheet. The peaks at O_U (1) and O_U (2) represent the uranyl oxygens, and a line between them is bisected by the uranium atom at the expected distance of 1.91 Å from each oxygen. The highest peak in the electron density map could represent nothing else except the silicon position. Using the silicon position as the center of an SiO_4 tetrahedron and the uranyl position, a model was constructed and resulted in the conclusion that only one reasonable arrangement of atoms could be possible. The model was constructed before the electron density map shown in Fig. 3 was obtained. The uranyl, calcium, and silicon coordinates were obtained from an early Fourier summation based on poor intensities from a previously photographed large crystal. The electron density in Fig. 3 verifies the sheet determined in the model with two of the SiO_4 oxygen peaks at O_{Si} (3) and O_{Si} (4) and the other two, O_{Si} (1) and O_{Si} (2) both very near the uranium position in this projection.

Figure 4 is an isometric drawing of the uranyl silicate sheet as determined in the structure, and its formula is $[(UO_2)_2(SiO_4)_2]^{-4}$. Independent SiO_4 tetrahedra are bonded to the uranium atom to make up the sheet. One of the corners of the tetrahedra is pointing out of the sheet. The coordination around the uranium atom is seven, with five oxygen atoms forming a ring around the uranium atom in the plane of the sheet. Seven oxygen atoms around the uranium is an unusual coordination pattern and is attributed to the common sharing of two oxygens by a silicon and uranium as shown in Fig. 4, which is also unusual. Bond distances and angles to the oxygen atoms from the uranium atom are listed in Table 3. The SiO_4 tetrahedra are not distorted and are the major control on these bond patterns. The bond angle $O_{Si}(1)$—U—$O_{Si}(2)$ is the smallest angle in the structure and is caused by the fact that the oyxgens are both in the same SiO_4 tetrahedron thus being pulled closer together than any other pair of oxygens around the uranium atom. The uranium-oxygen distances normal to the uranyl axis are in fair agreement with values found in the other uranyl structures. Further refinement of the structure may bring these values closer together.

It has already been mentioned that the uranophane structure has been considered both as an Si_2O_7 structure type and as an Si_2O_6 chain structure. A consideration of the pseudo-symmetry $P2_1/a$ and the cell constants will give a strong argument against the chain structure. Because only four silicon atoms are present in the unit cell, the chain would have to lie either along the screw axes or exactly between two screw axes. The repeat distance therefore would be 5.28 Å which does not agree with the 7.07 Å found in uranophane.

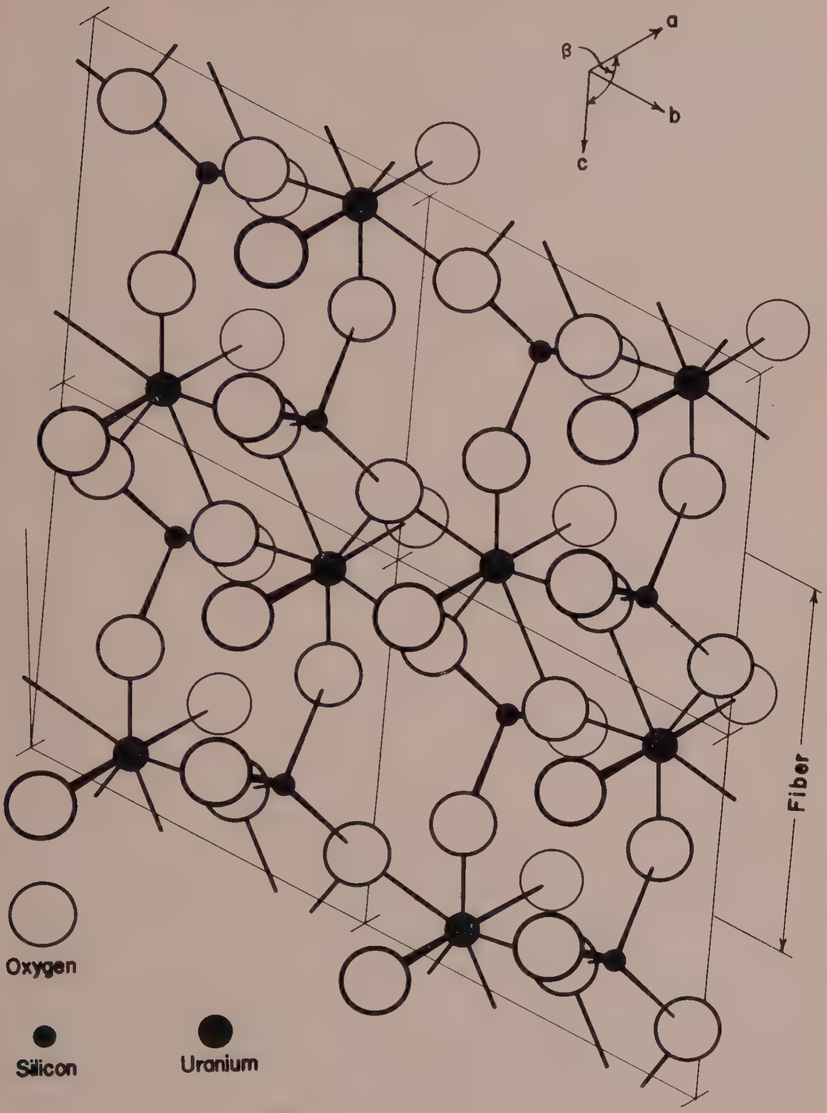

FIG. 4. Isometric drawing of the uranyl silicate sheet.

The arguments against an Si_2O_7 structure are more subtle. An Si_2O_7 group is only possible if the bridging oxygen lies on the pseudo-center of symmetry. This condition would require the peak labeled Ca on Fig. 3 to represent a silicon atom. Assuming this location for the silicon, the shortest possible U—Si distance would be around 4 Å, a reasonable distance. However, because the Si—O—Si bond must pass through the

TABLE 3. BOND DISTANCES AND BOND ANGLES

Bond distances around the uranium atom:		
U—O_U(1)	1.91 Å	oxygens of the uranyl ion
U—O_U(2)	1.91 Å	
U—O_{Si}(1)	2.5 Å	oxygens in the same SiO_4 tetrahedron
U—O_{Si}(2)		
U—O_{Si}(1)	2.3 Å	oxygens not in the same SiO_4 tetrahedron
U—O_{Si}(2)		
U—O_{Si}(3)	2.2 Å	bond between fibers
Bond angles around the uranium in order:		
O_{Si}(1)—U—O_{Si}(2)	61.0°	oxygens in the same SiO_4 tetrahedron
O_{Si}(2)—U—O_{Si}(1)	70.0°	oxygens not in the same SiO_4 tetrahedron
O_{Si}(1)—U—O_{Si}(3)	79.5°	
O_{Si}(3)—U—O_{Si}(2)	79.5°	
O_{Si}(2)—U—O_{Si}(1)	70.0°	
Bond distances in the SiO_4 tetrahedra:		
Si—O_{Si}	1.7 Å	
O_{Si}—O_{Si}	2.6 Å	
Bond distances on the surface part of the sheet:		
O_U(1)—O_U(2)	4.1 Å	
O_U(1)—O_{Si}(4)	2.9 Å and 3.6 Å	
O_U(2)—O_{Si}(4)	4.1 Å	
Bond distances between the sheets:		
Ca—O_{Si}(4)	2.4 Å	
Ca—O_U(1)	2.2 Å	
Ca—O_U(2)	2.4 Å	
O_U(1)—O_U(2)	4.6 Å	

origin, which also requires the *y* coordinate of the silicon atom to be near zero, the nearest possible corner of the double tetrahedron to a uranium atom would be over 2.5 Å away. This distance is too long to be accepted. A further objection to an arrangement of this type is based on the fact that the oxygen bridge between uranium and silicon atoms should be stronger than the bridges involving the calcium atom and would not be expected to be nearly normal to the cleavage or fiber direction.

The seven-fold coordination around the uranium atom also explains the fibrous habit of the mineral. Figure 4 shows four unit cells of the sheet, and the fiber direction is indicated. This fiber consists of two $[(UO_2)(SiO_4)]^{-2}$ chains with twice as many oxygen bridges across the fiber between the uranium and silicon atoms as between the fibers. This difference results from the common sharing of two oxygens by each silicon and uranium within the fiber and the sharing of only one oxygen by each uranium and silicon between the fiber. An apparent cleavage parallel to (001) may be observed in some of the larger crystals under the microscope. This cleavage is still questionable, but if present it would be caused by the breaking of the uranium oxygen bonds between fibers.

The *R*-factor, where $R=\Sigma|F_o-F_c|/\Sigma F_o$, for the whole sheet and the calcium atoms is 14.2 per cent for the 303 observed *h*0*l* reflections with *h* even. If the two oxygens, $O_{Si}(1)$ and $O_{Si}(2)$, located near the uranium atom are not included, the *R*-factor drops to 12.3 per cent. This apparent discrepancy is believed to be caused by anomalous scattering effects and uncertainty in the relative phases of the uranium and oxygen atoms and not by an erroneous structure. A three-dimensional study planned for the future should resolve the problem. The 0*kl* zone supports the location of the oxygen atoms in these positions. The electron density map in Fig. 3 shows an excess of scattering matter around the uranium position, but this excess does not resolve into any well defined peaks. Placing of the oxygen atoms, therefore, had to be done primarily by steric considerations based on the known size of the SiO_4 tetrahedron and the location of the silicon atom from the Fourier summation.

Figure 5 is a map of the error synthesis using the residuals from the calculated structure factors based on the sheet and calcium atoms as coefficients for the Fourier summation. A negative region now exists in the location of the sheets. Absorption effects, which affect the low order reflections most, are probably the principal cause of the negative regions. A second cause which affects the strong intensities most, which also are mostly low order reflections, is secondary extinction phenomena. Table 4 gives the observed and calculated structure factors for the *h*0*l* zone with *h* even and the (002), (004), (006), and (008) observed structure factors in particular are decidedly lower than the corresponding calculated values. The residuals of all these reflections would subtract in the region of the sheet. Some of the features such as the low minimum near $O_{Si}(3)$ were present on the difference Fourier with just the uranium atoms removed, Fig. 3. This low value, therefore, probably does not indicate that $O_{Si}(3)$ should be moved.

The error synthesis in Fig. 5 should also contain information concerning the location of the five water molecules present in the structure. Five possible positions are indicated by crosses, and these five peaks may be seen on the difference Fourier in Fig. 3 also. As has been previously mentioned, the peaks will be half the expected height and twice as numerous as they are in the structure. However, because the calcium position has been set, each water position now must be picked so its structure factor combines with the calcium structure factors to fit the *h*0*l* values with *h* odd. The only difference in the odd *h* structure factors for the two possibilities is the reversed sign for all values. Because the observed odd *h* values are relatively few in number a visual comparison of the calculated to observed structure factors will probably be more useful than the *R*-factor. Many of the odd *h* reflections are visible on the photographs of the large crystal used; and although these intensities are unreliable, they

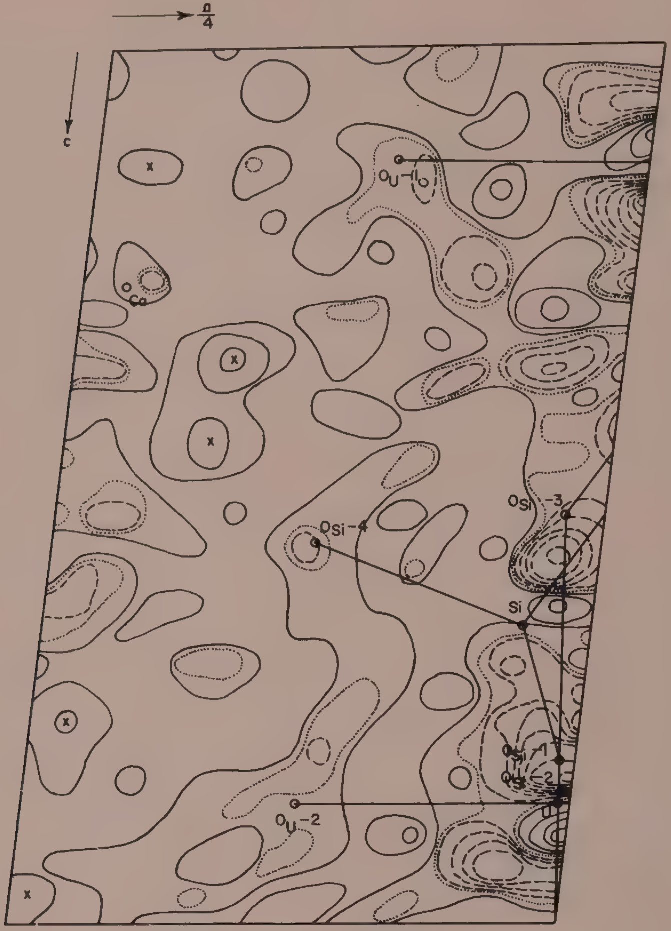

FIG. 5. Error synthesis of the uranyl silicate sheets and calcium atoms projected along *b* axis. A projection of the structure is superimposed. Negative contours are dashed; zero contour is dotted. Contours are at 0, 1, 3, 5, etc. electrons/Å^2.

are indicative and can be used to supplement the reliable odd *h* structure factors when compared with the calculated values. Table 5 gives observed structure factors where they are reliable. Where the reflection was observed on the unreliable photographs and not on reliable ones an asterisk is used. The calculated structure factors for reflections marked with the asterisk should be nearer the limiting value of observation than those not marked.

Because the structure is an independent tetrahedron type of silicate, one calcium ion between the sheets is not enough to balance the −4 charge of the sheet. Therefore, to make up this deficiency two hydronium

TABLE 4. OBSERVED AND CALCULATED STRUCTURE FACTORS FOR THE [$h0l$] ZONE WITH h EVEN. DASH INDICATES UNOBSERVED REFLECTIONS

hkl	F_o	F_c	hkl	F_o	F_c
001	190.4	202.5	400	325.3	384.6
002	95.5	−106.8	401	107.4	94.2
003	268.6	−289.0	402	104.2	−121.9
004	255.5	−260.3	403	215.2	−217.3
005	119.9	− 98.2	404	183.6	−191.1
006	130.9	120.6	405	62.5	− 40.2
007	203.6	188.7	406	137.5	138.3
008	153.6	125.6	407	143.5	136.8
009	64.4	22.2	408	135.5	105.7
0.0.10	99.6	−110.0	409	—	− 21.5
0.0.11	113.9	−116.8	4.0.10	71.4	−101.1
0.0.12	77.7	− 65.3	4.0.11	106.1	− 89.0
0.0.13	—	7.4	4.0.12	78.2	− 46.5
0.0.14	—	82.1	4.0.13	—	23.2
0.0.15	85.6	90.9	4.0.14	—	77.2
200	348.8	−459.2	4.0.15	64.7	72.9
201	157.6	−156.9	$40\bar{1}$	275.6	255.2
202	48.5	51.9	$40\bar{2}$	123.6	− 99.2
203	265.1	302.2	$40\bar{3}$	191.4	−209.5
204	239.6	240.4	$40\bar{4}$	185.5	−187.4
205	74.7	51.0	$40\bar{5}$	141.0	−119.3
206	152.8	−153.9	$40\bar{6}$	98.3	85.6
207	147.4	−132.7	$40\bar{7}$	173.4	157.0
208	139.0	−106.9	$40\bar{8}$	142.1	120.5
209	—	− 25.3	$40\bar{9}$	67.0	30.0
2.0.10	84.9	110.2	$4.0.\overline{10}$	73.0	− 79.7
2.0.11	120.8	115.0	$4.0.\overline{11}$	113.1	−107.1
2.0.12	73.8	54.1	$4.0.\overline{12}$	73.3	− 68.3
2.0.13	—	− 32.6	$4.0.\overline{13}$	—	7.0
2.0.14	—	− 71.1	$4.0.\overline{14}$	—	55.2
2.0.15	73.0	− 72.2	$4.0.\overline{15}$	82.4	90.7
$20\bar{1}$	224.0	−248.7	600	297.7	−346.8
$20\bar{2}$	37.4	66.2	601	80.4	−109.5
$20\bar{3}$	242.1	241.6	602	80.4	93.4
$20\bar{4}$	279.0	288.9	603	228.6	273.8
$20\bar{5}$	123.4	89.5	604	220.8	220.7
$20\bar{6}$	143.4	−127.5	605	—	− 20.5
$20\bar{7}$	167.0	−158.9	606	125.9	−135.9
$20\bar{8}$	149.5	−110.2	607	131.0	−127.1
$20\bar{9}$	77.4	− 44.1	608	151.7	−106.6
$2.0.\overline{10}$	75.7	82.0	609	—	12.0
$2.0.\overline{11}$	124.8	138.0	6.0.10	101.9	110.6
$2.0.\overline{12}$	77.3	69.3	6.0.11	92.6	110.2
$2.0.\overline{13}$	—	− 18.5	6.0.12	74.4	32.5
$2.0.\overline{14}$	—	− 70.4	6.0.13	—	− 33.9
$2.0.\overline{15}$	78.5	− 84.2	6.0.14	—	− 80.7

TABLE 4—*Continued*

hkl	F_o	F_c	*hkl*	F_o	F_c
6.0.15	67.3	−63.4	10.0.0	224.5	−253.7
$60\bar{1}$	197.2	−240.8	10.0.1	71.2	−78.7
$60\bar{2}$	66.4	−6.0	10.0.2	88.7	102.9
$60\bar{3}$	207.2	217.5	10.0.3	249.8	284.2
$60\bar{4}$	230.5	226.3	10.0.4	164.9	142.7
$60\bar{5}$	155.0	135.3	10.0.5	26.8	−34.3
$60\bar{6}$	110.1	−87.2	10.0.6	106.8	−131.7
$60\bar{7}$	175.0	−165.5	10.0.7	123.5	−118.7
$60\bar{8}$	124.8	−97.5	10.0.8	123.2	−93.7
$60\bar{9}$	90.3	−58.9	10.0.9	61.1	39.6
$6.0.\overline{10}$	59.6	60.3	10.0.10	110.0	112.8
$6.0.\overline{11}$	119.3	119.6	10.0.11	90.3	86.0
$6.0.\overline{12}$	77.3	89.6	10.0.12	67.8	26.4
$6.0.\overline{13}$	—	−14.9	10.0.13	—	−47.5
$6.0.\overline{14}$	—	−57.8	10.0.14	73.5	−74.2
$6.0.\overline{15}$	82.4	−76.2	$10.0.\bar{1}$	255.8	−275.4
800	307.7	376.0	$10.0.\bar{2}$	44.5	−21.0
801	81.4	47.2	$10.0.\bar{3}$	141.5	157.4
802	100.1	−107.4	$10.0.\bar{4}$	236.9	235.0
803	244.5	−274.3	$10.0.\bar{5}$	186.1	143.0
804	183.7	−193.8	$10.0.\bar{6}$	30.4	−29.4
805	39.6	−3.1	$10.0.\bar{7}$	174.0	−169.3
806	127.6	141.7	$10.0.\bar{8}$	133.6	−121.0
807	171.0	163.3	$10.0.\bar{9}$	89.0	−57.8
808	128.1	94.3	$10.0.\overline{10}$	—	28.8
809	—	−38.7	$10.0.\overline{11}$	120.6	122.0
8.0.10	94.6	−110.9	$10.0.\overline{12}$	89.7	106.5
8.0.11	108.4	−93.0	$10.0.\overline{13}$	—	7.0
8.0.12	72.9	−46.4	$10.0.\overline{14}$	—	57.8
8.0.13	—	34.1	$10.0.\overline{15}$	66.5	−81.8
8.0.14	—	96.3	12.0.0	180.0	185.4
8.0.15	58.7	60.6	12.0.1	61.3	33.1
$80\bar{1}$	310.4	312.2	12.0.2	108.4	−113.9
$80\bar{2}$	37.2	−13.8	12.0.3	206.0	−198.0
$80\bar{3}$	190.4	−225.9	12.0.4	146.2	−118.4
$80\bar{4}$	198.4	−224.5	12.0.5	—	27.4
$80\bar{5}$	154.8	−135.8	12.0.6	112.9	126.7
$80\bar{6}$	—	21.0	12.0.7	117.3	120.2
$80\bar{7}$	195.3	185.6	12.0.8	73.0	61.7
$80\bar{8}$	145.2	137.1	12.0.9	—	−64.7
$80\bar{9}$	74.9	61.2	12.0.10	68.8	−78.5
$8.0.\overline{10}$	59.9	−66.6	12.0.11	78.5	−71.7
$8.0.\overline{11}$	126.0	−119.5	12.0.12	—	−25.4
$8.0.\overline{12}$	85.1	−88.0	12.0.13	—	46.7
$8.0.\overline{13}$	—	−10.7	12.0.14	—	76.9
$8.0.\overline{14}$	—	56.2	$12.0.\bar{1}$	235.8	264.1
$8.0.\overline{15}$	78.5	89.8	$12.0.\bar{2}$	59.8	29.6

TABLE 4—*Continued*

hkl	F_o	F_c	*hkl*	F_o	F_c
12.0.$\bar{3}$	146.1	−160.7	16.0.6	108.8	132.5
12.0.$\bar{4}$	179.3	−160.5	16.0.7	122.2	133.5
12.0.$\bar{5}$	159.4	−112.6	16.0.8	63.6	31.6
12.0.$\bar{6}$	33.5	− 7.1	16.0.9	—	− 64.1
12.0.$\bar{7}$	138.4	130.1	16.0.10	67.1	− 85.1
12.0.$\bar{8}$	145.8	134.6	16.0.11	90.7	− 74.7
12.0.$\bar{9}$	78.3	57.3	16.0.$\bar{1}$	232.5	233.5
12.0.$\overline{10}$	—	− 39.8	16.0.$\bar{2}$	108.7	88.4
12.0.$\overline{11}$	88.3	− 95.0	16.0.$\bar{3}$	112.4	−123.3
12.0.$\overline{12}$	94.6	− 89.9	16.0.$\bar{4}$	165.9	−184.5
12.0.$\overline{13}$	—	− 10.7	16.0.$\bar{5}$	121.6	−105.5
12.0.$\overline{14}$	—	36.7	16.0.$\bar{6}$	60.8	− 43.8
12.0.$\overline{15}$	69.2	78.1	16.0.$\bar{7}$	107.3	111.9
14.0.0	167.4	−171.8	16.0.$\bar{8}$	131.5	142.8
14.0.1	69.5	− 50.3	16.0.$\bar{9}$	71.4	82.3
14.0.2	115.9	126.2	16.0.$\overline{10}$	—	− 23.6
14.0.3	210.8	218.3	16.0.$\overline{11}$	73.8	− 91.9
14.0.4	107.3	92.6	16.0.$\overline{12}$	82.8	− 94.8
14.0.5	27.5	− 59.4	16.0.$\overline{13}$	—	− 35.4
14.0.6	77.4	−102.8	16.0.$\overline{14}$	—	38.8
14.0.7	129.9	−118.1	16.0.$\overline{15}$	60.4	68.3
14.0.8	82.9	− 62.4	18.0.0	139.1	−138.0
14.0.9	—	60.3	18.0.1	52.0	− 32.4
14.0.10	74.2	93.6	18.0.2	143.2	150.2
14.0.11	79.2	75.8	18.0.3	163.5	193.2
14.0.12	—	5.2	18.0.4	69.7	48.1
14.0.$\bar{1}$	213.1	−201.3	18.0.5	—	− 48.3
14.0.$\bar{2}$	96.5	− 74.1	18.0.6	98.8	−114.5
14.0.$\bar{3}$	116.1	119.8	18.0.7	113.9	−106.5
14.0.$\bar{4}$	196.9	170.1	18.0.8	—	− 38.7
14.0.$\bar{5}$	147.4	129.5	18.0.9	—	68.9
14.0.$\bar{6}$	36.6	10.2	18.0.10	—	87.3
14.0.$\bar{7}$	138.8	−135.0	18.0.11	66.5	60.6
14.0.$\bar{8}$	112.0	−111.5	18.0.$\bar{1}$	186.1	−193.1
14.0.$\bar{9}$	66.0	− 60.6	18.0.$\bar{2}$	108.0	− 86.1
14.0.$\overline{10}$	—	17.9	18.0.$\bar{3}$	61.6	67.7
14.0.$\overline{11}$	88.8	81.0	18.0.$\bar{4}$	156.9	177.1
14.0.$\overline{12}$	90.5	106.3	18.0.$\bar{5}$	136.9	127.8
14.0.$\overline{13}$	—	18.5	18.0.$\bar{6}$	57.2	37.3
14.0.$\overline{14}$	—	− 49.0	18.0.$\bar{7}$	94.3	−106.2
14.0.$\overline{15}$	62.0	− 64.5	18.0.$\bar{8}$	129.2	−137.2
16.0.0	165.3	159.4	18.0.$\bar{9}$	73.8	− 64.6
16.0.1	28.8	11.6	18.0.$\overline{10}$	—	− 0.3
16.0.2	108.9	−112.8	18.0.$\overline{11}$	67.1	75.5
16.0.3	180.3	−205.6	18.0.$\overline{12}$	91.6	107.8
16.0.4	101.9	− 90.6	18.0.$\overline{13}$	—	45.4
16.0.5	—	39.7	18.0.$\overline{14}$	—	− 41.7

TABLE 4—*Continued*

hkl	F_o	F_c	*hkl*	F_o	F_c
20.0.0	102.3	91.2	24.0.3	102.9	−124.7
20.0.1	—	5.7	24.0.4	—	− 35.8
20.0.2	107.6	−129.0	24.0.5	—	58.6
20.0.3	123.0	−138.2	24.0.6	70.3	114.0
20.0.4	82.7	− 53.9	24.0.7	79.0	75.0
20.0.5	—	51.5	24.0.$\bar{1}$	124.8	149.7
20.0.6	98.8	115.0	24.0.$\bar{2}$	79.8	108.7
20.0.7	97.8	85.4	24.0.$\bar{3}$	—	− 25.9
20.0.8	—	5.3	24.0.$\bar{4}$	108.4	−147.6
20.0.$\bar{1}$	160.3	173.6	24.0.$\bar{5}$	87.0	− 94.4
20.0.$\bar{2}$	101.1	99.6	24.0.$\bar{6}$	—	− 44.5
20.0.$\bar{3}$	61.4	− 70.4	24.0.$\bar{7}$	64.8	39.9
20.0.$\bar{4}$	136.6	−147.4	24.0.$\bar{8}$	98.8	103.6
20.0.$\bar{5}$	107.9	− 94.4	24.0.$\bar{9}$	67.1	88.9
20.0.$\bar{6}$	57.7	− 34.4	24.0.$\overline{10}$	—	8.9
20.0.$\bar{7}$	66.4	58.1	24.0.$\overline{11}$	—	− 60.1
20.0.$\bar{8}$	125.2	122.4	24.0.$\overline{12}$	65.5	− 74.4
20.0.$\bar{9}$	67.7	78.6	26.0.0	80.4	− 86.4
20.0.$\overline{10}$	—	− 9.5	26.0.1	—	27.0
20.0.$\overline{11}$	67.7	− 65.2	26.0.2	105.2	143.5
20.0.$\overline{12}$	85.5	− 86.2	26.0.3	80.4	101.1
20.0.$\overline{13}$	—	− 37.0	26.0.4	—	13.0
20.0.$\overline{14}$	—	23.4	26.0.5	—	− 51.6
22.0.0	98.7	−107.4	26.0.6	79.2	− 99.2
22.0.1	—	2.5	26.0.7	74.4	− 67.6
22.0.2	121.2	146.1	26.0.$\bar{1}$	107.0	−137.9
22.0.3	97.5	128.3	26.0.$\bar{2}$	72.7	− 83.0
22.0.4	—	25.6	26.0.$\bar{3}$	—	− 0.2
22.0.5	—	− 55.3	26.0.$\bar{4}$	85.3	113.9
22.0.6	73.3	− 89.9	26.0.$\bar{5}$	105.6	114.8
22.0.7	81.9	− 87.3	26.0.$\bar{6}$	65.5	50.8
22.0.8	—	− 4.3	26.0.$\bar{7}$	—	− 37.7
22.0.$\bar{1}$	98.5	−132.4	26.0.$\bar{8}$	86.0	−106.8
22.0.$\bar{2}$	78.1	− 90.8	26.0.$\bar{9}$	67.8	− 74.2
22.0.$\bar{3}$	—	32.7	26.0.$\overline{10}$	—	− 16.4
22.0.$\bar{4}$	125.0	127.6	28.0.0	77.0	50.8
22.0.$\bar{5}$	112.8	109.1	28.0.1	—	− 30.6
22.0.$\bar{6}$	60.4	44.5	28.0.2	85.1	−113.7
22.0.$\bar{7}$	65.3	− 66.7	28.0.3	74.2	− 77.1
22.0.$\bar{8}$	110.8	−102.9	28.0.4	—	− 20.6
22.0.$\bar{9}$	66.2	− 66.9	28.0.5	—	65.5
22.0.$\overline{10}$	—	1.5	28.0.6	66.5	87.7
22.0.$\overline{11}$	67.7	42.7	28.0.$\bar{1}$	92.1	110.9
22.0.$\overline{12}$	85.1	83.0	28.0.$\bar{2}$	87.8	93.7
24.0.0	62.2	86.6	28.0.$\bar{3}$	—	0.2
24.0.1	—	− 23.3	28.0.$\bar{4}$	73.0	− 99.8
24.0.2	95.7	−129.3	28.0.$\bar{5}$	85.1	− 96.8

TABLE 4—*Continued*

hkl	F_o	F_c	*hkl*	F_o	F_c
28.0.$\bar{6}$	66.9	− 30.5	30.0.$\bar{1}$	69.9	− 96.1
28.0.$\bar{7}$	—	13.9	30.0.$\bar{2}$	69.7	− 71.3
28.0.$\bar{8}$	67.8	76.3	30.0.$\bar{3}$	—	− 9.8
30.0.0	—	− 58.4	30.0.$\bar{4}$	69.7	65.7
30.0.1	—	49.6	30.0.$\bar{5}$	74.4	89.2
30.0.2	91.6	108.5	30.0.$\bar{6}$	—	46.4
30.0.3	67.4	55.7	32.0.2	79.2	− 94.2
30.0.4	—	4.4	32.0.$\bar{1}$	—	93.8
30.0.5	—	− 55.7	32.0.$\bar{5}$	—	− 89.0
30.0.6	—	− 69.9			

TABLE 5. OBSERVED STRUCTURE FACTORS FOR [*h*0*l*] ZONE WITH *h* ODD. REFLECTIONS OBSERVED ON FIRST CRYSTAL ONLY ARE MARKED WITH *. DASH INDICATES UNOBSERVED REFLECTIONS

hkl	F_o	F_{Ca}	*hkl*	F_o	F_{Ca}
101	31.2	− 8.5	30$\bar{7}$	*	7.7
102	33.4	−28.5	500	29.7	25.4
103	35.7	12.8	501	—	−19.1
104	*	17.6	502	37.7	−16.8
105	*	−12.7	503	—	18.9
106	—	− 9.8	504	*	8.4
107	*	12.4	505	*	−15.9
10$\bar{1}$	40.2	− 0.4	506	30.4	− 2.7
10$\bar{2}$	—	−31.0	507	*	13.5
10$\bar{3}$	47.4	7.2	50$\bar{1}$	22.3	13.6
10$\bar{4}$	*	20.6	50$\bar{2}$	28.3	−25.9
10$\bar{5}$	*	− 9.6	50$\bar{3}$	47.4	− 4.8
10$\bar{6}$	*	−12.5	50$\bar{4}$	*	21.1
10$\bar{7}$	*	10.3	50$\bar{5}$	27.5	− 1.0
300	15.6	31.6	50$\bar{6}$	*	−15.7
301	34.2	−15.3	50$\bar{7}$	*	4.6
302	34.7	−23.2	700	*	17.9
303	26.0	16.8	701	18.5	−21.0
304	*	13.2	702	29.4	−10.6
305	—	−15.0	703	*	19.3
306	*	− 6.3	704	*	3.6
307	—	13.5	705	—	−15.8
30$\bar{1}$	36.4	7.4	706	31.2	0.7
30$\bar{2}$	24.5	−30.0	70$\bar{1}$	26.0	17.1
30$\bar{3}$	58.4	0.9	70$\bar{2}$	17.8	−20.9
30$\bar{4}$	21.6	21.9	70$\bar{3}$	34.6	− 9.6
30$\bar{5}$	—	− 5.5	70$\bar{4}$	26.0	18.8
30$\bar{6}$	*	−14.5	70$\bar{5}$	26.8	2.9

TABLE 5—*Continued*

hkl	F_o	F_{Ca}	*hkl*	F_o	F_{Ca}
$70\bar{6}$	—	−15.2	13.0.0	*	0.3
$70\bar{7}$	—	1.2	13.0.1	*	−16.6
900	*	11.1	13.0.2	31.2	3.8
901	*	−20.8	13.0.3	—	14.0
902	26.8	− 4.6	13.0.4	30.4	− 6.8
903	*	18.0	13.0.5	—	−10.5
904	31.2	− 0.5	$13.0.\bar{1}$	*	17.2
905	—	−14.7	$13.0.\bar{2}$	—	− 4.7
906	*	3.9	$13.0.\bar{3}$	—	−15.0
$90\bar{1}$	23.7	18.8	$13.0.\bar{4}$	*	8.0
$90\bar{2}$	—	−15.3	$13.0.\bar{5}$	—	11.3
$90\bar{3}$	*	−12.8	$13.0.\bar{6}$	*	− 9.9
$90\bar{4}$	40.2	15.4	15.0.0	*	− 3.4
$90\bar{5}$	26.0	6.6	15.0.1	—	−14.1
$90\bar{6}$	*	−14.3	15.0.2	—	6.8
$90\bar{7}$	26.0	− 2.0	15.0.3	—	11.3
11.0.0	*	5.0	$15.0.\bar{1}$	*	15.8
11.0.1	—	−19.0	$15.0.\bar{2}$	*	− 0.6
11.0.2	*	0.1	$15.0.\bar{3}$	—	−14.9
11.0.3	*	16.4	$15.0.\bar{4}$	*	4.3
11.0.4	*	− 4.0	$15.0.\bar{5}$	*	12.3
11.0.5	*	−12.9	17.0.0	*	− 6.2
$11.0.\bar{1}$	*	18.4	17.0.1	*	−11.5
$11.0.\bar{2}$	23.7	− 9.6	17.0.2	*	8.9
$11.0.\bar{3}$	—	−14.3	$17.0.\bar{1}$	—	13.6
$11.0.\bar{4}$	26.8	11.8	$17.0.\bar{2}$	—	2.7
$11.0.\bar{5}$	—	9.2	$17.0.\bar{3}$	*	−13.8
$11.0.\bar{6}$	—	−12.2	$17.0.\bar{4}$	*	0.9
$11.0.\bar{7}$	*	− 5.0			

ions are considered present instead of three water molecules. Chemical analyses discussed by Gorman and Nuffield (1955) indicate that six water molecules best fit the data, although Schoep (1927) has assumed seven. If six are accepted, and there are two hydronium ions, five water positions should be expected in the structure. The determination of these five positions is still in the experimental stage, and the positions given in Table 2 are not to be considered final. However, no good agreement of the water molecules has been found and three-dimensional data is bebelieved necessary to resolve these positions.

Because the structure of the sheet was determined by evaluation of the *h*0*l* zone coupled with steric considerations, some test of the *y* coordinates had to be made to verify the correctness of the structure. The 0*kl* zone has given the structure this test even though the zone has not been

Table 6. Observed and Calculated Structure Factors for the [0*kl*] Zone. Dash Indicates Unobserved Reflections

hkl	F_o	F_c
001	204.0	202.4
002	95.3	−107.4
003	270.5	−289.6
004	239.6	−259.8
005	111.6	− 98.3
006	119.7	120.5
007	164.4	189.0
008	133.7	125.8
009	—	22.3
010	0.0	0.0
011	224.8	275.7
012	372.7	379.4
013	128.3	137.4
014	—	− 93.6
015	137.0	−190.5
016	230.0	−211.1
017	69.5	− 64.7
018	92.4	124.0
019	137.6	167.6
020	364.9	−404.0
021	109.0	−135.1
022	—	30.6
023	161.6	187.0
024	229.6	231.0
025	118.8	125.6
026	68.2	− 88.3
027	158.8	−185.0
028	140.6	129.9
029	39.3	− 15.5
030	0.0	0.0
031	195.6	−208.1
032	280.2	−266.2
033	98.6	− 83.5
034	61.3	78.8
035	143.2	135.5
036	155.2	149.5
037	34.5	44.8
038	48.1	− 91.5
040	215.8	269.2
041	92.9	93.4
042	34.7	− 61.1
043	99.8	−135.8
044	127.1	−122.8
045	72.4	− 50.7
046	—	59.6
047	82.6	105.0
048	76.0	68.3
050	0.0	0.0
051	—	72.6
052	111.4	97.1
053	60.6	38.9
054	—	− 15.2
055	74.4	− 54.4
056	74.6	− 84.8

completely analyzed. Figure 6 is the Patterson function for this zone, and although only five orders of *k* are included, reflected in the lack of resolution of distinct peaks, it still contains considerable information. Figure 7 is the Patterson function of the structure that was determined from the *h*0*l* zone and inspection of the 0*kl* photographs which determine the *y* coordinate of the uranium atom. Only interactions with the uranium can be expected to be present, because the calcium-calcium interaction is $18\cdot 18=324$ with respect to the uranium-oxygen interaction which is $92\cdot 8=736$. Twelve uranium-uranium interactions, four single peaks with heights 8464 and four double peaks with heights 16928, dominate the pattern. Other peaks present are 16 uranium-silicon interactions, eight single peaks with heights 1268 and four double ones with heights 2536; eight single uranium-calcium interactions with heights 1656; and 64 uranium-oxygen interactions (not counting the uranyl oxygens which lie

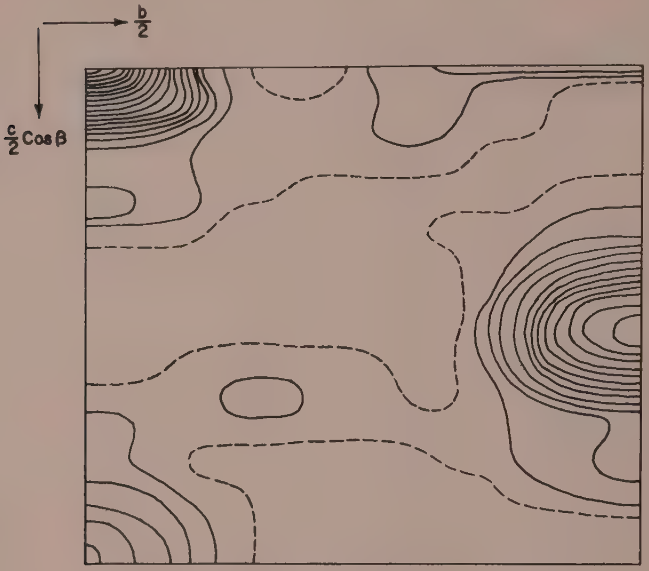

FIG. 6. Patterson projection along *a* axis.

on the uranium in this projection), 32 single peaks with heights 736 and 16 double ones with heights 1472. All these peaks are plotted in their respective positions in Fig. 7. If Fig. 7 is superimposed on Fig. 6 the strong similarity is evident. The uranium-calcium interactions are the only in-

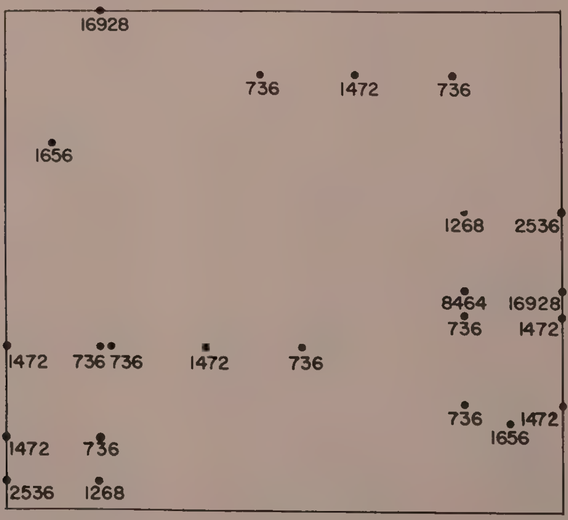

FIG. 7. Predicted Patterson projection along *a* axis based on structure.

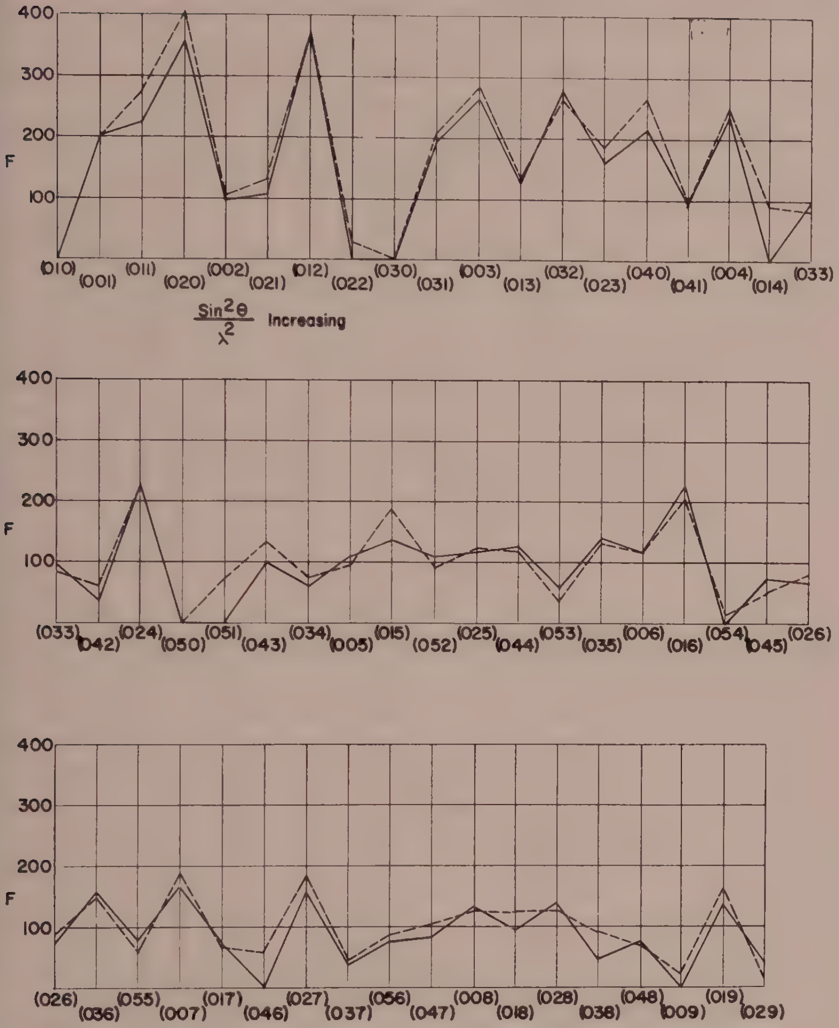

FIG. 8. Graphical representation of $0kl$ structure factors. Solid line represents observed values; dashed line represents calculated values.

dications of the y coordinate of the calcium position. The short bond distance Ca—$O_U(1)$ of 2.2 Å is probably a sign that the calcium is still not quite correctly placed.

The structure was further checked by calculating the structure factors for the $0kl$ zone. The values were scaled by correlation of the $00l$ reflections with the same reflections in the $h0l$ zone. Using the same temperature factor, $B=.35$ Å^2, as in the $h0l$ calculations and including the cal-

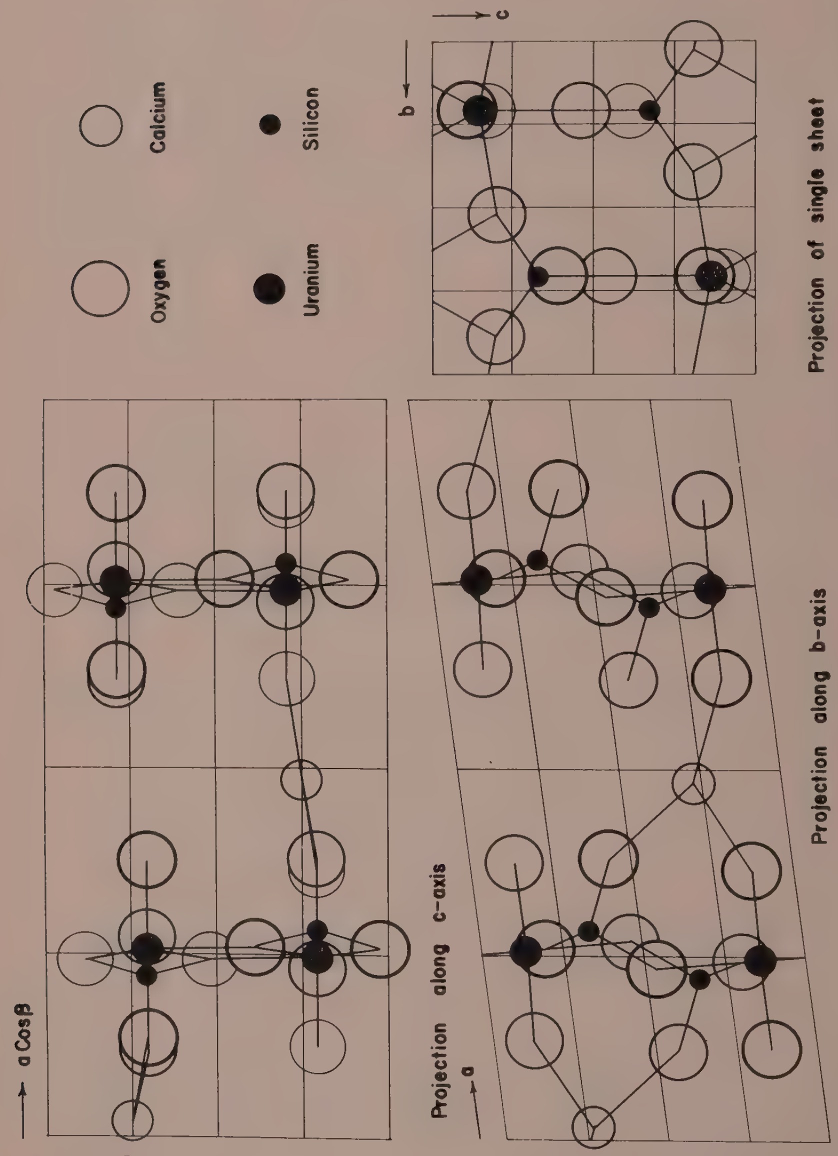

FIG. 9. Orthogonal projections of the crystal structure.

cium atoms, the *R*-factor is 13.2 per cent. Figure 8 graphically represents the agreement between the observed and calculated structure factors for each reflection in the order of increasing $\sin^2\theta/\lambda^2$. Table 4 gives the numerical values for these same structure factors. This reasonably good agreement of structure factors indicates the correctness of the structure.

Table 2 lists the complete atomic coordinates for all but the water molecules. These coordinates have been shifted to conform with the general coordinates of the space group $P2_1/a$ with its center of symmetry located at the origin. Figure 9 gives three orthogonal views of the structure, also without water molecules. The relative shifting of the sheets is easily seen in these diagrams. The oxygens in the sheets are densely packed leaving room only for the uranium. Considerable open space is found between the sheets, but much of this space should be occupied by the water molecules. The spacing between the sheets is controlled by the calcium, since calcium is bonded directly to the oxygen atoms of the sheets, and loss of water molecules should not cause collapse of the structure.

Conclusions

The structure of uranophane furthers the understanding of the nature of uranium in uranyl minerals. The odd coordination of seven is intermediate between the coordination of six and eight which had been reported previously. Sklodowskite, which is considered iso-structural with uranophane, and beta-uranophane may have structures based on uranophane. Its independent SiO_4 tetrahedra are somewhat surprising considering its fibrous habit. It indicates that many of the uranyl structures are perhaps based on structural sheets regardless of habit.

Acknowledgment

The writers wish to acknowledge the assistance received in the early part of this investigation from Dr. Peter J. Wheatley, The University of Leeds, England and Dr. Abraham Rosenzweig, University of New Mexico, Albuquerque, New Mexico.

References

Appleman, D. E. (1956), personal communication.

Beintema, J. (1938), $H5_9$-Type; Autunite $Ca(UO_2)_2(PO_4)_2\cdot 10\frac{1}{2}H_2O$: Strukturbericht, VI, p. 25.

Beintema, J. (1938), $H5_{10}$-Type; Meta-autunite $Ca(UO_2)_2(PO_4)_2\cdot 6\frac{1}{2}H_2O$: Strukturbericht, VI, p. 26.

Beintema, J. (1938), On the Composition and Crystallography of Autunite and the Meta-autunites: *Rec. Trav. Chim. Pays-Bas*, **57**, 155.

Billet, V. (1936), Uranotile and Sklodowskite: *Natur. Tijd. Gent.*, **18**, 184.

Clark, Joan R., and Christ, C. L. (1956), Some Observations on Rutherfordine: *Am. Mineral.*, **41**, 844.

COCHRAN, W. (1948), The Correction of *X*-Ray Intensities for Polarization and Lorentz Factors: *Jour. Sci. Inst.*, **25,** 253.

DIEKE, G. H., AND DUNCAN, A. B. F. (1949), Spectroscopic Properties of Uranium Compounds; Nat'l. Nuclear Energy Series Div. III **2,** p. 27, McGraw-Hill.

FRONDEL, CLIFFORD, RISKA, DAPHNE, AND FRONDEL, JUDITH (1956), *X*-Ray Powder Data for Uranium and Thorium Minerals: *U. S. Geol. Surv.* T.E.I. Rept. 575, 82.

GORMAN, D. H., AND NUFFIELD, E. W. (1955), Studies of Radioactive Compounds: VIII —Uranophane and Beta-Uranophane: *Am. Mineral.*, **40,** 634.

Internationale Tabellen zur Bestimmung von Krystallstrukturen, Zweiter Band, Mathematische und Physikalische Tafeln Gebrüder Borntraeger Berlin.

LARSEN, E. S., HESS, F. L., AND SCHALLER, W. T. (1926), Uranium Minerals from Lusk, Wyoming: *Am. Mineral.*, **11,** 155.

SCHOEP, ALFRED (1927), Isomorphism of Sklodowskite and Uranophane: *Natur. Tijd. Gent.*, **9,** 30.

SUNDBERG, INGRID, AND SILLEN, L. G. (1949), On the Crystal Structure of Carnotite KUO_2VO_4 (Synthetic Anhydrous): *Arkiv für Kemi*, Band 1, Nr. 42.

WASER, J. (1951), The Lorentz and Polarization Correction for the Buerger Precession Method: *Rev. Sci. Inst.*, **22,** 567.

WEBSKY, M. (1853), Über die geognostichen Verhältnisse der Erzlagerstäten von Kupferberg u. Rudelstadt in Schlesien: *Zs. d. Deutsch. Geol. Ges.*, **V,** 391.

WEBSKY, M. (1859), Ueber Uranophan: *Zs. d. Deutsch. Geol. Ges.*, **XI,** 384.

WEEKS, A. D., AND THOMPSON, M. E. (1954), Identification and Occurrence of Uranium and Vanadium Minerals from the Colorado Plateau: *U. S. Geol. Surv. Bull.* 1009B.

ZACHARISEN, W. H. (1948), Crystal Chemical Studies of the 5f Series of Elements III—The Disorder in the Crystal Structure of Anhydrous Uranyl Fluoride: *Acta Cryst.*, **1,** 277.

ZACHARISEN, W. H. (1948), The Crystal Structure of $Ca(UO_2)O_2$ and $Sr(UO_2)O_2$: *Acta Cryst.*, **1,** 281.

Manuscript received March 26, 1957.

THE AMERICAN MINERALOGIST, VOL. 42, SEPTEMBER-OCTOBER 1957

NOLANITE, A NEW IRON-VANADIUM MINERAL FROM BEAVERLODGE, SASKATCHEWAN

S. C. Robinson, *Geological Survey of Canada, Ottawa,* and H. T. Evans, Jr., W. T. Schaller, and J. J. Fahey, *U. S. Geological Survey, Washington, D. C.*

Abstract

A new iron vanadium oxide mineral from Fish Hook Bay, Beaverlodge region, Saskatchewan, has been named nolanite, after Dr. Thomas B. Nolan, Director of the U. S. Geological Survey. The mineral occurs as small, black, opaque, hexagonal plates with a submetallic luster, usually intimately associated with another unidentified iron vanadium oxide mineral. The unit cell is hexagonal, with $a=5.85_4$, $c=9.29_5$ Å, and space group $P6_3/mmc$, $P6mc$, or $P\bar{6}2c$. Chemical analyses of samples of nolanite, extracted by differential solubility in acid and by hand picking, lead to inconclusive results regarding the formula, owing to the great difficulty experienced in removing impurities. On crystal chemical grounds, it is proposed that Fe substitutes for V in the crystal structure and that the formula may be approximately $Fe_{2.5}{}^{+2}V_{1.7}{}^{+3}V_{5.5}{}^{+4}O_{16.0}$, or $Fe_{2.8}{}^{+2}V_{1.5}{}^{+3}V_{5.5}{}^{+4}O_{16.0}$. The mineral is best identified by its *x*-ray powder pattern.

Introduction

A small hand specimen from the "A" zone of Eldorado Mining and Refining Limited, on the shore of Fish Hook Bay, Lake Athabaska, in the Beaverlodge region[1] of Saskatchewan, was found to contain a new mineral, an iron vanadium oxide. This specimen and several others from the same area were *x*-rayed in Washington and in Ottawa and gave identical patterns unlike that of any known mineral.

The new mineral has been named nolanite in honor of Dr. Thomas B. Nolan, Director of the U. S. Geological Survey, and geologist in the Survey since 1924, in recognition of his outstanding geological work and his constant appreciation of the value of mineralogical data in geological problems.

Occurrence

In addition to the original discovery, nolanite has been identified from the first level of the No. 2 mine of Consolidated Nicholson Mines Limited, from several levels of the Ace Mine, and from the main showing on the Pitche group of claims on the southwest shore of Beaverlodge Lake. In the Pitche group vanadium assays were high enough to raise hopes that the element might be recovered economically. It is possible that nolanite may be found in sufficient quantity to become an ore mineral of vanadium.

---

[1] The Beaverlodge region was referred to as the Goldfields region in some earlier publications.

All the deposits containing nolanite are thought to be hydrothermal in origin. They are described in a bulletin on the mineralogy of the region by Robinson (1955). Although fissure filling has been the dominant mechanism in most deposits of the Beaverlodge region it is noteworthy that evidence of replacement has been observed in three of the four deposits in which nolanite has been identified.

The typical occurrence of nolanite is as concentrations of discrete subhedral to euhedral hexagonal plates from 10 to 20 microns in diameter. Locally these plates have coalesced into massive material containing residual inclusions. In the dolomite matrix of the Fish Hook Bay deposit, nolanite crystals attain diameters up to 1 mm. (Fig. 1). In leached zones some of these crystals have been freed by differential weathering of the dolomite. In the Nicholson Mine, nolanite forms radiating crusts on the dolomitized walls of the veins. Pitchblende, calcite, and sulfides in turn form an inner layer toward the center of the vein and fill interstices in the nolanite crust.

Minerals intimately associated with nolanite are dolomite, quartz, calcite, pyrite, hematite, pitchblende, chalcopyrite, ilmenite, and galena. Nolanite fills cracks in euhedral pyrite but is mantled or cemented by massive pyrite. It is also mantled by chalcopyrite, pitchblende, dolomite, and quartz. Hematite in part is veined by nolanite, but crystals of hematite, together with crystals of nolanite, are embedded in chalcopyrite and pyrite (Fig. 2). Ilmenite and nolanite in coalescing subhedral grains occur together, cemented by quartz, calcite, and pitchblende. In the Pitche group showing, carnotite has been identified, presumably having been formed as a weathering product of nolanite and pitchblende.

Description

Massive nolanite is black, but in powdered form it is brownish black. In polished section it is pleochroic from dark brown to deep blue. Plates with the *c* crystallographic axis normal to the surface are virtually isotropic, but sections containing the *a* and *c* axes are markedly anisotropic with parallel extinction. Charles Milton of the U. S. Geological Survey, in a polished section of the sample from the "A" zone of the Eldorado Mining and Refining Limited, observed two phases, one with a brownish reflection and the other with a bluish reflection. The two phases were in the ratio of approximately four to one in abundance. The chemical analysis by Fahey tended to confirm the presence of two phases by differential solubility, nolanite being the phase of greater abundance.

In thin section nolanite is opaque, but thin splinters are slightly translucent. The hardness is approximately 5; the determination was difficult owing to very small grain size. The specific gravity, as determined by

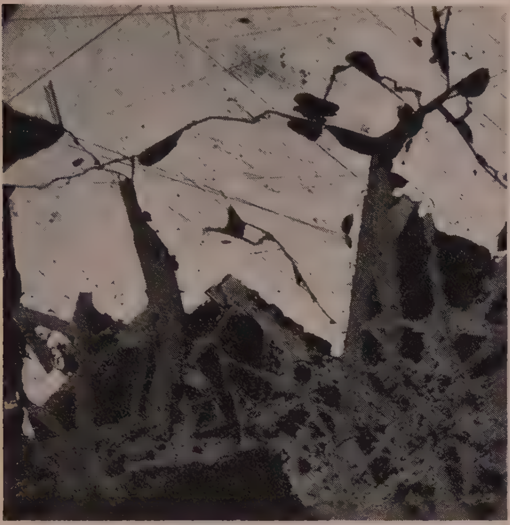

FIG. 1. Boxwork of nolanite (gray) in chalcopyrite (white) and dolomite (black). Polished section of weathered specimen, Zone "A," Eldorado Mining and Refining Ltd., Fish Hook Bay. Magnification 100×.

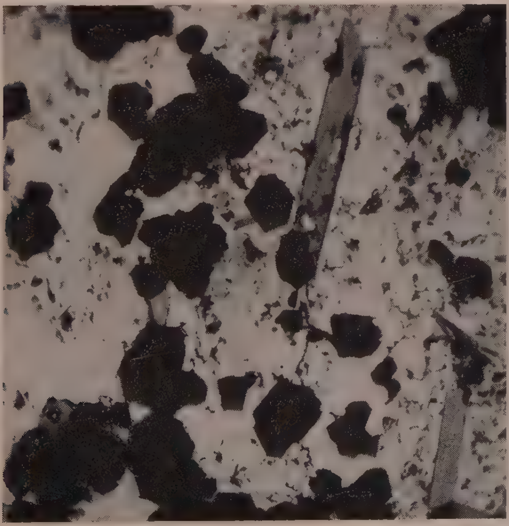

FIG. 2. Crystals of nolanite (dark gray) and laths of hematite (gray) in chalcopyrite and pyrite (white). Polished section under oil immersion. Main showing, Pitche Group, S.W. shore of Beaverlodge Lake. Magnification 500×.

Alice D. Weeks of the U. S. Geological Survey on a crushed sample from the Pitche group, is 4.65. On crystals from Fish Hook Bay the forms $c\ \{0001\}$, $m\ \{10\bar{1}0\}$, and $p\ \{10\bar{1}1\}$ were identified.

Barnes and Qurashi (1952) published results of preliminary *x*-ray studies of nolanite ("iron vanadate . . . from Goldfields, Saskatchewan," unnamed at the time) in which they show that the unit cell is hexagonal, with $a=5.854\pm0.005$ Å and $c=9.295\pm0.010$ Å and the space group $P\bar{6}2c$, $P6mc$ or $P6/mmc$. The axial ratio based on these *x*-ray measurements is $a{:}c=1{:}1.588$.

Table 1 lists the calculated spacings based on the unit-cell data of Barnes and Qurashi, the observed spacings and intensities from a film made by F. A. Hildebrand of the U. S. Geological Survey using CrKα radiation, and the observed spacings of Miss A. P. Sabina of the Geological Survey of Canada using CuKα radiation.

It should be noted that identification of nolanite as reported by Robinson (1955) rests on *x*-ray powder diffraction patterns. The same *x*-ray powder pattern has been obtained from approximately a dozen different specimens from Canada.

CHEMICAL SEPARATION

It was obvious, because of the intimate intergrowth of nolanite and the other opaque mineral, that separation of the two species by mechanical means would be impossible. In an effort to find a solvent for these two opaque minerals, and if possible to find a differential solvent, various concentrations of acetic, hydrochloric, nitric, and sulfuric acids were tried. Portions of the ground sample were treated with these acids at room temperature, at the temperature of the steam bath, and at boiling temperatures for periods of time ranging from a few minutes to several months. A solution of one volume of concentrated sulfuric acid in four volumes of water, cooled to room temperature, was found to be a suitable differential solvent. The treatment of the sample was as follows:

To a 2.000-gm. sample in an Erlenmeyer flask, from which the air had been displaced by CO_2, 100 ml. of the (1+4) H_2SO_4 at room temperature was added, and the flask lightly stoppered until the evolution of CO_2, due to the dolomite, ceased. The flask was then tightly closed.

Within a few minutes the acid solution assumed a faintly blue green color that gradually deepened for about five days. After this time there was no visual evidence of further solution of the sample. The flask was allowed to stand for two weeks, with frequent agitation, and then the blue green solution was carefully decanted into another flask from which the air had been displaced by CO_2. From this flask aliquots (25 ml. =0.500 g. sample) were pipetted and analyzed (Analysis 1, Table 2).

TABLE 1. *X*-RAY POWDER DATA FOR NOLANITE

Calculated spacings based on hexagonal unit cell, space group $P6_3/mmc$, $a=5.85_4$, $c=9.29_5$ Å

Evans measured spacings in Å based on Hildebrand's film no. 5865, CrKα radiation (2.2909 Å), 114.7 mm. diameter camera, cutoff at 20.0 Å

Sabina measured spacings in Å based on film made with CuKα radiation (1.5418 Å), 114.7-mm. diameter camera, cutoff at 12.0 Å

b indicates broad line

hkl	*d* (*calc.*) Å	Evans		Sabina	
		d (*obs.*) Å	*I*(100)	*d* (*obs.*) Å	*I*(10)
10.0	5.07	5.09	16		
00.2	4.65	4.66	55	4.63	3
10.1	4.45	4.47	8		
10.2	3.43	3.44	100	3.43	6
11.0	2.93	2.95	16	2.92	1
10.3	2.63	2.66	90	2.64	5
20.0	2.54	2.55	16	2.54	½
11.2	2.48	2.49	90	2.47	10
20.1	2.45	2.46	40	2.44	6
00.4	2.32	2.33	6		
20.2	2.23	2.23	50	2.23	3
10.4	2.11	2.12	1		
20.3	1.962	1.969	30	1.962	4
21.0	1.916				
21.1	1.913				
11.4	1.818				
21.2	1.772	1.779	9	1.777	½
10.5	1.745	1.750	6		
20.4	1.713	1.719	20	1.718	2
30.0	1.690				
30.1	1.663				
21.3	1.630	1.636	25	1.634	4
30.2	1.588	1.595	13	1.594	1
00.6	1.549	1.543	4	1.541	½
20.5	1.499	1.495	60	1.503	6
30.3	1.484				
10.6	1.482				
21.4	1.478			1.470*b*	3
22.0	1.454	1.461*b*	22		
31.0	1.406				
31.1	1.390				
22.2	1.387				
11.6	1.369				
30.4	1.367	1.357	1		
31.2	1.346	1.346	3		
21.5	1.334	1.333	6		
20.6	1.322	1.320	6		
10.7	1.285	1.282*b*	20	1.287	2
31.3	1.280				
40.0	1.268	1.269	1		
40.1	1.256	1.256	4	1.261*b*	1
30.5	1.251				
22.4	1.232	1.238	3		
40.2	1.223	1.223	3		
21.6	1.205				
31.4	1.203				
20.7	1.176	1.176	5		

After displacing with CO_2 the air in the flask containing the undissolved portion of the sample, an additional 100 ml. of (1+4) H_2SO_4 at room temperature was added and the flask tightly stoppered. For about two weeks the acid remained colorless. Then a faint blue green color appeared that slowly deepened for about two weeks, after which no further increase in depth of color was noticed. After another period of two weeks (total time six weeks), the solution was carefully decanted into another flask that had been filled with CO_2. From this flask aliquots were pipetted as before and analyzed (Analysis 2, Table 2).

To determine whether all of the vanadium and iron had been dissolved, another 100 ml. of (1+4) H_2SO_4 at room temperature was added to the remaining undissolved portion of the sample after displacing the air in the flask with CO_2. The flask was tightly stoppered and allowed to stand for two weeks at room temperature, with frequent shaking. Aliquots were then taken and analyzed colorimetrically for iron and vanadium.

Chemical Analyses

The chemical analyses of the first and second leachings of the mineral, as described above, are given in Table 2, analyses 1 and 2, respectively, in terms of weight percentages of the original sample. The aliquot taken of the third leaching was also analyzed for iron and vanadium, giving V_2O_4 0.40 per cent and FeO 0.10 per cent (percentages of original sample). The ratio of V_2O_4 to FeO in this third leaching indicates that it corresponds to the mineral dissolved in the second leaching. The mol ratios obtained from these analyses indicate that the formula of the mineral dissolved in the first leaching, corresponding to the crystallized nolanite, is $4FeO \cdot V_2O_3 \cdot 4V_2O_4$; and that the formula of the mineral dissolved in the second leaching is $FeO \cdot 2V_2O_4$.

Twenty-five milligrams of nolanite crystals were hand-picked from a dolomitic specimen from the Fish Hook Bay deposit. A microchemical analysis by A. M. Sherwood of the U. S. Geological Survey is listed in Table 1, analysis 3. This analysis indicates that water is absent and suggests the formula $3FeO \cdot V_2O_3 \cdot 3V_2O_4$ for nolanite.

The formula $4FeO \cdot V_2O_3 \cdot 4V_2O_4$ computed from analysis 1, Table 2, by Fahey and that, $3FeO \cdot V_2O_3 \cdot 3V_2O_4$, obtained from Sherwood's microchemical analysis 3, Table 2, are not greatly different. When one considers that more than 40 per cent of the sample analyzed by Fahey was made up of minerals other than nolanite, and that Sherwood analyzed only 25 milligrams of sample, the agreement is notably close. However, the correct formula will probably not be known until a complete structural study of nolanite has been made.

TABLE 2. CHEMICAL ANALYSES OF NOLANITE

(*a*) Wt. per cent analysis
(*b*) Mol ratios calculated from (*a*)

	1		2		3	
	a	*b*	*a*	*b*	*a*	*b*
V_2O_3	8.18	1.05	none		16.5	0.96
V_2O_4	34.40	3.97	10.86	1.96	59.8	3.14
FeO	14.90	3.97	2.50	1.04	24.0	2.90
Total	57.48		13.36		100.3	

1. Analysis of first (1+4) H_2SO_4 leaching of 2-gram sample of material from Fish Hook Bay, Beaverlodge, Saskatchewan. J. J. Fahey, analyst.
2. Analysis of second leaching of the same sample. J. J. Fahey, analyst.
3. Microanalysis of 25-mg. hand-picked sample from Fish Hook Bay. A. M. Sherwood, analyst.

Table 3 contains the gross chemical analysis of the sample from Fish Hook Bay, from another portion of which nolanite and the other vanadium mineral (Table 2, Nos. 1 and 2) had been separated by differential solution. The component minerals, computed from the analysis in Table 3, are listed in Table 4. Due to the organic matter present, the figure for H_2O+(110° C.) in Tables 3 and 4 is probably a little high.

TABLE 3. CHEMICAL ANALYSIS OF THE GROSS SAMPLE FROM FISH HOOK BAY, BEAVERLODGE REGION, SASKATCHEWAN, CANADA
By J. J. Fahey

	Per cent
V_2O_3	8.18
V_2O_4	45.66
FeO	17.50
CaO	4.78
MgO	3.64
CO_2	9.61
U_3O_8	1.26
H_2O- (110° C.)	1.50
H_2O+ (110° C.)	3.32
Inorganic insoluble (1+4) H_2SO_4	1.13
Organic insoluble (1+4) H_2SO_4	2.30
SO_3	0.03
Total	98.91

TABLE 4. PROBABLE MINERAL COMPOSITION OF ANALYZED SAMPLE COMPUTED FROM TABLE 3

	Per cent
More soluble mineral (nolanite)	57.48
Less soluble mineral ($FeO\cdot 2V_2O_4$)	13.86
Dolomite (computed from 4.78% CaO)	15.74
MgO (excess)	0.23
CO_2 (excess)	2.06
U_3O_8	1.26
H_2O- (110° C.)	1.50
H_2O+ (110° C.)	3.32
Inorganic insoluble (1+4) H_2SO_4	1.13
Organic insoluble (1+4) H_2SO_4	2.30
SO_3	0.03
Total	98.91

CRYSTAL CHEMICAL CONSIDERATIONS

In the absence of conclusive chemical data, the principal criteria for the identification of nolanite are its characteristic crystallography and *x*-ray powder diffraction pattern. The unit-cell dimensions and symmetry place rather severe restrictions on the chemical constitution of nolanite, although, unfortunately, they do not in themselves lead to a unique chemical formula for the mineral.

Using the data of Barnes and Qurashi (1952) the unit-cell volume is 275.9 Å³. The cell will just accommodate 16 oxygen atoms, assuming the specific volume of oxygen to be 17.2 Å³. This value of the specific volume is entirely consistent with that found for other oxides of the same type. For example, the specific volume of oxygen in goethite is 17.2 Å³; in montroseite, (V, Fe)O(OH) (Evans and Block, 1953) it is 17.1 Å³; and in duttonite, $VO(OH)_2$ (Evans and Mrose, personal communication), it is 17.2 Å³. On the basis of 16 oxygen atoms in the unit cell, the chemical analyses in Table 2 may be formulated:

$Fe_{2.5}^{+2}V_{1.7}^{+3}V_{5.5}^{+4}O_{16.0}$ (analysis 3)
$Fe_{2.8}^{+2}V_{1.5}^{+3}V_{5.5}^{+4}O_{16.0}$ (analysis 1)

Concerning the structure itself, it seems likely that the 16 oxygen atoms are arranged in closest packing, either purely hexagonal, or half hexagonal and half cubic. An ideal closest packing of oxygen atoms with specific volume 17.2 Å³, four layers high, would have the hexagonal unit cell dimensions $a=5.80$ Å and $c=9.46$ Å. As pointed out by Barnes and Qurashi, the permissible space groups provide only 2-, 4-, and 6-fold equipoints for the cations in the structure. The formulations given above consistent with the chemical analytical data suggest that the unit cell probably contains a total of 10 cations (analysis 1 give 9.8, analysis 3 gives 9.7).

The crystal chemical considerations are complicated by the fact that iron may be expected to substitute for vanadium in one or more of the crystallographic sites in the nolanite structure, so that the Fe/V or V^{+3}/V^{+4} ratios need not be rational. In montroseite (Weeks, Cisney and Sherwood, 1953), Fe^{+2} substitutes for V^{+3} to the extent of as much as 8 weight per cent. For these reasons, and also because of the recognized uncertainties in the chemical analyses (mainly because of the difficulty of purifying samples), it is not possible to write a valid chemical formula for nolanite at this time. It is probable that the true formula may be revealed only by a complete crystal-structure determination, which is now in progress (W. H. Barnes, personal communication).

SUMMARY

Although it is not possible at the present time to write a conclusive chemical formula for nolanite, the mineral has been established as a new species on crystallographic evidence. This situation is common among low-valence vanadium oxide minerals because such minerals are frequently intermixed on a fine scale and impossible to separate. The crystals are hexagonal and have a crystal structure based on a close packed arrangement of 16 oxygen atoms in the unit cell. The structure as a whole is unknown, and, especially in view of the possibility of partial substitution of Fe for V, a rational chemical formula cannot be written at the present time. The mineral is most easily characterized by means of its *x*-ray powder pattern, which has been completely accounted for in terms of the single-crystal data.

ACKNOWLEDGMENTS

Grateful acknowledgment is made to W. H. Barnes, National Research Council of Canada, and to J. A. Maxwell, Geological Survey of Canada, for information and helpful criticism of this paper; to the following members of the U. S. Geological Survey: A. M. Sherwood for his analysis of nolanite, Mrs. A. D. Weeks for the determination of its specific gravity, J. M. Axelrod and F. A. Hildebrand for making and measuring many *x*-ray powder diffraction patterns; and to Miss A. P. Sabina, Geological Survey of Canada, for other *x*-ray powder patterns.

REFERENCES

BARNES, W. H., AND QURASHI, M. M. (1952), Unit cell and space group data for certain vanadium minerals: *Am. Mineral.*, **37**, 407–422.

Evans, H. T., Jr., and Block, Stanley (1953), The crystal structure of montroseite, a vanadium member of the diaspore group: *Am. Mineral.*, **38,** 1242–1250.

Robinson, S. C. (1955), Mineralogy of uranium deposits, Goldfields, Saskatchewan: *Geol. Survey Canada Bulletin* **31.**

Weeks, A. D., Cisney, E., and Sherwood, A. M. (1953), Montroseite, a new vanadium oxide from the Colorado Plateaus: *Am. Mineral.*, **38,** 1235–1241.

Manuscript received March 26, 1957.

THE AMERICAN MINERALOGIST, VOL. 42, SEPTEMBER-OCTOBER 1957

SYNTHESIS, STABILITY AND POLYTYPISM OF NICKEL AND GALLIUM PHLOGOPITE*

Cyrus Klingsberg and Rustum Roy, *The Pennsylvania State University, University Park, Pennsylvania.*

Abstract

Phlogopites have been synthesized with Ni^{2+} substituting for Mg^{2+} and Ga^{3+} for Al^{3+}. The Ni-phase was prepared only as the 3T polytype; the Ga-member could not be indexed on any simple basis. Their decomposition temperatures under hydrothermal conditions have been determined and compared to that for phlogopite. The nickel substitution hardly affects the stability, whereas replacement of aluminum by gallium lowers the equilibrium dissociation temperature by 100° C.

Introduction

The aim of this work is to provide data upon which generalizations relating ionic composition to properties may be based. Theoretical approaches to crystal chemistry are severely limited by both the absence of thermochemical data on all but the commonest phases, and by the complexity of the mathematical treatment of the crystal energetics approach to any but the simplest arrangements. The general problem at hand is to relate the composition of a mica with its equilibrium thermal stability. The effect of composition on polytypism has also been examined.

For this purpose we have compared the following phases:

$KMg_3AlSi_3O_{10}(OH)_2$
$KNi_3AlSi_3O_{10}(OH)_2$
$KMg_3GaSi_3O_{10}(OH)_2$

The nickel phlogopite represents the substitution (only in the octahedral layer) of a more polarizable non-noble gas ion for the magnesium with hardly any change in size. The gallium on the other hand, presumably, enters only the tetrahedral layer, and again reflects the influence of increased polarizability, but also of slightly increased size.

Experimental

Mixtures of the desired compositions were prepared by the nitrate-organic silica method described by Roy (1956). The concentrated aqueous solution of the desired nitrates (of Mg, Ni, Al or Ga) are added to a solution of ethyl orthosilicate in absolute ethyl alcohol. A large excess of water is added and enough alcohol to give a clear solution. The mixture is heated not higher than 60° C. for several hours, and after a very loose gel-like structure is formed, the potassium hydroxide solution is added and the whole stirred. The gel is allowed to set and is dehydrated and ignited at about 350° C.

---

* Contribution No. 56–47, College of Mineral Industries, The Pennsylvania State University; University Park, Pennsylvania.

These starting materials are amorphous to x-rays and are several orders of magnitude more reactive than a mechanical mixture of the oxides. They are placed in platinum envelopes and heated at the appropriate temperatures and pressures in test-tube-type stellite vessels. The experimental methods have been described by Roy, Roy and Osborn (1950).

RESULTS

The mixtures both yielded well-crystallized micas (as evidenced by their powder x-ray patterns) when heated at moderate temperatures and pressures ($\sim$700° C., 15,000 psi). The crystals were very small and only rarely were small hexagonal flakes visible at the highest magnification of the polarizing microscope. The following table compares some properties of the micas:

TABLE 1

	Mg Phlog. (Yoder)	Ni Phlog.	Ga Phlog.
Basal spacing	10.15 Å	10.17 Å	10.26 Å
Refractive index (γ)	1.588	1.652	1.598

Forty-three runs were made to determine the two p-t curves for the decomposition of the nickel and gallium phase. The runs reported in Table 2 are in general somewhat more conclusive than those reported by Yoder and Eugster (1954) in the same pressure range for the Mg-phlogopite. Still they are not long enough to establish equilibrium unequivocally. While it would be very desirable to make longer runs than those reported, the temperatures and pressures are very near the limit for the vessels. In the absence of unequivocal data the results must be interpreted with considerable circumspection. For most of the cases each run was started with two starting materials: one, a pre-crystallized synthetic mica, and the other the "amorphous" gel. However, even under these conditions, during the few minutes (15–30 min.) required for the vessel to come to temperature the "amorphous" material undoubtedly had crystallized partly to a mica. It is not feasible to avoid this crystallization in this case by taking up the temperature first and then letting in the water pressure, since this causes the anhydrous phases including NiO to be formed before the run starts. These anhydrous phases persist metastably for very long periods. In the light of these facts certain nonrigorous criteria are necessary to decide where the univariant equi-

TABLE 2

Temp. (° C.)	Pressure (psi)	Time (hrs.)	Initial Condition	Results
Ni-Phlogopite				
900	2,000	71	xl.	Phlog.
900	2,000	71	gel	NiO and Leucite
910	3,300	72	xl.	Phlog.
910	3,300	72	gel	Phlog.
950	2,000	11½	xl.	Phlog.
950	2,000	11½	gel	NiO and Leucite
975	5,000	45	xl.	Phlog.
975	5,000	45	gel	Phlog.
1002	6,000	17½	xl.	Phlog. and Leucite
1002	6,000	17½	gel	Phlog. and Leucite
Ga-Phlogopite				
799	2,000	47	xl.	Phlog. and Forsterite
799	2,000	47	gel	Phlog. and Forsterite
850	5,000	240	gel	Phlog.
900	7,500	48	xl.	Phlog.
900	7,500	48	gel	Phlog.
900	11,000	117	xl.	Phlog.
900	11,000	117	gel	Phlog.
900	10,000	120	xl.	Phlog.
900	10,000	120	gel	Phlog.
920	13,000	48	xl.	Phlog.
920	13,000	48	gel	Phlog.
920	5,000	144	xl.	Forst.+Leucite
920	5,000	144	gel	Forst.+Leucite
950	6,000	138	xl.	Phlog.+Forst.
950	6,000	138	gel	Phlog.+Forst.
970	15,000	10	xl.	Phlog.
970	15,000	10	gel	Phlog.
985	15,000	9½	xl.	Phlog.
985	15,000	9½	gel	Phlog.+Forst.
990	15,000	13	xl.	Phlog.+Forst.
990	15,000	13	gel	Phlog.+Forst.
1014	10,000	5½	xl.	Phlog.+Forst.
1014	10,000	5½	gel	Phlog.+Forst.

Abbreviations: Phlog.=phlogopite; Forst.=forsterite; xl=crystal.

librium curve lies. Runs in which both starting materials yield the anhydrous phases—even in part only—are obviously points above the curve. Runs in which well-formed mica is obtained from both starting materials have to be repeated for longer and longer times to be sure that it is not metastable persistence of the mica. Confirmation is sought by obtaining decomposition with very much shorter runs at about 10° C. above the long runs which gave only the mica.

The reaction involved in both cases is presumed to be analogous to the Mg-phlogopite decomposition, i.e.: 2 phlogopite$\rightleftarrows$3 $Mg(Ni)_2SiO_4$+$KAl(Ga)Si_2O_6$+$KAl(Ga)SiO_4$. Evidence for the actual formation of the forsterite and leucite phases is ample in both cases, whereas even the detection of $KAlSiO_4$ is questionable in the hydrothermal decomposition products of both micas. Dry decomposition attempted at 1200° C. for 48 hours caused melting of the gallium composition and the formation of only NiO as a crystalline phase from the nickel member. Evidence that these are the equilibrium anhydrous phases is therefore not conclusive.*

From the curves of Fig. 1 it can be seen that where data have been obtained the Ni curve is almost identical with the Mg curve. It actually lies about 10–20° C. lower than the Mg-mica curve of Yoder and Eugster but this is well within the limits of error and correspondence across laboratories. The Ga-mica curve on the other hand is definitely (~100° C.) lower than the aluminum counterpart. DeVries and Roy (1955) have discussed elsewhere the significance of the influence of the ionic size and polarizability on stability of the layer lattice minerals. Crystal growth seemed to be quite unaffected by these ionic substitutions. There was no marked tendency for either of these micas to grow much faster or larger than the other.

POLYTYPISM OF THE Ni AND Ga PHLOGOPITES

(By F. H. Gillery)

Specimens of the nickel and gallium phlogopites (respectively $K_2Ni_6(Al_2Si_6)O_{20}(OH)_4$ and $K_2Mg_6(Ga_2Si_6)O_{20}(OH)_4$), were examined by *x*-ray powder techniques to determine the polymorphic varieties. The former was found to have a one-layer monoclinic or a three-layer trigonal structure. A consideration of the stacking possibilities of mica layers showed that these two types of structure should be indistinguishable from powder photographs of trioctahedral micas. An indexed powder pattern is given in Table 3.

The gallium phlogopite proved to be a more difficult problem. It was impossible to index the *x*-ray diagram completely on either a 1M, 2M, 3T, or 6T basis. The pattern appears to be more complex than any of these types.

---

* A long, low-P, high-T run gave, in addition to leucite and forsterite, diffraction peaks which could very well represent Ga-kaliophilite.

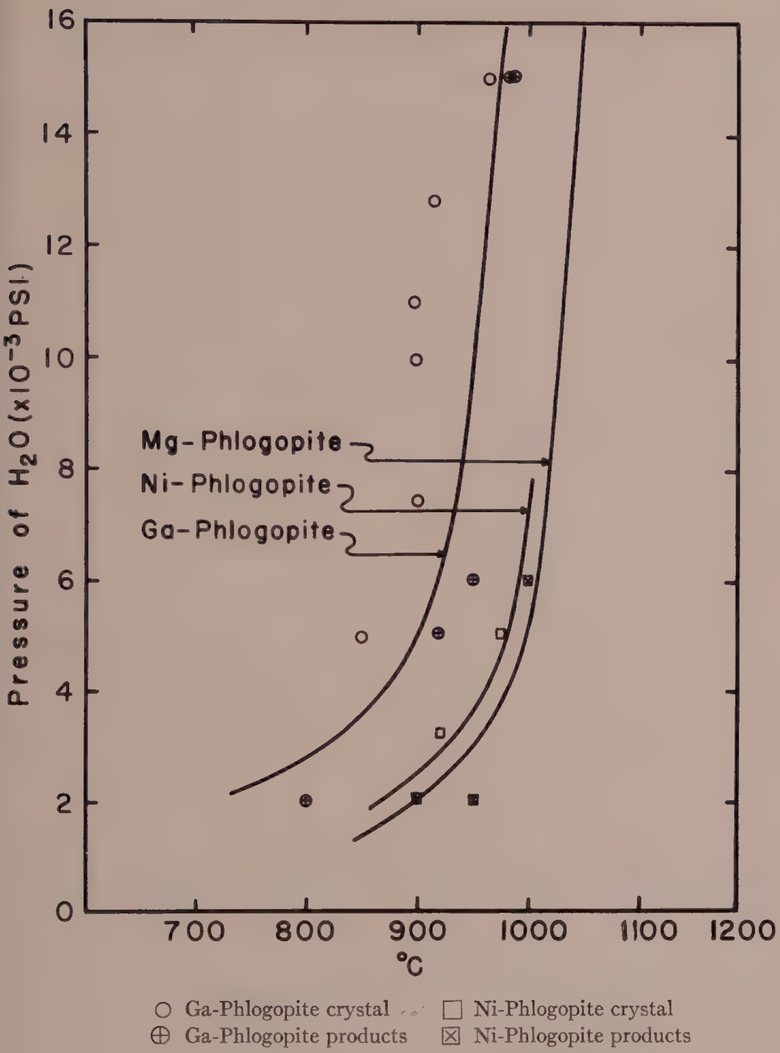

FIG. 1. Curves showing stability relationships.

ACKNOWLEDGMENTS

This work was done under the sponsorship of the Chemical Physics Branch of the Signal Corps Engineering Laboratories under Contract DA-36-039 SC-71214. We are grateful to Dr. Gillery for the indexing of the nickel phlogopite.

TABLE 3. INTERPLANAR SPACINGS AND INDICES OF NICKEL PHLOGOPITE (3T BASIS)

d(Å), *obs.*	Int., est.	*hkl*	*d*(Å), *calc.*
10.15	10	00.3	10.17
5.512	4	?	—
5.065	5	00.6	5.083
4.557	6	10.0; 10.1	—
3.927	5	10.4	3.932
3.672	6	10.5	3.668
3.389	10	00.9	3.389
3.164	6	10.7	3.160
2.928	6	10.8	2.932
2.720	4	10.9	2.726
2.612	10	11.2	2.611
2.542	6	00.12	2.542
2.501	4	11.4	2.503
2.430	10	11.5	2.431
2.359	2	?	—
2.291	3	20.0	2.295
2.264	5	11.7	2.264
2.176	9	11.8	2.176
2.089	8	20.6	2.092
1.997	7	11.10	2.000

Cell Parameters	
$a = 5.300$ Å	$c = 30.51$ Å

REFERENCES

DEVRIES, R. C., AND ROY, RUSTUM (1955), Influence of ionic substitution on the stability of micas and chlorites: *Bull. Geol. Soc. Am.*, **66**, 1550.

ROY, RUSTUM (1956). Aids in hydrothermal experimentation: II, Methods of making mixtures for both dry and wet phase equilibrium studies: *J. Am. Ceram. Soc.*, **39**, No. 4.

ROY, DELLA, ROY, RUSTUM, AND OSBORN, E. F. (1950), Compositional and stability relationships among eucryptite, spodumene and petalite: *J. Am. Ceram. Soc.*, **33**, 153–159.

YODER, H. S., AND EUGSTER, H. P. (1954), Phlogopite synthesis and stability range: *Geochim. et Cosmochim. Acta*, **6**, 157–185.

Manuscript received February 7, 1957.

THE AMERICAN MINERALOGIST, VOL. 42, SEPTEMBER-OCTOBER 1957

ANDALUSITE- AND CORUNDUM-BEARING PEGMATITES IN YOSEMITE NATIONAL PARK, CALIFORNIA

ROBERT L. ROSE, *School of Mineral Sciences, Stanford University, Stanford, California.*

ABSTRACT

Five andalusite- and corundum-bearing pegmatites occupy the *ac* joints of interbedded pelitic hornfels and quartzite in the marginal portion of a roof pendant at May Lake, Yosemite National Park, California. The pegmatites are composed of quartz, orthoclase, biotite, muscovite, andalusite, corundum, etc. Andalusite ($N_x = 1.646$, $2V_x = 84°$) is concentrated in the margin zones and is partly replaced by muscovite. Small biaxial corundum crystals with margins of diaspore are enclosed in the muscovite in the interior of the altered andalusite crystals. The pegmatites are thought to have formed by magmatic injection and reaction of the magma with the wall rocks, with the formation of andalusite in the reaction zones. Later potash metasomatism partly converted the andalusite to a mixture of muscovite, corundum, and diaspore.

The age of biotite from one of the pegmatites (88.2 million years) indicates they are genetically related to the Sentinel granodiorite rather than the adjacent Mt. Hoffmann quartz monzonite.

INTRODUCTION

Andalusite has been reported in granitic pegmatites from many localities; indeed, the best specimens of andalusite have come from pegmatites and related andalusite-quartz veins (Lacroix, 1892, p. 32–33, Murdoch and Webb 1938, p. 47, Hintze 1897, p. 135–136). Although such pegmatites are not uncommon they are interesting from a genetic standpoint. Most andalusite pegmatites and veins are apparently located in aluminous metamorphic rocks near acid plutonic bodies. Consequently their genesis is usually interpreted as being related to their environment; e.g. magmatic reaction with aluminous xenoliths. A few andalusite pegmatites, however, are located in rocks that are not notably aluminous, and in such cases, because their genesis is not obvious, various hypotheses have been offered to account for their origin. Macdonald and Merriam (1938, p. 592–594) for example, suggested that the andalusite and corundum of a Fresno County pegmatite are of pneumatolytic origin, the aluminum having been introduced by "aluminous vapors" after crystallization of the surrounding minerals.

The purpose of this paper is to describe a group of andalusite- and corundum-bearing pegmatites in a Sierran roof pendant and to consider their origin.

LOCATION

Five small tabular andalusite- and corundum-bearing pegmatite dikes are exposed on the rocky north shore of May Lake in the central part of Yosemite National Park, California (Fig. 1). They are enclosed in thermally metamorphosed sedimentary rocks in the northwestern margin of a roof pendant. They are limited to a small area about 100 feet from the contact with the Mt. Hoffmann quartz monzonite although none of them adjoins the quartz monzonite at the surface.

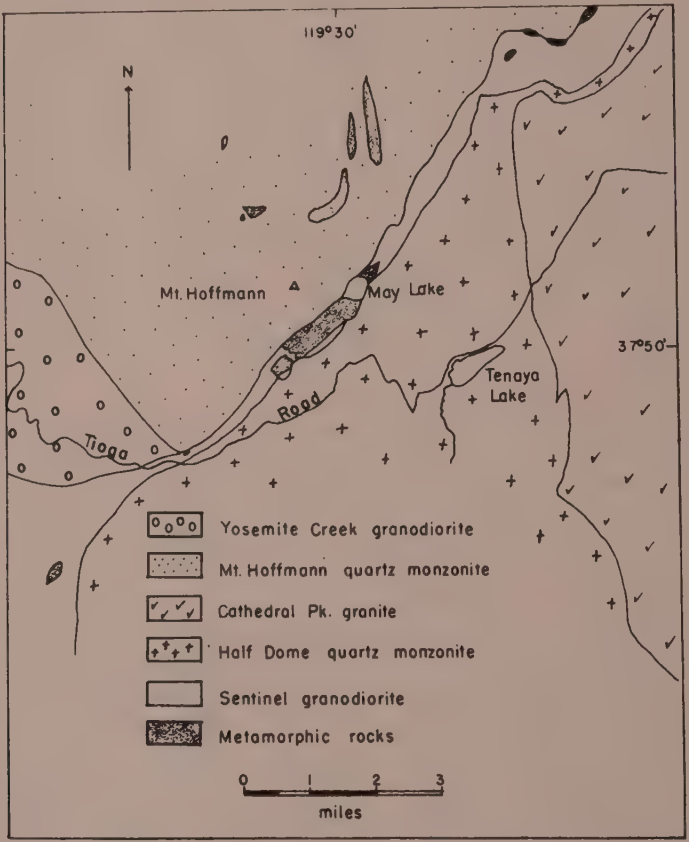

FIG. 1. Geological sketch map showing portion of Yosemite National Park.

GENERAL GEOLOGICAL SETTING

The pendant of metamorphic rock, a northeast-trending mass about 2 miles long and $\frac{1}{2}$ to $\frac{3}{4}$ of a mile wide, is the largest of a group of pendants near May Lake. It is partly enclosed by the Sentinel granodiorite and its northwestern boundary is in contact with the Mt. Hoffmann quartz monzonite. The southeastern border of the pendant is locally in contact with the Half Dome quartz monzonite but a thin band of Sentinel granodiorite usually separates them. The oldest of these granitic rocks is the

Sentinel granodiorite and the youngest is the Mt. Hoffmann quartz monzonite. The sketch map (Fig. 1) shows the general relationships.

Small, fine- and medium-grained pegmatite dikes are common in the marginal portions of the granitic masses and in the adjacent metamorphic rocks. They are mineralogically simple and most of them consist of quartz, perthitic potash feldspar, oligoclase, and biotite with the usual accessories. Allanite and monazite in megascopically conspicuous crystals are not uncommon in the pegmatites associated with the Sentinel granodiorite. Muscovite is common in pegmatites cutting meta-pelitic rocks, and hornblende is a conspicuous constituent of those cutting diopside hornfels. In general the mineral composition of each pegmatite seems to be genetically related to its wall rock.

The metamorphic rocks that make up the May Lake pendant are mainly quartzite and pelitic hornfelses with minor amounts of marble, calc-silicate hornfels, and amphibolite. About 2500 feet of strata are present and although no fossils have been found within them they are thought to be of late Paleozoic Age.

The pendant itself trends northeast but the structural trend of the metamorphic rocks is to the northwest, the rocks having been folded into a series of anticlines and synclines that plunge N. 40°–80° W. at 50°–70°. The rocks are lineated and show prominent *b* lineations and conspicuous *ac* joints. Locally they show schistosity parallel to the bedding. In general their fabric is highly discordant with that of the adjacent granitic rocks, contacts are sharp, and all field and laboratory evidence indicate that the granites were magmatically emplaced.

Pegmatites

The pegmatites range from 10 to 47 feet in length and from 0 to 18 inches in thickness. The two best exposed ones are only 2 to 4 feet apart and appear to be connected by thin quartz-feldspar veins between half an inch and an inch in thickness. All five are in a zone about 110 feet wide and are essentially parallel, striking N. 15°–20° E. and dipping 50°–55° S.E. They gradually thin toward their ends and *ac* joints with the same attitude extend away from them. In general the pegmatites seem to be fillings of *ac* joints.

The sides of the dikes are nearly parallel so that major irregularities in opposite walls seem to match. In detail, however, the walls are minutely irregular and not strictly parallel, suggesting the pegmatites have partially replaced their walls.

Mineralogy of the Pegmatites

The pegmatites are vaguely zoned with marginal, fine-grained andalusite-bearing zones, a poorly defined medium-grained core composed mainly of quartz and feldspar, and intermediate zones. The central of the five pegmatites is the thickest and best zoned, but all of them show the same general characteristics. Their mineral composition is difficult to estimate because of variation in grain size and the tendency of minerals to occur in clusters. Table 1 is an estimate of the modal composition of the central pegmatite; the others are essentially similar but may contain less andalusite and more tourmaline.

The quartz of the pegmatites is anhedral and colorless and in thin section shows numerous minute irregular cavities containing both a liquid phase and a bubble of gas. Individual grains are usually about 1 to 3 inches in greatest dimension but range up to 8 inches. The potash feldspar is orthoclase micro-perthite. It appears to be optically monoclinic $(\perp X,\ Z\wedge a=5^\circ;\ \perp Z,\ X\wedge b=0^\circ)$, with an optic axial angle of about $55^\circ(-)$. This corresponds to about 75% Or and 25% (Ab-An) (MacKenzie and Smith 1956, p. 406). The feldspar is pale pink and occurs as anhedral to subhedral crystals ranging in size up to 10 inches in greatest dimension. Locally it contains irregular patches and streaks of muscovite concentrated along grain boundaries, fractures, and cleavage planes; apparently the mica has replaced the orthoclase. The plagioclase is oligoclase (An_{25}) and occurs as subhedral white crystals seldom more than two inches in greatest dimension. The margins of many grains are partly replaced by muscovite and in places the plagioclase is cloudy and partially argillized.

TABLE 1. ESTIMATED MINERAL COMPOSITION OF THE CENTRAL PEGMATITE
(volume per cent)

Quartz	37
Potash Feldspar	35
Plagioclase (An_{25})	15
Andalusite	5
Biotite	3
Muscovite	2
Titaniferous Hematite plus Corundum	1
Tourmaline	1
Other accessories	1

Tourmaline is found principally in clusters of subradiating black prisms one quarter to three eighths inch in diameter and several inches in length but isolated crystals are enclosed in most of the principal minerals. Many individual crystals of tourmaline pass uninterruptedly through several mineral grains, seemingly replacing everything in their way. Small granular patches of tourmaline occur chiefly in the margins of the pegmatite bodies, apparently replacing feldspar. In general the

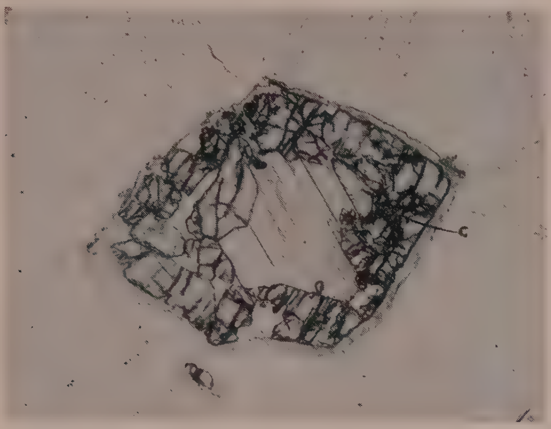

PLATE 1. Andalusite crystal enclosed in quartz and largely replaced by muscovite. Arrow points to small isolated crystal of corundum which is actually separated from andalusite by a sheath of muscovite. Lack of corundum elsewhere is possibly due to adequate supply of silica at time of introduction of potash. Radial cracks in quartz may have been permeability channels for potash introduction. Plain light, ×18.

tourmaline is erratically distributed and individual crystals show no obvious preferred orientation. The mineral is pleochroic from dark green to pinkish-brown in thick sections, ϵ is about 1.65, corresponding to intermediate schorlite.

Biotite is present as subhedral, platy crystals that range from 1 to 4 inches in greatest width. Individual crystals show no preferred orientation and many plates stand at high angles to the walls of the pegmatite. Muscovite (2V about 40°) is generally subhedral and occurs in clusters erratically distributed throughout the pegmatite. Fine-grained muscovite is also present in or marginal to orthoclase and plagioclase, apparently replacing both.

Small tabular crystals of titaniferous hematite are scattered throughout but seem to be more abundant in the marginal zones with the andalusite. The crystals are euhedral to subhedral with prominent development of the basal pinacoid, but the faces are generally rough and imperfect. The crystals are one tenth to one half inch wide and up to one tenth of an inch in thickness and many of them contain small inclusions of rutile and quartz. A positive qualitative reaction for titanium was obtained by boiling a hydrochloric acid solution of the fused mineral with tin. The specific gravity was determined on a Berman microbalance to be 5.13 ±0.01 (average of three determinations) which corresponds to a mixture of 74.2% hematite and 25.8% ilmenite by weight or 72.3% and 27.7% by volume respectively.

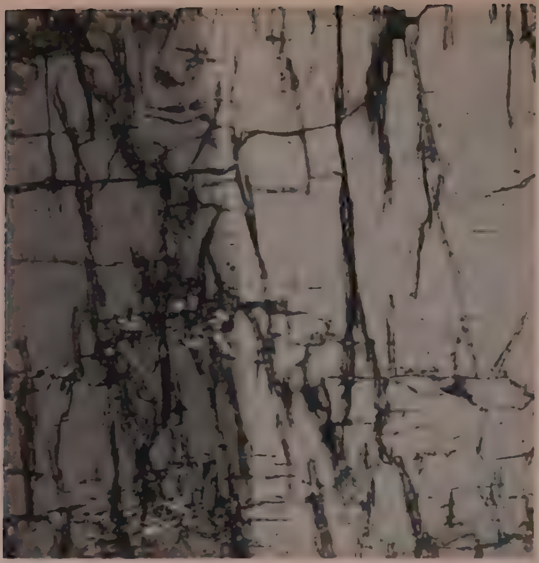

Plate 2. Zoned andalusite showing {110} cleavage and parting parallel to {001}. Section ⊥ *a* with X approximately N.S. Note minor development of fine-grained muscovite (bright material) along cleavage and parting cracks, but absence of corundum. Crossed nicols with analyzer 45° from X, ×27.

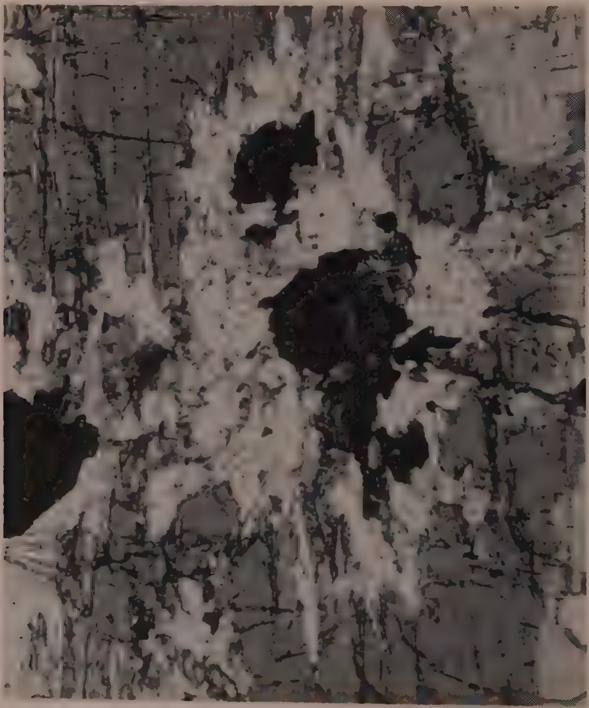

Plate 3. Part of crystal shown in Plate 2. Black grains are dark blue corundum, surrounding white is muscovite, and light and medium gray is andalusite. Note irregular zoning of andalusite. Slide is about 0.04 mm. thick so zoning is more pronounced than in sections of standard thickness. Crossed nicols with analyzer about 45° to cleavage, ×27.

Andalusite occurs as striated brown, prismatic, tapering crystals with a silvery white coating of muscovite. Individual crystals range up to 4 inches in length and three quarters of an inch in diameter. They are concentrated in the marginal zones but in some cases occur well within the pegmatites. The crystals show a preferred orientation, the *c* axis of most individuals lying at high angles to the walls of the pegmatite. In thin section the andalusite is weakly pleochroic with X, pale pink, Y and Z pale greenish to colorless and $X > Y = Z$, $\alpha = 1.646$, and $\gamma = 1.656$, the 2V is 84°, negative and the dispersion about X is strong with $r < v$. The specific gravity of andalusite free from inclusions is 3.14 ± 0.01 (average of three determinations on a Berman microbalance); this along with the optical properties indicates that the andalusite contains about 5% of the Fe_2SiO_5 molecule (Tröger 1952, p. 44). Some crystals are zoned with irregular bands that have slightly lower birefringence and stronger pleochroism than most of the andalusite. These portions probably contain slightly more than 5% of the iron molecule. The andalusite apparently shows all stages of replacement by muscovite, the margins of the crystals being replaced by coarse mica, and veinlets and irregular patches of coarse- and fine-grained colorless mica are present in all of the crystals. Embedded in the muscovite in the interior of the andalusite crystals are small crystals of corundum and diaspore, the corundum constituting 10 to 15% of most crystals and diaspore less than 1%. Neither of these minerals was observed in the marginal portions of the altered andalusite crystals.

Corundum is present as small equant six-sided euhedral to subhedral crystals ½ to 2 mm. in diameter scattered throughout the andalusite-muscovite mixture but apparently always embedded in the muscovite. The crystals are pleochroic, biaxial, and generally zoned in shades of blue, but some zones are colorless and in some cases the Y and Z directions are bright yellow. A few grains were observed to have one end with Y = yellow and the other end Y = blue. Bluish grains have the following optical properties:

$\alpha = 1.761$	bluish-green to nearly colorless
$\beta =$ about 1.768	deep to pale blue
$\gamma = 1.769$	deep to pale blue
$X < Y = Z$	
$2V_x = 17°$	(average of 3 measurements)
$X = c$	

Yellow grains seem to have a smaller 2V and slightly higher indices of refraction but these properties were not accurately measured. Although the corundum crystals are enclosed in muscovite they show no obvious evidence of being replaced by the mica; instead small colorless subhedral crystals of diaspore are occasionally attached to their margins and locally the diaspore replaces the margins of the corundum grains.

Minor accessories rutile, zircon, and apatite are distributed throughout the pegmatites in small euhedral crystals but only the rutile is megascopically apparent.

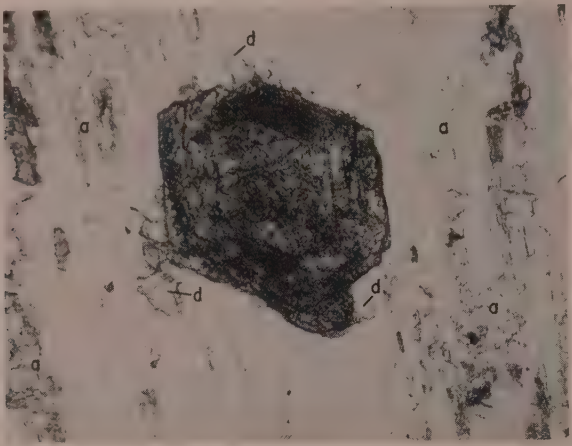

PLATE 4. Zoned corundum in muscovite that has replaced andalusite. Light colored marginal portions of crystals and adjacent colorless grains with high relief are diaspore (d). Grains with high relief near margins of picture are andalusite (a). Plain light, ×27.

METAMORPHIC ROCKS

The rocks enclosing the pegmatites are dominantly pelitic hornfels with minor interbedded quartzite. The hornfels is medium to dark gray, and banded with a vague schistosity parallel to the bedding, apparently because of the subparallel orientation of biotite crystals. Microscopically the hornfels is typically porphyroblastic with small (1 to 3 mm.) poikilitic andalusite crystals embedded in a fine-grained hornfelsic ground-mass that consists mainly of cordierite, andalusite, potash feldspar, and biotite with minor amounts of muscovite, quartz, magnetite, rutile, sillimanite, tourmaline, and monazite(?). Table 2 gives the estimated mode of a typical hornfels. The most variable constituent is apparently muscovite which occurs principally as fine-grained material replacing the marginal portions of andalusite grains and potash feldspar. Some of the muscovite is intergrown with biotite and this may be primary, although a replacement origin is suggested by some fabric relationships. In general the muscovite is thought to be mainly a secondary mineral and a retrograde product.

The quartzite is typically light gray, well-bedded to cross-bedded, and medium- to coarse-grained with a granoblastic texture. It shows well-developed mosaic structure with interlocking anhedral grains of quartz, interstitital potash feldspar and small grains of biotite, magnetite, and zircon. Locally small crystals of plagioclase, cordierite, and andalusite are conspicuous constituents. Muscovite is present in small amounts in most specimens, apparently replacing feldspar. In general quartz constitutes 85 to 95% of the bulk and potash feldspar 3 to 12%, with the accessories and biotite varying from 3 to 10%.

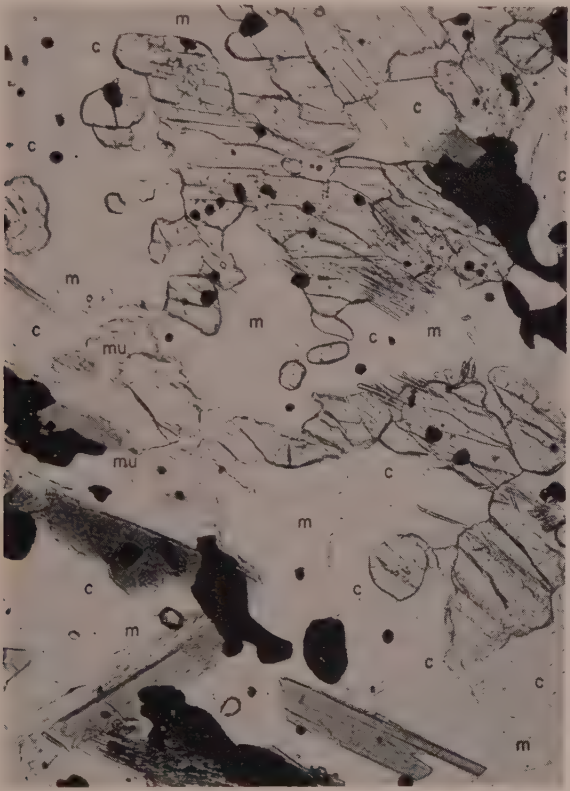

Plate 5. Pelitic hornfels from wall of middle pegmatite. Composed mainly of andalusite (gray grains, high relief), opaque ore (black grains), biotite (dark gray), cordierite (c), microcline (m), sillimanite (acicular crystals), and muscovite (mu). Muscovite and biotite intergrowth in left central part of picture probably replaces microcline, andalusite and cordierite. Plain light, ×80.

Petrogenesis

Pegmatites are commonly thought to have originated either by (a) magmatic injection, (b) partial fusion of the host rock and migration of pegmatitic fluid into fractures or other suitable locis, or (c) metasomatic replacement of the host rock (Turner and Verhoogen 1951, p. 328). It is difficult however to account for the May Lake pegmatites by any one of the above mechanisms; apparently they were formed by a combination of processes.

The mineralogy of the pegmatites and adjacent rocks suggests that the mineral composition of the pegmatites was influenced by that of the wall rocks. Spatial relationships, however, indicate that the pegmatites are essentially joint fillings with only limited replacement of the adjacent meta-sediments. Lack of preferred orientation of the micaceous minerals and the tendency for the andalusite prisms to stand at high angles to the walls indicate that the pegmatite did not flow into place as a mixture of crystals and liquid unless it has been recrystallized. Can the pegmatite have crystallized in situ from a magma that was injected in a completely molten state? If so how can one account for the presence of corundum in the crystalline product of such a silica-rich melt?

Table 2. Estimated Mineral Composition of a Typical Pelitic Hornfels (volume per cent)

Potash feldspar	40
Andalusite	25
Cordierite	15
Biotite	6
Quartz	5
Opaque ore	4
Muscovite	2
Sillimanite	2
Accessories (rutile, monazite, apatite)	1

If it is assumed that the corundum and andalusite were both present before the muscovite crystallized then the corundum-andalusite assemblage has several features suggestive of an exsolution origin (Schwartz 1942, p. 363–364):

a. The corundum occurs as small individual crystals scattered throughout the andalusite.

b. It is restricted to the andalusite, and all andalusite crystals contain corundum.

c. The amount of corundum is small, only varying within narrow limits.

d. The chemical composition of the host is similar to that of its inclusions; the two are not incompatible.

But the corundum crystals show no preferred orientation and they are not equally distributed. Only where the muscovite replacement of the andalusite is uniform is the corundum uniformly distributed. Further-more the corundum is always separated from the andalusite by muscovite; the corundum crystals, in other words, are actually enclosed in muscovite that replaces the andalusite. However, the corundum shows no signs of replacement by muscovite, instead it is partly replaced by diaspore. An exsolution origin for the corundum and andalusite therefore seems improbable. More likely the corundum was formed contemporaneously with the muscovite.

Andalusite has a very low silica content (36.8%) even though it can exist in equilibrium with quartz. Consequently, conversion of andalusite to muscovite (silica 45.6%) requires not only addition of potash and water but also silica. Complete conversion to muscovite is possible only if considerable silica is available:

$$3Al_2SiO_5 + 2H_2O + K_2O + 3SiO_2 \rightarrow 2KAl_3Si_3O_{10}(OH)_2$$

andalusite+water+potash+silica→muscovite

If andalusite reacts with water and potash to form muscovite without introduction of silica, then considerable alumina will be left over which may crystallize as corundum or, if it reacts with water, as diaspore.

$$6(Al_2SiO_5) + 2H_2O + K_2O \rightarrow 2KAl_3Si_3O_{10}(OH)_2 + 3Al_2O_3$$

andalusite+water+potash→ muscovite +alumina

It seems probable, therefore, that the corundum and diaspore formed as by-products of the conversion of andalusite to muscovite in a silica-deficient environment. These reactions must have occurred after the initial crystallization of the pegmatite and under conditions such that silica from the pegmatite was unable to migrate to the interior of the andalusite crystals to participate in the process.

The occurrence and distribution of the tourmaline are rather difficult to explain. The manner in which isolated crystals penetrate all of the other major minerals—individual tourmaline prisms often extending through two or more other mineral grains—suggests that they are of replacement origin. Moreover, the erratic concentration of the tourmaline suggests that the requisite boron was introduced along structurally controlled permeability channels. If so, then tourmalinization must have occurred after the pegmatites had largely or completely crystallized.

The fabric of the pegmatites indicates that the andalusite crystals formed in place and did not flow into position as crystals suspended in a fluid medium. Their concentration in the marginal zones and the way they tend to stand at high angles to the pegmatite walls is reminiscent of reaction structures often seen in volcanic rocks, e.g. rims of fibrous pyroxene on the margins of quartzite xenoliths in olivine basalt. Although the compositional difference between a typical pelitic hornfels and a granite is not as striking as that between quartzite and olivine basalt, the contrast is enough to cause significant concentration and temperature gradients to form between the hornfels and a granitic magma. The melting point of a pelitic hornfels is probably considerably higher than that of granite, as the composition of the average pelitic rock is similar to that of quartz diorite (Nockolds 1954, p. 1019; Shaw 1956, p. 928). Consequently if a granitic magma is injected into pelitic hornfels the two will tend to react without appreciable melting of the hornfels, unless of course, the magma is superheated, which is improbable. If melting did occur it would probably be restricted to differential melting along quartz-potash feldspar boundaries immediately adjacent to the granite contact where the temperature of the hornfels was a maximum. Thus, the composition, fabric, and geometry of the pegmatites and their wall rocks all seem to indicate that the pegmatites were formed both by injection of granitic magma and by reaction with and partial replacement of the wall rocks.

AGE OF PEGMATITES

Biotite collected from the central pegmatite was determined to be 88.2 million years old by the potash-argon method by J. Lipson, J. E. Evernden, and G. Curtis.* This value is only slightly less than that obtained for biotite from the Sentinel granodiorite but considerably greater than the value for the Mt. Hoffmann quartz monzonite and other nearby granitic rocks. Therefore the andalusite pegmatites are genetically related to the Sentinel granodiorite rather than to the nearby Mt. Hoffmann quartz monzonite. The effect of the latter and other nearby granitic rocks on the minerals of the pegmatite is apparently negligible as the potash-argon balance of the biotite was apparently not disturbed after emplacement of the Sentinel granodiorite.

CONCLUSIONS

A pegmatitic magma was injected into the *ac* joints of pelitic hornfelses, partially replacing them by reaction. Large andalusite crystals that formed in the reaction zone were partially replaced by mixtures of muscovite, corundum, and diaspore, the corundum and diaspore forming only in the interior of the andalusite crystals where the supply of silica was insufficient to convert all of the alumina to a silicate. Late in the history of the pegmatites, the feldspars were partly replaced by muscovite and many minerals were locally replaced by tourmaline.

Potash-argon dating of the pegmatitic biotite indicates that the andalusite pegmatites were emplaced about the same time as the Sentinel granodiorite.

---

* Personal communication, J. E. Evernden.

ACKNOWLEDGMENTS

The present study was carried out at the University of California, Berkeley, as part of an investigation of the igneous and metamorphic rocks of the May Lake area. The writer wishes to express his appreciation to the University for financial assistance during the field work, and to Dr. F. J. Turner, Dr. Adolf Pabst, and Dr. C. M. Gilbert for assistance in the field and laboratory work. The writer is also grateful to Dr. Howel Williams and Dr. A. Pabst for critical reading of the manuscript.

BIBLIOGRAPHY

CALKINS, F. C. (1930), The granitic rocks of the Yosemite region, *in* Matthes, F. E., Geologic history of the Yosemite Valley, *U. S. Geol. Survey*, Prof. Paper **160.**

HINTZE, CARL (1897), *Handbuch der Mineralogie*, Vol. 2.

LACROIX, A. (1893), Mineralogie de la France et de ses Colonies, **1,** 32–33.

MACDONALD, G. A. AND MERRIAM, RICHARD (1938), Andalusite in pegmatite from Fresno County, California. *Am. Mineral.*, **23,** 588–594.

MACKENZIE, W. S. AND SMITH, J. V. (1956), The alkali feldspars, III, An optical and *x*-ray study of high-temperature feldspars, *Am. Mineral.*, **41,** 405–427.

MURDOCH, JOSEPH AND WEBB, ROBERT W. (1948), Minerals of California, California State Div. Mines, Bull. 136, San Francisco, California.

NOCKOLDS, S. R. (1954), Average chemical composition of some igneous rocks, *Bull. Geol. Soc. Amer.*, **65,** 1007–1032.

SCHWARTZ, G. M. (1942), Progress in the study of ex-solution in ore minerals, *Econ. Geol.*, **37,** 345–364.

SHAW, D. M. (1956), Geochemistry of pelitic rocks, Part III: Major elements and general geochemistry, *Bull. Geol. Soc. Amer.*, **67,** 919–934.

TRÖGER, W. E. (1952), Tabellen zur optischen Bestimmung der gesteins-bildenden Minerale: E. Schwerzerbart'sche Verlagsbuchkandlung, Stuttgart.

TURNER, F. J. AND VERHOOGEN, JEAN (1951), Igneous and metamorphic petrology: McGraw-Hill Book Company.

Manuscript received December 11, 1956.

THE AMERICAN MINERALOGIST, VOL. 42, SEPTEMBER-OCTOBER 1957

PYRITE-URANINITE POLYCRYSTAL*

A. G. King, *U. S. Geological Survey, Washington, D. C.*†

Abstract

A texture was observed in a sample of ore in which pyrite and uraninite occurred as thin alternate layers paralleling crystal faces of a pyrite nucleus. This texture could be formed either by replacement or by syntaxis. Although syntactic growth forming polycrystals of two chemically dissimilar minerals has not been previously described, this explanation fits the observed data better than the explanation offered by replacement. It is proposed, therefore, that this occurrence is an example of a polycrystal of uraninite and pyrite and that the mechanism of formation is syntaxis.

INTRODUCTION

Growth-zoning phenomena in minerals are fairly common, and many authors have published descriptions of zoning in a wide variety of materials, including pyrite. The zoning has been shown by a color change between successive layers due to compositional differences or by symmetrically arranged inclusions.

A third type of growth zoning—two-phase zoning—is described in the following pages. This zoning is observed in a sample, collected by Art Baker, Vulcan Silver and Lead Co., and submitted to the Geological Survey for analysis by the U. S. Atomic Energy Commission. The sample is a highly mineralized siliceous boulder which was found in a stream bed about 4 miles ENE of Marshall Pass, Saguache County, Colorado. The rock contains pyrite, uraninite, quartz, and sphalerite(?) as primary minerals; and hematite, limonitic material, secondary uranium minerals, and quartz as alteration products and later introductions. An estimated 80 per cent of the pyrite in the sample does not show zoning. Of the remaining 20 per cent, about 19 per cent is single-phase zoned and 1 per cent two-phase zoned. The zoned pyrite occurs only in certain areas of the sample studied. The occurrence and distribution of the three types of pyrite suggest that there were at least two, and possibly three, different introductions of pyrite. As the three types of pyrite are spatially separated in the sections studied, it was not possible to establish the paragenesis.

Most of the uraninite is present in ring-shaped botryoidal textures surrounded and partly replaced by secondary uranium minerals and quartz (Fig. 1). Some uraninite occurs as small irregular blebs dispersed in the gangue and as an irregular peripheral replacement of pyrite.

This short study is an outgrowth of a program conducted by the U. S.

---

* Publication authorized by the Director, U. S. Geological Survey.

† Present address: 2-B Boyd St., Worcester, Mass.

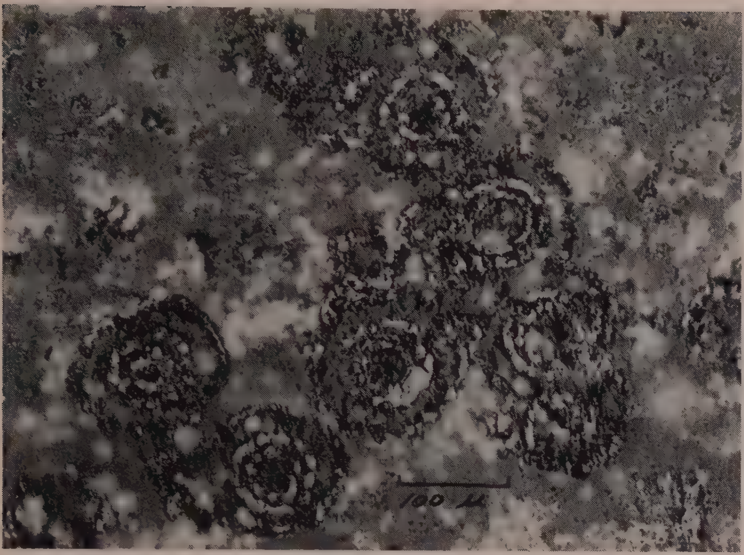

FIG. 1. Uraninite ring texture.

Geological Survey on behalf of the Division of Raw Materials of the U. S. Atomic Energy Commission.

SINGLE-PHASE ZONING

This type of zoning in the pyrite appears as layers that are visible in polished sections owing to relatively slight differences in color. The colors range from light brassy yellow to a pale pinkish lavender. In a few crystals the dark-colored layers are a light gray-lavender.

The two large crystals (Fig. 2) measure about 50 microns in diameter, with the dark zones being from 2 to 3 microns thick. The dark banding is not uniform in color across the width of a layer but contains subtle variations in shading. The color at any one layer is probably related to composition, darker colors indicating greater amounts of atoms other than iron and sulfur.

The maximum color contrast between these layers and normal pyrite is shown in the large central crystal of Fig. 2. Various authors have published descriptions of similar material (Edwards, 1954; Ramdohr, 1950), and this occurrence is not considered unique. It is included as evidence that this single-phase growth zoning seems to be a separate phenomenon from the two-phase zoning described in the following pages.

The presence of a compositional difference might affect the pyrite unit-cell dimension. A few pyrite grains were handpicked from the sample and were analyzed by *x*-ray diffraction—using powder technique and

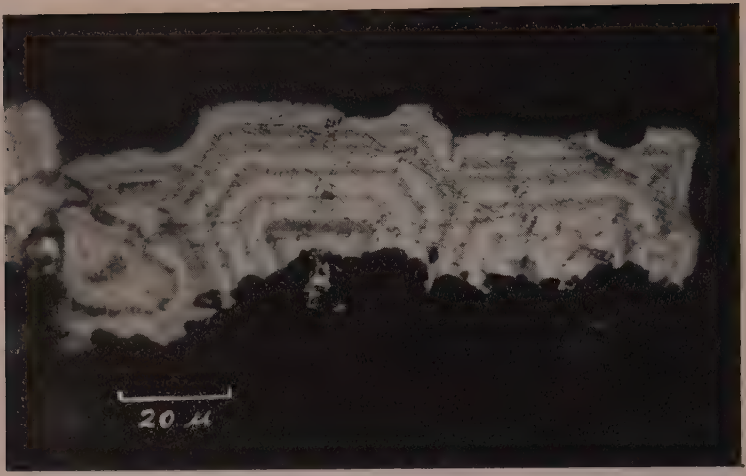

FIG. 2. Single-phase zoning in pyrite.

manganese-filtered iron radiation. It was not possible to determine whether the grains analyzed were the zoned crystals or the more common unzoned pyrite. The small size of the pyrite crystals precluded separation of the three types of pyrite for more detailed investigation. The resultant diffraction pattern matched our pyrite standard except that the lattice was slightly expanded. The unit-cell dimensions were calculated by the method of Bradley and Jay (1932).

The pyrite has a unit-cell dimension of 5.4275±0.001 Å. Normally pyrite has a unit-cell dimension of 5.405 Å (Palache *et al.*, 1946).

An attempt was made to separate a pure pyrite fraction for analysis, to determine the amount and kind of trace elements present. A pulp was separated by heavy liquids (methylene iodide) and then by differential chemical leaching (20 per cent H_2SO_4 on a steam bath for two hours). No pyrite was recovered.

TWO-PHASE ZONING

A few of the pyrite crystals have zoning that seems to be different from the color zoning described in the preceding pages (Fig. 3). The dark zones are thinner, with sharper edges, and are composed of a material that in polished section is dark gray. The color contrast between this type of zone and the pyrite is much greater than that between the most intense individual color zones noted in pyrite (Fig. 2). In the polished surfaces studied no crystal was found to exhibit both types of zoning, and it is assumed that they occur independently of each other. The interfaces between some of these zones and the pyrite have a small amount of relief.

This was interpreted as evidence for a slight difference of hardness between the pyrite and the gray zones.

A thinned polished section of this material was coated with a nuclear track emulsion (nuclear track emulsion in gel form, type C.2, Ilford Ltd., London), and a six-day exposure was made. The resultant alpha-track pattern in the emulsion indicated that these zoned crystals are radioactive. A camera-lucida tracing was made of a zoned crystal and its alpha-track pattern (Fig. 4). The lines within the crystal and paralleling the faces show the position of the dark-gray zones. Because of the necessary magnification and the presence of an emulsion, it was not possible to draw the dark zones with their true width. The center of each zone is indicated by the lines. The dark zones in this particular sample are from about 0.25 to 0.5 micron in width. The large circles at one end of the projected alpha-tracks indicate the point of emergence of the alpha particle from the polished surface.

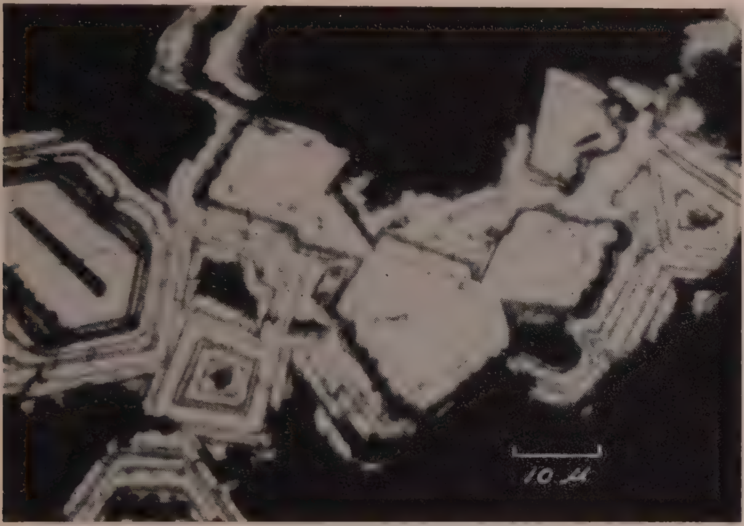

Fig. 3. Two-phase zoning in pyrite.

Only those tracks were plotted that either showed both ends or whose ends could be inferred. More than half of the tracks shown are actual plots. The points of origin of the remaining tracks were inferred by extending the trajectory of the tracks to the polished surface as the microscope focus was lowered. At this magnification the inferred origin of the track is within about 0.5 micron of its true position. This particular nuclear track emulsion is in direct contact with the polished surface, whereas with stripping films it is separated by a cellulose ester backing. The projection in these circumstances does not have as great an error in the contact emulsion as it does in stripping film. Alpha-tracks can be seen to originate from the dark-gray zones, showing that the zones are radioactive. Considering the width of the zones in this crystal, the length of exposure, and the fact that more than half of the tracks could not be plotted, the zones are at least moderately radioactive.

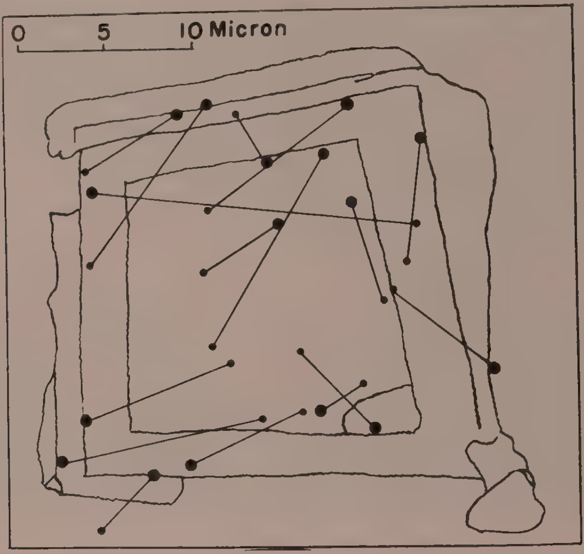

FIG. 4. Zoned pyrite crystal with alpha tracks.

The mineral that comprises the dark-colored zones in the pyrite crystals is tentatively identified as uraninite. It is radioactive, has the color of uraninite in polished section, and is slightly softer than the pyrite. Most of the evidence is indirect, and there is some possibility of error. Because of the extremely small size of these crystals and structural similarities between uraninite and pyrite, more direct methods of identification failed.

If we assume that this identification is correct, a very interesting hypothesis can be derived concerning the origin of this zoning.

The zoning in the color bands is rather obviously a crystal growth phenomenon. The composition, temperature, or pressure of the ore solution was rhythmically fluctuating as these crystals were deposited. One zoned pyrite crystals shows what may be a systematic offset of the crystallographic directions as the deposition progressed (Fig. 5).

The rest of the zoning is much more regular, and the axes of the seed crystal are faithfully paralleled in subsequent layers.

One possible explanation of the zoning between pyrite and uraninite (?) is replacement. Compositional differences between color zones in pyrite might have permitted selective replacement by uraninite. A significant difference in solubility would be expected and might be magnified by galvanic action.

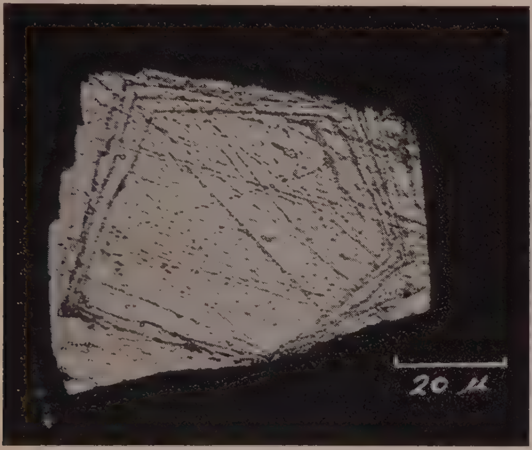

FIG. 5. Zoned pyrite crystal with systematic angular offset.

This explanation has a number of shortcomings. It is doubtful that a replacement of this sort would be so highly selective as to produce the sharp contacts between zones that are present. Few veinlets are seen connecting successive zones that would permit an exchange of material (Fig. 3). No gradation is present between color zoning and two-phase zoning; either one or the other is present in a single crystal, but not both. There is also a difference in size of the two types of zoned pyrite crystals, the color-zoned crystals being larger by a factor of at least two and more usually about four. The dark zones in the single-phase crystals are about 2 to 3 microns in width, whereas the dark zones in the two-phase crystals are 0.25 to 0.5 micron in width. The variation in size and width of zoning suggests that these two types of crystals formed under different conditions and possibly at different times. If replacement processes produced the two-phase zoning, we would expect the interfaces to be more irregular, more interconnecting veinlets to be present, the two types of crystals to have the same size distribution, and at least a few crystals with the zones partly replaced by uraninite(?). As such is not the case, this explanation was questioned.

An alternate explanation is offered. The literature cites numerous examples of crystals (Buckley, 1951), both natural and artificial, that are composed of one mineral containing oriented inclusions of another. A growing crystal face attracts atoms or structural fragments from the solution in which the crystal is growing. As these forces originate from atoms arranged in a lattice, the bounding forces also extend into the solution as an orderly array. An atom or structural fragment that is attracted to the crystal will, under ideal conditions, position itself so as best to satisfy the magnitude, "sign," and arrangement of these forces. This can result in the inclusion growing crystallographically oriented with respect to the host.

By careful control of crystal-growth conditions it might be possible to form a continuous shell of the inclusion mineral, which could completely encase the host mineral.

The term polycrystal was coined by G. Donnay (1953) to describe the syntaxic intergrowth of two distinct species. These polycrystals have been reported (G. Donnay and J. D. H. Donnay, 1953) forming from the species bastnaesite, $CeFCO_3$; parisite, $2CeFCO_3 \cdot CaCO_3$; roentgenite, $3CeFCO_3 \cdot 2CaCO_3$; and synchisite, $CeFCO_3 \cdot CaCO_3$. If growth conditions reversed rhythmically so as to favor alternate deposition of the host and inclusion, it would be possible to build up parallel shells of the two minerals. This would not be likely to occur if the two minerals were of dissimilar structures. We are concerned here with uraninite (?) and pyrite. Both minerals are isometric. Uraninite has a variable unit-cell dimension of about 5.47 Å. The unit-cell dimension of the pyrite in this sample measured 5.4275±0.001 Å. Uraninite is face-centered hexoctahedral. Pyrite is diploidal and is based on a *P* lattice. However, the iron atoms occur in face-centered positions. The sulfur atoms are arranged in dumbbell-shaped pairs in the lattice and thus lower the symmetry displayed by the iron atoms alone. When these two unit cells are fitted together, the uranium and iron match atom to atom and the continuity of the face-centered lattice is preserved through both minerals. The sulfur atoms fit (or partly fit) in the depressions in the uraninite cell face between uranium atoms. Because of the structural similarities between these two minerals, it may be possible for them to fit together in this manner.

The large central zoned crystal in Fig. 6 started as euhedral pyrite. When the nature of the ore fluid or physical environment changed to favor the deposition of uraninite (?), a thin layer of this mineral was deposited on the surface of the crystal. If this layer were not crystallographically oriented with the pyrite, the next and successive layers of pyrite could not have nucleated with the same orientation as the first. If this is the case, then this occurrence is an example of a polycrystal between two compounds, very dissimilar chemically.

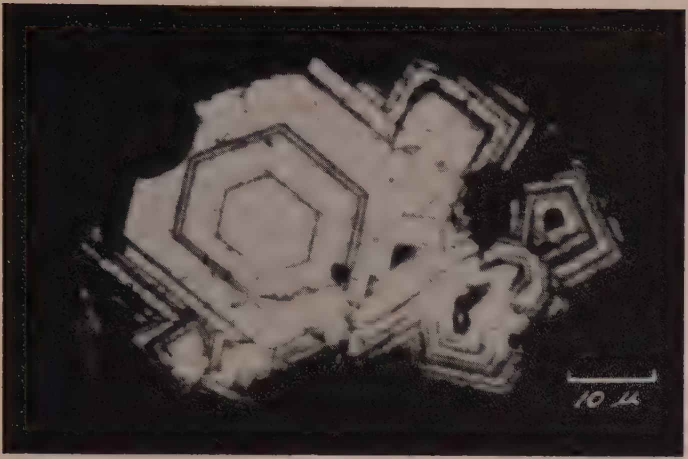

FIG. 6. Two-phase zoning in pyrite.

A similar type of zoning as that described here has been found on the Colorado Plateau in the Mi Vida mine (A. D. Weeks, written communication) and the Happy Jack mine (A. F. Trites, Jr., written communication).

SUMMARY

The concept of polycrystals offers an alternate explanation to certain ore textures that in the past have been attributed to replacement processes. It may be possible to explain these textures more satisfactorily by crystal-growth phenomena, the explanation in certain instances being simpler and more direct than that offered by replacement.

The evidence presented here is largely inferential. Many of the uncertainties can be more satisfactorily answered when larger crystals exhibiting the same textures are found. Such materials could be analyzed by precession photographs, and if the two phases have the same crystallographic orientation, this evidence would be considered definitive.

The development of polycrystals may offer a satisfactory explanation of this two-phase zoning. In the material studied, this process is thought to offer a better explanation of the textures observed than a process involving replacement.

REFERENCES

BRADLEY, A. J., AND JAY, A. H. (1932), A method for deducing accurate values of the lattice spacing from *x*-ray powder photographs taken by the Debye-Scherrer method: *Phys. Soc. Proc.*, **44**.

BUCKLEY, H. E. (1951), Crystal growth, New York, John Wiley and Sons.

DONNAY, GABRIELLE (1953), The "polycrystal," a product of syntaxic intergrowth (abstract): Am. Crystallographic Assoc. meeting, Ann Arbor, Michigan, June 22–26, 1953.

DONNAY, GABRIELLE, AND DONNAY, J. D. H. (1953), The crystallography of bastnaesite, parisite, roentgenite, and synchisite: *Am. Mineral.*, **38**, 932–963.

EDWARDS, A. B. (1954), Textures of the ore minerals and their significance, 2d ed., Melbourne, Australasian Inst. Mining Met.

PALACHE, C., BERMAN, H., AND FRONDEL, C. (1946), Dana's system of mineralogy, 7th ed., New York, John Wiley and Sons.

RAMDOHR, PAUL (1950), Die Erzmineralien und ihre Verwachsungen, Berlin, Akad. Verlag, 826 p.

Manuscript received March 16, 1957.

THE AMERICAN MINERALOGIST, VOL. 42, SEPTEMBER–OCTOBER 1957

UMOHOITE FROM THE LUCKY MC MINE, WYOMING*

ROBERT G. COLEMAN AND DANIEL E. APPLEMAN, *U. S. Geological Survey, Washington 25, D. C.*

ABSTRACT

A new occurrence of the hydrous uranium-molybdenum mineral umohoite is described from the Lucky Mc mine, Wyoming. *X*-ray investigation shows that umohoite is monoclinic, $P2_1(C_2^2)$ or $P2_1/m(C_{2h}^2)$, $a=14.30$ Å, $b=7.50$ Å, $c=6.38$ Å, $\beta=99°05'$. Optically umohoite is biaxial negative with α(calc.) 1.66 ± 0.01, $\beta 1.831\pm0.005$, and γ 1.915 ± 0.005, 2V (Na) $65°\pm2°$; pleochroism X dark blue, Y light blue, Z olive green; dispersion $r>v$, strong. The strongest lines of the *x*-ray powder pattern are 7.31–6.96 (broad) (100), 3.22 (50), 14.10 (25), and 3.18 (25). Indexed *x*-ray powder diffraction data are listed.

INTRODUCTION

The uranium deposits of the Gas Hills area in Fremont County, Wyoming, contain a complex suite of uranium minerals. More than twenty distinct species have been identified from this area. These deposits are localized in coarse arkosic sandstones and conglomerates of the upper part of the Wind River formation (Eocene). Mudstones and siltstones are also mineralized to a lesser extent.

The abundant molybdenum in these deposits has given rise to uranium molybdates in the early stages of oxidation. The unoxidized ore contains uraninite, coffinite, iron sulfides, and "jordisite" as an interstitial cement in the sediments. The fine-grained nature of these minerals and the high porosity of the sediments allow rapid oxidation by moist air above the water table. Umohoite, as described by Brophy and Kerr (1953), is present in limited amounts at the Lucky Mc mine where it crystallizes in the early stages of oxidation. The umohoite is commonly intergrown with gypsum in juxtaposition with iron sulfides and uranium oxides. At this stage of oxidation, secondary uranium minerals containing UO_2^{+2} have not yet formed; however, this stage must be transitory, as schoepite and uranophane may be found within several inches of the umohoite.

The umohoite forms delicate rosettes of tabular plates terminated by rather sharply angled points. These rosettes are rarely more than 2 mm. across and the individual crystals are all less than 0.5 mm. in their longest dimension. The unaltered crystals are splendent blue black or in some cases dark green. In the areas where the secondary uranyl minerals have begun to form the umohoite is seen to alter to an undefined yellow uranium molybdate.

---

* Publication authorized by the Director, U. S. Geological Survey.

UNIT CELL AND SPACE GROUP

X-ray examination of the crystalline umohoite described above reveals that most of the material is not suitable for single-crystal studies. The typical "crystal" of umohoite is composed of many extremely thin, platy individuals stacked in disordered aggregates. Efforts to separate the plates cause bending, cleaving, and fracturing of the fragile crystals. Fairly good precession photographs were obtained with MoKα radiation from a small specimen, with approximate dimensions $97\times85\times2\ \mu$, comprising only two or three individual plates.

Umohoite is monoclinic, with space group $P2_1$ (C_2^2) or $P2_1/m$ (C_{2h}^2). The cell dimensions of the crystals studied are:

$$a=14.30\pm0.05\ \text{Å}$$
$$b=\ 7.50\pm0.03$$
$$c=\ 6.38\pm0.03$$
$$\beta=99°05'\pm10'$$

There is a prominent pseudo-rhombohedral multiple cell; the *c*-axis of the pseudo-*R* cell is parallel to a^* of the monoclinic cell and has a spacing of 42.36 Å.

OPTICAL PROPERTIES

Umohoite is biaxial (−), with the following optical properties:

	n	*Pleochroism*
α (calc.)	$1.66\ \pm0.01$	dark blue
β	1.831 ± 0.005	light blue
γ	1.915 ± 0.005	olive green

2V (Na) = 65° ± 2°; dispersion $r>v$, strong, Different plates show inclined or symmetrical extinction, depending on the face development; in a few cases (010) is present. The optic orientation is:

$$\mathrm{X}\approx a^*(X\wedge a\approx 9°05')$$
$$\mathrm{Y}=b$$
$$\mathrm{Z}\approx c$$

CHEMICAL FORMULA

Brophy and Kerr (1953) give the tentative chemical formula of umohoite as $UO_2MoO_4H_2O$, and the observed specific gravity as 4.55 to 4.66. If this formula is correct, the cell contains $4[UO_2MoO_4\cdot 4H_2O]$ and the calculated specific gravity is 4.93. An analysis of the Lucky Mc material by *x*-ray fluorescence spectroscopy, made by I. Adler of the U. S. Geological Survey, confirms the U:Mo ratio of 1:1. However, the following observations cast doubt on the formula as given: (1) umohoite occurs with partly oxidized ore at the Lucky Mc mine, at a stage at which typi-

TABLE 1. *X*-RAY POWDER DIFFRACTION DATA FOR UMOHOITE

CuKα radiation, $\lambda = 1.5418$ Å, camera diameter 114.59 mm.
Corrected for film shrinkage. Cutoff at 15 Å.

hkl	$d_{calc.}$ (Å)	$d_{obs.}$ (Å)	*I*
100	14.12	14.10	25
200	7.06	7.31–6.96b[1]	100
110	6.62		
001	6.30	6.31	9
$\bar{1}01$	6.12		
101	5.44	5.44	4
210	5.14		
$\bar{2}01$	5.12	5.11	2
011	4.82	4.82	4
$\bar{1}11$	4.74	4.74	18
300	4.71		
111	4.41	4.41	1
201	4.37		
$\bar{2}11$	4.23	4.23	2
$\bar{3}01$	4.09		
310	3.99	3.96	1
211	3.78		
020	3.75	3.74	4
120	3.62		
$\bar{3}11$	3.59		
400	3.53	3.54	9
301	3.52		
220	3.31	3.32	3
$\bar{4}01$	3.30		
021	3.22	3.22	50
$\bar{1}21$	3.20		
410	3.20		
$\bar{1}02$	3.18	3.18	25
311	3.18		
002	3.15		
121	3.09	3.10	12
$\bar{2}02$	3.06	3.06	3
$\bar{4}11$	3.03	3.03	18
$\bar{2}21$	3.02		
102	2.98	2.98	12
320	2.93	2.93	3
$\bar{1}12$	2.93		
012	2.90		
401	2.89	2.88	2
221	2.85		
$\bar{2}12$	2.84	2.85–2.83b[1]	18
$\bar{3}02$	2.83		
500	2.82		
112	2.77		
$\bar{3}21$	2.77	2.77	2
$\bar{5}01$	2.76		
202	2.72		
411	2.70		
$\bar{3}12$	2.65		
510	2.64	2.64	1
$\bar{5}11$	2.59		
420	2.57	2.57	6
321	2.56		
$\bar{4}02$	2.56		
212	2.56		
$\bar{4}21$	2.48	2.48	4
130	2.46		
302	2.45		
501	2.44		
$\bar{1}22$	2.43		
$\bar{4}12$	2.42	2.42	2
022	2.41		
$\bar{2}22$	2.37	2.37	1
230	2.36		
600	2.35		
122	2.33		
$\bar{6}01$	2.33	2.33	2
312	2.33		
031	2.32		
511	2.32		
$\bar{1}31$	2.31		
$\bar{5}02$	2.29		
421	2.29	2.28	1
131	2.27		
		2.10	1
		2.04	18
		1.97	4
		1.92	1
		1.88	9
		1.85	6
		1.82	3
		1.79	6
		1.72	1
		1.66	2
		1.64	2
		1.62	6
		1.59	2
		1.57	1
		1.55	2
		1.54	2
		1.23	2

---

[1] b=broad.

cal secondary uranium minerals have not yet formed; (2) umohoite has a dark bluish color, whereas uranyl or molybdate compounds are characteristically brightly colored; (3) umohoite alters in the totally oxidized part of the ore to a yellow uranyl molybdate similar to synthetic uranyl molybdates. It therefore seems probable that the uranium or the molybdenum or both in umohoite are in an oxidation state lower than hexavalent.

X-RAY POWDER DIFFRACTION DATA

Umohoite has a variable lattice spacing normal to the perfect cleavage, as noted by Brophy and Kerr. If the mineral is prepared for *x*-ray powder photography by the usual grinding technique, the cell dimensions are altered, possibly due to a change in water content. In addition, the stacking of the layers in the structure is apparently disrupted, causing the virtual disappearance of the (*h*00) reflections. To overcome this difficulty F. A. Hildebrand of the U. S. Geological Survey prepared a sample of umohoite by fine chopping, rather than grinding; this process left the crystallographic characteristics of the mineral relatively unaltered. The powder-diffraction data listed in Table 1 are corrected for film shrinkage and are indexed on the basis of the single-crystal measurements. The following lines could not be indexed on the umohoite cell:

I	$d_{obs.}$ (Å)
1	8.24
9	6.02
3	5.74
1	2.15
6	2.07

The authors express their thanks to H. T. Evans, Jr., U. S. Geological Survey, for helpful advice. This work is part of a program being conducted by the U. S. Geological Survey on behalf of the Division of Raw Materials of the U. S. Atomic Energy Commission.

REFERENCE

BROPHY, G. P., AND KERR, P. F. (1953), Hydrous uranium molybdate in Marysvale ore: Annual Report for June 30, 1952 to April 1, 1953, U. S. Atomic Energy Comm. RME-3046, p. 26–44, issued by the U. S. Atomic Energy Comm. Tech. Inf. Service Extension, Oak Ridge, Tenn.

Manuscript received March 25, 1957.

THE AMERICAN MINERALOGIST, VOL. 42, SEPTEMBER-OCTOBER 1957

NOTES AND NEWS

ALLUAUDITES AND VARULITES

D. Jerome Fisher, *University of Chicago, Chicago 37, Illinois.*

These minerals may be described chemically as phosphates of Na, Ca, Fe″, Fe‴, and Mn. The ideal formula may be taken as W_{0-12} $(X+Y)_{12}$ $(PO_4)_{12}$, where W = Na, Ca; X = Mn″, Fe″; and Y = Fe‴; although if both W and X are zero, we would be dealing with heterosite, a mineral outside of this system. No success has been obtained in attempting to write a formula showing a simple coupling arrangement involving Ca-X and Na-Y. Thus the varulites are high in Na and low in Fe‴. Nevertheless it seems clear that these minerals are all members of one monoclinic isotypous series which has space group $I2_1/a$ with unit cell $a_0 = 11.0$, $b_0 = 12.5$, $c_0 = 6.5$ Å and $\beta = 97\frac{3}{4}°$ (Fisher, 1956). *X*-ray powder diffraction patterns are closely similar; differences are presumably explicable on the basis of the widely varying chemical composition. Except for the presence of Fe_2O_3 (which is as low as 5.3% in the varulites) these minerals are chemically very close to the dickinsonites (Fisher, 1954; 1955*a*); the latter however are readily differentiated optically or by *x*-ray photographs. The space group is $C2/c$ with $a_0 = 16.6$, $b_0 = 10.0$, $c_0 = 24.8$ and $\beta = 105°41'$. They invert to alluaudite on heating for a day in air at about 500° C. With the exception of hühnerkobelite, all known alluaudites (and varulites) are much richer in Na than Ca. It is thus suggested that the alluaudites be regarded as Na, Fe″, Fe‴, Mn phosphates with generally minor Ca. The end members may be referred to as mangano-alluaudite, ferri-alluaudite, and ferro-alluaudite. FeO was not reported in the analysis of the type alluaudite (Chanteloube); it is relatively low in all minerals heretofore classified as alluaudite. On this basis the known alluaudites could be grouped as shown in the table.

The numbers of the samples in the table correspond to those of Fig. 1, where the composition is shown in weight percentages with the sum of Fe″, Fe‴ and Mn recalculated as 100% (it is assumed that the Chanteloube and Buranga minerals lack FeO, though this oxide was not reported in these analyses nor in one of the Varuträsk analyses (7, Fig. 1)). The index of refraction (α) values used in plotting the isopleths in the figure are all taken from the literature except for the Chanteloube material which has $\alpha = 1.764$, $\beta = 1.779$, and 2V near 90°. The birefringence increases fairly regularly from 0.013 in the varulites to 0.060 in the Buranga alluaudite, though the low value (0.012) for the Sukula specimen seems out of line.

Mason (quoted in Quensel, pp. 46–51) considers that varulite is an alteration product of lithiophilite [but note that this involves replacement of Li by (Na, Ca); also oxidation of part of the iron] and that it in

NOMENCLATURE OF THE ALLUAUDITES

Ferroan-alluaudites	Manganoan-alluaudites	Ferrian-alluaudites
Norrö 1	Hagendorf	
	Hagendorfite 2	Buranga 10
	Varulites	
	Skrumpetorp 3	Black Hills 11
	Varuträsk 4, 5	Hühnerkobel
	Lemnäs 6	Hühnerkobelite* 12
	Varuträsk 7	
	Chanteloube 8	
	Sukula 9	

* Hühnerobelite could be designated as a calcian ferrian-alluaudite when it is important to be precise.

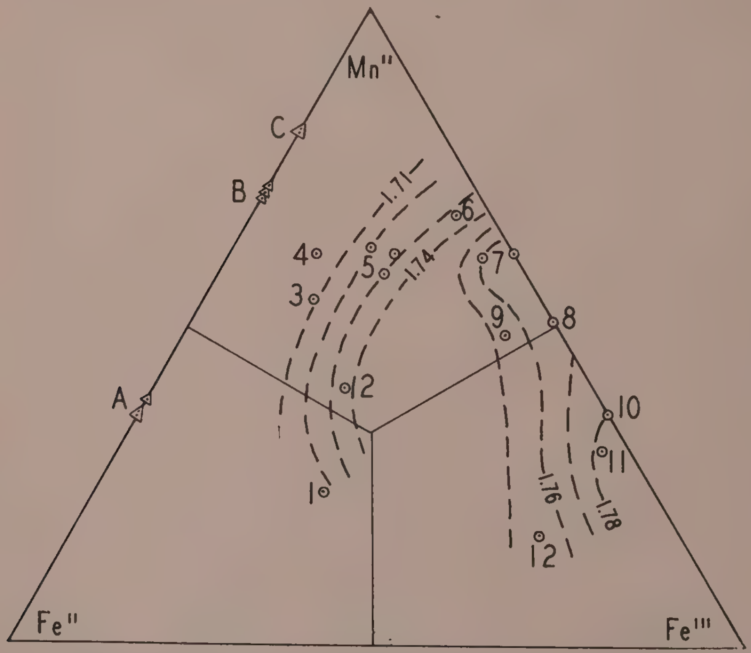

FIG. 1. Alluaudites and varulites plotted according to weight percentages of the three cations (numbered points in circles; see the table). The points in triangles represent ferrodickinsonites (A), mangano-dickinsonites (B), and fillowite (C). The isopleths show index of refraction (α) values.

turn may alter to alluaudite. "One thin section shows lithiophilite in contact with yellow-brown alluaudite, the latter mineral containing small grains of green varulite." Mason notes that the green varulite "is structurally similar to alluaudite (judging from x-ray powder photographs, measurements of which he gives), but is distinct in its . . . physical properties and in the presence of most of the iron in the bivalent state." The last phrase of Mason's statement that "the alteration of varulite to alluaudite involved the oxidation of the iron from the ferrous to the ferric state, with the concomitant removal of some sodium ions from the lattice to maintain electrical neutrality" is not borne out by the analyses presented, unless one assumes atomic sodium is present in alluaudite. The fact that dickinsonite is readily oxidized to alluaudite on heating in air for a day at about 500° also belies this concept.

If the investigators of the Varuträsk pegmatite have made no mistakes in their thin-section identification of the phosphate minerals, it is not readily apparent why varulite and alluaudite (their terminology) appear as separate physical entities if they are actually members of an isotypous series. Nevertheless it is not inconceivable that oxidation of the varulite would not go ahead uniformly through the specimen, but it might proceed by "leaps and bounds"; i.e., at certain places the material be more susceptible to oxidation than at others.

The remarks in this note are preliminary; detailed optical, chemical, thermal, and x-ray studies are in progress on all these minerals.

Appendix. In working out the unit cell of hagendorfite, I found that both it and alluaudite could be described using space group 15—C^6_{2h} in the orientation $I\ 2_1/a$ with a β-angle of $97\frac{3}{4}$°. This has advantages over the orientation $C\ 2/c$ of this same space group with β of 114°22′ used in my 1955*b* paper. This was noted on p. 1101 of this paper (where the transformation formula appears) but it was stated that the less-oblique orientation resulted in "systematic absent spectra which do not fit space group criteria." This statement is erroneous. Fig. 2 on p. 1104 in the preferred $I\ 2_1/a$ orientation should be labelled "sketch of (001) cleavage flake of alluaudite" and the face-trace on the right is 100 (instead of $\bar{1}00$); the indices of the face-traces on the top and bottom and on the left are correct if all signs are reversed. In short this change in orientation merely involves a change in the choice of the a-axis direction.

REFERENCES

All needed references are in vol. 2 of Dana's *System* (1951, pp. 669, 674 and 717) except as follows:

FISHER, D. J. (1954), Arrojadite is a ferro-dickinsonite: *Am. Mineral.*, **39**, 676–680.

———, (1955*a*), Soda Fe-Mn pegmatite phosphates, *Science*, **121**, 312.

———, (1955*b*), Alluaudite. *Am. Mineral.*, **40**, 1100–1109.

———, (1956), Hagendorfite unit cell: *Bull. Geol. Soc. Amer.*, **67**, 1694–1695 (abstract).

Quensel, P. (1956), The paragenesis of the Varuträsk pegmatite: *Arkiv för Mineralogi och Geologi*, **2**, no. 2, 125 pp.

Strunz, H. (1954), Hagendorfit, ein neues Mineral der Varulith-Hühnerkobelit-Reihe: *Neues Jahrb. Mineral.*, Monatshefte, 252–255.

THE AMERICAN MINERALOGIST, VOL. 42, SEPTEMBER–OCTOBER 1957

LATTICE CONSTANTS FROM WEISSENBERG PATTERNS

A. Pabst, *University of California, Berkeley.*

In a recent article Christ (1956) has called attention to the possibility of correcting for film shrinkage and related errors in the measurements from Weissenberg patterns by recording the powder pattern of a standard substance on the same film. This provides a scale of standard angular distances on the film. Christ discussed the procedures for calibration at length and claimed "that a precision of about 2 to 4 parts in 10,000 may be easily obtained." To record the powder pattern over but a limited strip of the film a "slotted brass cylinder" was added to the usual rotation shield. Judging from the appearance of the powder pattern shown at the left of Christ's Fig. 1, the width of the slot must have been just over one centimeter. Christ (p. 571) stated that "whenever possible spots measured on the Weissenberg part of the film were taken close to the calibration pattern."

A few years ago the writer (Pabst, 1951, footnote on p. 557) mentioned the use of a *c*-axis zero layer for calibration. Since then it has been regular practice in single crystal work in the Geology Department at Berkeley to use zero-layer strips of quartz *c*-axis rotation patterns recorded at each edge of the zero-layer Weissenberg patterns for calibration. Figure 1 shows a Weissenberg pattern calibrated in this manner. The calibration strips are recorded at each edge by insertion of the Weissenberg screen, whose slot width is 0.2 cm., and proper placing of the cassette. Ordinarily an exposure of one hour for each strip will suffice with copper radiation. The general procedure to be followed is that described by Christ and it yields about the precision that he claims.

For the method here reported one must have a suitable reference crystal perfectly oriented on the goniometer head before being placed on the Weissenberg apparatus so that no *x*-ray adjustment is needed. The writer has used very slim needles of quartz. That used for the pattern shown in Fig. 1 was just under 0.04 mm. in thickness and had been oriented on a Stoe two-circle goniometer fitted with adapter to accommodate the goniom eter head of the Weissenberg apparatus. It is convenient, if the operation is to be carried out at frequent intervals and a goniometer head can be spared for the purpose, to keep a standard crystal mounted and adjusted ready for use. The crystal under investigation in the film shown on Fig. 1, a mesolite from Kings Valley quarry, Benton County, Oregon, was also a slim needle. The α_1 and α_2 lines are well resolved for both the quartz and the mesolite in the outer part of the film.

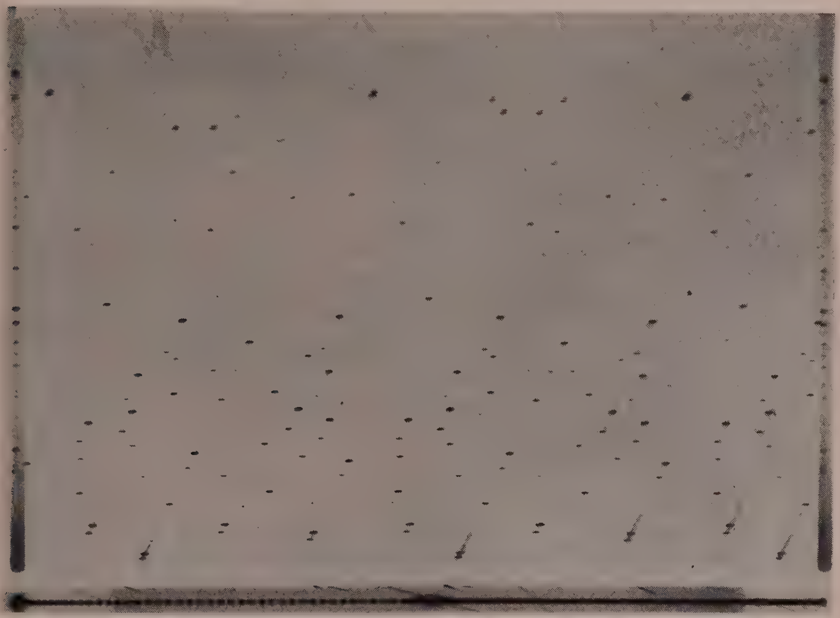

FIG. 1. One half of Weissenberg pattern calibrated with quartz *c*-axis layer strips at each side. Original overexposed to afford better reproduction.

Though a powder pattern offers a greater number of lines for calibration than does the zero layer of the same substance it turns out that the quartz *c*-axis zero layer furnishes a sufficient number of suitably spaced spots with most of the wave-lengths of *x*-rays commonly used. For copper radiation there are thirteen $hk\cdot 0$ lines from $10\cdot 0$ at $2\theta = 20.876°$ ($\alpha_{\text{unres.}}$) to $24\cdot 0$ at $2\theta = 147.602°$ (α_2) at 18° C. If β lines and the resolved α_1 and α_2 are considered, the calibration points are more numerous.

The method of calibration here reported has a number of advantages:

1. No modification of the standard Weissenberg apparatus is required.
2. No part of the Weissenberg pattern need be sacrificed to make room for the calibration pattern.
3. Any departure of the film from a cylindrical shape during exposure

is readily detected when the calibration strips are aligned on the usual measuring device. Since the cylindrical position of the film is supposed to be fixed when the film is fitted in the cassette in the dark room it will be subject to any small errors in trimming of film, folding of the protective black paper sheath or securing of the metal parts of the cassette.

4 If the two calibration strips have been found to indicate a satisfactory approach of the film to perfect cylindrical shape during exposure, measurements may be made with equal confidence on any part of the film and need not be confined to the region "close to the calibration pattern."

A limiting factor in any calibration method that involves the use of a standard substance is the constancy of the d values of that substance. The range of variation of cell dimensions cited for quartz by Frondel and Hurlbut (1955) is only of the order of 1/10,000. This is well within the limits of precision assigned to the method of calibrated Weissenberg patterns by Christ. Hence the arbitrary use of Wilson and Lipson's (1941) cell dimensions as a basis of 2θ values of quartz for calibration seems justified.

REFERENCES

Christ, C. L. (1956), Precision determination of lattice constants of single crystals using the conventional Weissenberg camera: *Am. Mineral.*, **41**, 569–580.

Frondel, C., and Hurlbut, C. S., Jr. (1955), Determination of the atomic weight of silicon by physical measurements on quartz: *Journ. Chem. Phys.*, **23**, 1215–1219.

Pabst, A. (1951), X-ray examination of uranothorite: *Am. Mineral.*, **36**, 557–562.

Wilson, A. J. C., and Lipson, H. (1941), The calibration of Debye-Scherrer x-ray powder cameras: *Proc. Phys. Soc.*, **53**, 245–250.

THE AMERICAN MINERALOGIST, VOL. 42, SEPTEMBER–OCTOBER 1957

SERPENTINES WITH 6-LAYER ORTHO-HEXAGONAL CELLS*

J. Zussman† and G. W. Brindley, *Department of Ceramic Technology, The Pennsylvania State University, University Park, Pennsylvania.*

A new variety of serpentine mineral from Unst, Shetland Isles, was described by Brindley and v. Knorring (1954). The most prominent lines of its powder pattern were indexed on the basis of an ortho-hexagonal cell with $a_0=5.322$ Å, $b_0=9.219$ Å, $c_0=14.53$ Å, but an additional series of eleven closely spaced weak lines following 020 could be associated with a superlattice parameter $S=43.8$ Å in either the x or z direction. The data then available were insufficient to distinguish between these alternatives. The former suggested an analogy with antigorite (Mikonui; $a_0=43.5$ Å, Aruja 1945) while the latter implied a large cell containing six serpentine layers. Some discussions of these alternatives occur elsewhere (Brindley and v. Knorring, *loc. cit.;* Zussman, 1956; Zussman, Brindley & Comer, 1957) but in the course of more recent studies on serpentine minerals new results have been obtained which throw light on the true nature of the serpentine from Unst.

---

* Contribution No. 56-38 from the College of Mineral Industries, The Pennsylvania State University.

† Present address: Department of Geology, Manchester University, Manchester 13, England.

Table 1 gives x-ray powder data obtained from a synthetic Mg-Ge serpentine, the preparation of which was described by Roy and Roy (1954), who kindly supplied us with the material; the first and second columns give reflection intensities and d values measured with a Norelco x-ray diffractometer. The pattern was first indexed using approximate cell dimensions and these were refined by least square solutions of two series of reflections, $20l$'s for a and c and $02l$'s for b and c. The orthohexagonal cell derived, $a_0=5.436$ Å, $b_0=9.415$ Å, $c_0=44.66$ Å $(=6 \times 7.443)$, gives good agreement between observed and calculated d values for a wide range of reflections (see Table 1, second and third columns).

The three last columns of Table 1 list corresponding powder data for the Unst serpentine as given by Brindley and v. Knorring (1954) but indexed for a 6-layer cell. Making allowance for differences in cell dimensions and intensities through substitution of Ge for Si, the similarity of the two patterns is evident. From the well-ordered Mg-Ge serpentine, however, an excellent pattern was obtained showing many strong lines of the 6-layer cell throughout its range.

Electron diffraction patterns were obtained from thin, platy single crystals of the Mg-Ge serpentine (Zussman, Brindley and Comer (1957); Fig. 7), which show a simple hexagonal array of spots with no evidence of a superlattice or "large cell" in the xy plane. This is in marked contrast to the patterns from antigorites in similar orientations (see Figures 4 and 5 in the above paper). The large parameter in the present case is c which is parallel to the electron beam and therefore is not indicated in the electron diffraction pattern.

Electron micrographs of the Unst serpentine show that it has a lath-like morphology. Electron diffraction patterns from single laths showed strong spots in positions similar to those of orthochrysotile which has cell dimensions $a_0=5.32$, $b_0=9.2$, $c_0=14.6$ Å, $\beta=90°$ (Whittaker and Zussman, 1956), and has a parallel to the fibre axis. (For illustrations see

TABLE 1. *X*-RAY POWDER DATA FOR 6-LAYER ORTHO-SERPENTINES

Synthetic Mg-Ge serpentine			Indices *hkl* for both structures	Serpentine (Unst), Brindley & Knorring (1954)		
I	*d*(obs.)	*d*(calc.)		*d*(obs.)	*d*(calc.)	*I*
58	7.46	7.44	006	7.33	7.265	10
30	4.695	4.707	020	4.597	4.610	6B
30	4.612	4.606	022			
57	4.484	4.488	023	4.403	4.393	1
18	4.340	4.338	024	4.250	4.245	1
13	4.167	4.165	025	4.088	4.075	1
30	3.981	3.979	026	3.903	3.892	½
12	3.792	3.788	027			
70	3.730	3.730	0, 0, 12	3.662	3.632	10
15	3.601	3.599	028	3.528	3.519	½
43	3.414	3.415	029	3.348	3.338	½
8	3.242	3.240	0, 2, 10	3.172	3.167	½
4	3.073	3.075	0, 2, 11	3.015	3.005	½
10	2.921	2.920	0, 2, 12	2.865	2.853	½
4	2.776	2.775	0, 2, 13	2.720	2.711	½
57	2.716	2.718	200			
25	2.673	2.674	203	2.623	2.618	3
5	2.644	2.641	0, 2, 14			
100	2.551	2.554	206	2.502	2.499	10
15	2.522	2.516	0, 2, 15	2.450	2.458	1
18	2.486	2.481	0, 0, 18	2.425	2.422	1
3	2.404	2.401	0, 2, 16			
17	2.386	2.384	209	2.335	2.332	7
2	2.327	2.325	043			
1	2.305	2.303	044			
1	2.291	2.294	0, 2, 17			
1	2.243	2.246	046			
50	2.196	2.195	2, 0, 12	2.149	2.147	6
2	2.168	2.169	048			
6	2.127	2.127	049			
1	2.103	2.103	0, 2, 19			
1	2.084	2.082	0, 4, 10			
3	2.034	2.036	0, 4, 11			
60	2.008	2.008	2, 0, 15	1.9629	1.9626	7
3	1.992	1.989	0, 4, 12			
9	1.941	1.938	0, 2, 21			
2	1.895	1.894	0, 4, 14			
13	1.863	1.861	0, 0, 24	1.8154	1.8162	½
3	1.847	1.847	0, 4, 15			
62	1.831	1.831	2, 0, 18	1.7905	1.7911	1
3	1.799	1.799	0, 4, 16			
½	1.794	1.795	0, 2, 23			
3	1.780	1.780	310	1.7392	1.7424	1B

TABLE 1—*Continued*

Synthetic Mg-Ge serpentine			Indices *hkl* for both structures	Serpentine (Unst), Brindley & Knorring (1954)		
I	*d*(obs.)	*d*(calc.)		*d*(obs.)	*d*(calc.)	*I*
5	1.774	1.774	312			
15	1.765	1.767	313			
4	1.758	1.757	314			
5	1.734	1.731	0, 2, 24			
2	1.695	1.695	318			
25	1.674	1.675	2, 0, 21	1.6360	1.6368	4
2	1.654	1.654	0, 0, 27			
1	1.618	1.620	0, 4, 20			
2	1.603	1.605	3, 1, 12			
7	1.580	1.580	3, 1, 13			
83	1.569	1.569	060	1.5354	1.5367	8
83	1.536	1.536	2, 0, 24	1.5013	1.5033	7
2	1.5011	1.5005	3, 1, 16			
7	1.4914	1.4885	0, 0, 30	1.4520	1.4530	¼
2	1.4629	1.4637	0, 2, 29			
40	1.4457	1.4459	0, 6, 12	1.4148	1.4152	2
2	1.4200	1.4188	3, 1, 19			
13	1.4144	1.4131	2, 0, 27	1.3793	1.3803	2
5	1.3662	1.3678	0, 6, 16			
7	1.3602	1.3591	400			
7	1.3550	1.3535	403	1.3271	1.3252	1
40	1.3362	1.3370	406	1.3092	1.3090	5
12	1.3264	1.3262	0, 6, 18	1.2958	1.2975	¼
			4, 0, 9	1.2832	1.2832	½
25	1.3076	1.3060	2, 0, 30	1.2759	1.2752	½
			0, 0, 36	1.2100	1.2108	1
				and six additional indexed reflections.		
Lattice parameters: $a_0=$ 5.436 Å $b_0=$ 9.415 Å $c_0=$44.66 Å				$a_0=$ 5.322 Å $b_0=$ 9.219 Å $c_0=$43.59 Å		

Since $b=\sqrt{3}a$, alternative indices can be assigned for equivalent planes of equal *d* values, but these are not listed.

Zussman, Brindley and Comer, 1957.) In these patterns, which are of a rotation type because the laths have components in all orientations about *a*, a few very weak spots were observed on the first layer line which could not be indexed with the above cell, but may belong to the $11l$ series of a cell having $c \simeq 43.8$ Å.

While studying the thermal transformation of serpentines to forsterite

(Brindley and Zussman, 1957) some x-ray fibre photographs were obtained from the blue columnar serpentine from Unst described by Brindley and v. Knorring (Specimen No. 3). This had given a powder pattern similar to that from the massive specimen but with weaker "superlattice" lines. The x-ray fibre photograph shows clearly the a axis rotation pattern of the two layer ortho-cell although misorientation within the fibre bundle prevents measurement of accurate cell dimensions. Careful study of the photograph reveals a series of additional arcs on the first layer-line proceeding from 110 on the high angle side which are approximately in positions for $11l$'s of a six-layer cell.

CONCLUSIONS

A synthetic Mg-Ge platy serpentine possesses a six-layer ortho-hexagonal cell. The similarity between its x-ray powder pattern and that of serpentine from Unst, Shetland Isles, together with other evidence described, suggests that the latter mineral also has a 6-layer ortho-cell rather than one of the antigorite type; the name "ortho-antigorite" is therefore no longer apposite for the Unst serpentine.

This investigation is part of a program of research made possible by a grant from the National Science Foundation.

REFERENCES

ARUJA, E. (1945), An x-ray study of the crystal-structure of antigorite: *Mineral. Mag.*, **27,** 65–74.

BRINDLEY, G. W., AND VON KNORRING, O. (1954), A new variety of antigorite (ortho-antigorite) from Unst, Shetland Islands: *Am. Mineral.*, **39,** 794–804.

BRINDLEY, G. W., AND ZUSSMAN, J. (1957), A structural study of the thermal transformation of serpentine minerals to forsterite: *Am. Mineral.*, **42,** 461–474.

ROY, D. M., AND ROY, R. (1954), An experimental study of the formation and properties of synthetic serpentines and related layer silicate minerals: *Am. Mineral.*, **39,** 957–975.

WHITTAKER, E. J. W., AND ZUSSMAN, J. (1956), The characterisation of serpentine minerals by x-ray diffraction: *Mineral. Mag.*, **31,** 107–126.

ZUSSMAN, J. (1956), Antigorite: Superlattice and structural formula: *Am. Mineral.*, **41,** 148–151.

ZUSSMAN, J., BRINDLEY, G. W., AND COMER, J. J. (1957), Electron diffraction studies of serpentine minerals: *Am. Mineral.*, **42,** 133–153.

THE AMERICAN MINERALOGIST, VOL. 42, SEPTEMBER-OCTOBER 1957

RARE EARTHS AND THORIUM IN LYNDOCHITE

J. R. BUTLER, *Imperial College, London, England.*

INTRODUCTION

In 1927 Ellsworth described an occurrence of and gave an analysis for a black niobate associated with the feldspar of a pegmatite dike in Lyndoch Township, Renfrew County, Ontario. Compositionally and in crystal form the mineral resembled euxenite except that it was low in U_3O_8 (0.74%) and high in CaO (4.86%) and ThO_2 (4.95%); further the Nb_2O_5 and the total $Nb_2O_5+Ta_2O_5+TiO_2$ were higher than for then known euxenites, even allowing for the presence of microscopic inclusions of columbite. The mineral was named lyndochite and it has not been recorded outside the type locality since.

Lyndochite has been re-examined with a view to ascertaining the distribution of rare earths (Sc, Yt and the lanthanons) in euxenites and closely allied minerals. It is clear that the original analysis is not wholly correct and the evidence suggests that chemically the mineral resembles eschynite more than euxenite.

EXPERIMENTAL

The crystals of lyndochite available from the type locality exhibited no faces and, as Ellsworth found, they contained foreign microscopic inclusions. A polished section was prepared and I am indebted to my colleague, Anthony P. Millman, for the following description of the material. "Lyndochite takes an excellent polish and is pale greyish white in reflected light in air with weak yellowish internal reflections. With crossed nicols and oil immersion the mineral is isotropic and shows strong yellowish brown internal reflections. The lyndochite in polished section is seen to contain as principal impurity a mineral (*P*) occurring as unreplaced residuals with deeply carious margins indicating replacement by lyndochite. *P* is white in reflected light in air compared with lyndochite and shows no reflection pleochroism or internal reflections. With crossed nicols (polariser rotated 5°) *P* shows distinct anisotropism from pale greyish white to dark grey. Twinning is absent but an incipient parting is visible and the mineral contains minute exsolution spindles or rods. The reflectivity as determined with the Cooke microphotometer was 14.7% for green light in air (Ilford spectrum green filter). This is extremely close to the published data for columbite of 15% for green light in air. A subsidiary mineral (*Q*) occurs as curvilinear veinlets (20 thick) replacing the lyndochite along fractures and partings with characteristic embayed margins. *Q* is darker in reflected light in air than both lyndochite and *P*. The total content of impurities in the lyndochite was judged to be below 4%."

Presumably the mineral *P* in the lyndochite is that which Ellsworth satisfactorily showed by a partial chemical analysis to be columbite. No attempt was made to purify the lyndochite and it is to be observed that the concentrations of thorium and the rare earths determined on the impure mineral must be very near to those for the pure lyndochite. Rare earths plus thorium were determined via the fluorides, perchlorates and oxalates using a modified method after Gordon *et al.* (1949) described elsewhere (Butler 1957). Thorium was determined by decomposing the HF-insoluble fluorides with sodium bisulphate and precipitating thorium as iodate using the method of Meyer and Speter (1910); it was found advantageous to ice-cool the solution prior to addition of sodium sulphite and to allow the solution to become completely decolorised (i.e. iodine-free) prior to addition of ammonium hydroxide. The low U_3O_8 content was confirmed by the method of Bowie (1949). Individual rare earths were determined spectrographically by a method to be described elsewhere. The percentages of ThO_2 and rare earth oxides in the mineral were found to be 10.77 and 21.05 respectively (analyst: Miss Rosemary Hall); ThO_2 was examined spectrographically and found to be free from rare earths, etc. Results for the individual rare earths are presented in Table 1.

Discussion

The new ThO_2 percentage is more than twice that originally obtained and the value of 10.77% is unprecedentedly high for a euxenite; moreover, the ratio Th/U (atomic) must exceed 10 which, together with the low U_3O_8 content is quite atypical of euxenites. Eschynites or priorites, on the other hand, have comparable ThO_2 and low U_3O_8 contents (e.g. Chernik, 1929). The original analysis of lyndochite showed $(Ce,La,Di)_2O_3$ as 4.34% and $(Yt,Er)_2O_3$ as 18.22% which was compatible with the mineral being considered as a relative to the polycrase-euxenite group. Goldschmidt and Thomassen (1924) noted the preponderance of Yt and the heavier lanthanons in euxenites, and unpublished results from this laboratory have confirmed their findings. To date, 17 members of the euxenite-polycrase group and 2 tanteuxenites have been analysed for rare earths, and Yt invariably exceeds the lanthanons on an atomic basis; further the ratio heavier/lighter lanthanons is always greater than 2:1 and can exceed 10:1. Polycrase-euxenite from Mattawan Township, Nipissing District, Ontario, shows a typical rare earth distribution (Table 1, Col. 4) with Dy, Er and Yb the dominant lan-

TABLE 1

	1	2	3	4
Sc_2O_3	*	—	*	*
Yt_2O_3	13.1	5	28.8	74.5
La_2O_3	1.50	7	2.28	*
CeO_2	13.5	5	19.5	.49
Pr_6O_{11}	1.69	7	2.46	*
Nd_2O_3	17.0	5	25.0	.71
Sm_2O_3	4.40	5	6.26	.69
Eu_2O_3	*	—	*	*
Gd_2O_3	5.41	6½	7.41	2.57
Tb_4O_7	0.50	10	.66	.77
Dy_2O_3	2.94	5	3.91	4.90
Ho_2O_3	—	—	—	—
Er_2O_3	1.09	13	1.41	5.28
Tm_2O_3	0.48	9	.62	.79
Yb_2O_3	1.20	5	1.51	8.38
Lu_2O_3	0.2	35	.25	.92
ThO_2	33.80	—	—	—
Total	96.81		(100.07)	(100.00)

Col. 1. Percentage composition of rare earths plus thorium, separated from lyndochite, Lyndoch Township, Renfrew County, Ontario. Sc_2O_3 and Eu_2O_3 below the sensitivity limit of 0.1%.

Col. 2. Percentage standard deviations of estimates of individual rare earths from duplicated spectrograms.

Col. 3. Atomic percentage composition of rare earths except Ho from lyndochite. (Calculated to 100%).

Col. 4. Atomic percentage composition of rare earths from polycrase-euxenite, Mattawan Township, Nipissing District, Ontario. (Calculated to 100%.) Sc_2O_3, La_2O_3 and Eu_2O_3 were below 0.1% in the oxides; Pr_6O_{11} was below 0.5%. Ho_2O_3 was very approximately half as abundant as Tm_2O_3. The sum of the spectrographic estimates was 94.52% and the mineral contained 27.71% RE_2O_3 (Analyst: Miss Rosemary Hall).

thanons. The new analysis of lyndochite shows a similar rare earth total —21.05% against 22.56%—but the distribution of the individual rare earths shows quite a different pattern. Yt, Nd and Ce are, in that order, the chief constituents on an atomic basis (Table 1, Col. 3); together they account for 75% of the rare earths, although 10 of the remaining rare earths are represented. The distribution of the lanthanons (Fig. 1) shows that Nd and Ce were preferentially accepted in the lyndochite structure but the tolerance of the mineral in accepting ions of smaller size (eg. Dy^{+3}, radius 0.92 Å) was more limited. Thus the preponderance of Yt^{+3} (radius 0.92 Å) was probably due to its relatively high concentra-

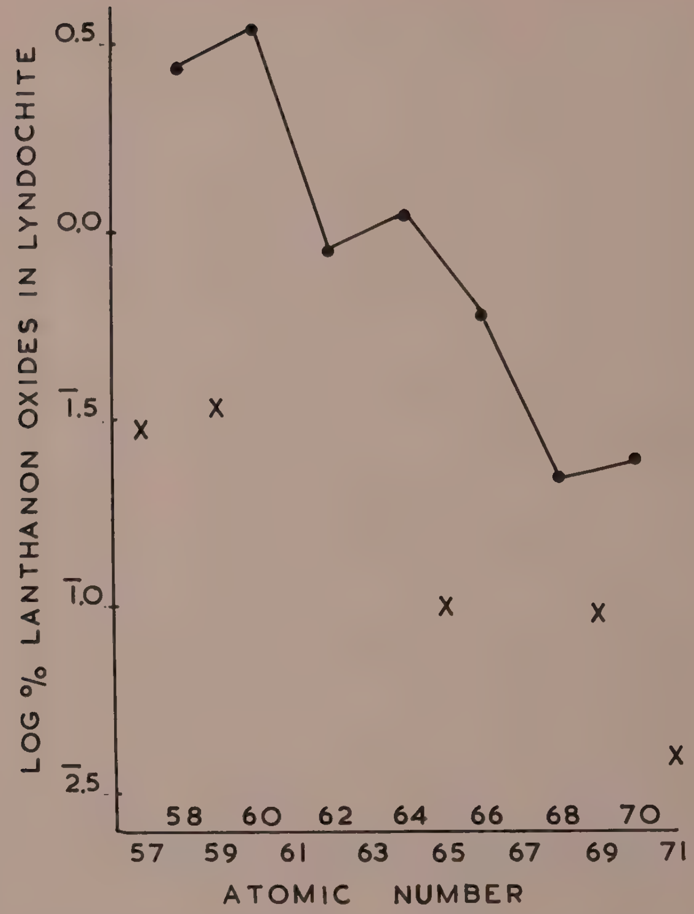

FIG. 1. Distribution of the lanthanons in lyndochite from Lyndoch Township, Renfrew County, Ontario. Points representing the Z-even lanthanons are joined.

tion in the solutions giving rise to lyndochite, rather than its being easily accommodated in the lyndochite structure. The mineral shows moderate selective assemblage tendencies in its lanthanon content (Goldschmidt and Thomassen, 1924) although the degree of selectivity is not so high as in, say, the monazites which contain but low amounts of Gd and the heavier lanthanons (Wylie, 1950, Murata *et al.* 1953) and have La/Ce ratios 4 or more times higher than in lyndochite; a further distinction is that monazites are poor in Yt. Among the Nb-Ta minerals containing essential rare earths both eschynite and polymignite show cerium earths in excess of yttrium earths; polymignite contains essential ZrO_2 and cannot, thus, be considered with either the euxenite-polycrase series (Ti varying) or the eschynite-priorite series (ratio light/heavy lanthanons varying). It is evident that lyndochite *chemically* resembles eschynite rather than previously analysed members of the euxenite-polycrase group.

Morphologically, however, lyndochite is distinct from eschynite, and Ellsworth observed that "Owing to the roughness and distortion of the faces it has not been possible to make sufficient exact measurements to be sure to what extent the interfacial angles differ from those of euxenite, but several fairly accurate contact measurements suggest a close similarity of forms and angles." The forms he identified as present were {100}, {010}, {110}, {310} or {410} or both, {201} and {111}. The angles between faces of these forms cannot be reconciled with those between observed faces of eschynite which has an axial ratio very different from that of euxenite; they would, however, compare with angles between faces of the same forms in columbite and it is recalled that Ellsworth observed inclusions in the lyndochite to be " . . . plainly remnants of columbite in process of assimilation by the lyndochite . . . " Dr. Millman's observations confirm that lyndochite has partly replaced columbite and it is thus possible that lyndochite is a pseudomorph of eschynite after columbite. Against this, however, it is to be noted that either {310} or {410} is rare in columbite and, further, that the habit of the columbite associated with lyndochite and described by Miller (1897) is either platy or nodular. Further, Berman (1955) found that 7 suitably heated specimens of euxenite gave x-ray diffraction patterns very similar to that of suitably heated lyndochite. If this evidence is taken to preclude the likelihood of lyndochite being a pseudomorph after columbite, then lyndochite can be regarded as a cerian-thorian-U-poor variety of euxenite in the euxenite-polycrase series, chemically analogous to eschynite in the eschynite-priorite group.

ACKNOWLEDGMENTS

My thanks are due to Mr. J. E. T. Horne (Atomic Section, H. M. Geological Survey) for supplying the lyndochite, Dr. A. P. Millman for his description of the polished section properties and many helpful discussions, Miss R. Hall for the chemical analyses involved and to the Director of Rothamsted and Head of the Pedology Department for their permission to use the Mannkopff spectrograph there.

REFERENCES

BERMAN, J. (1955), Identifying metamict minerals by x-ray diffraction: *Am. Mineral.*, **40**, 817.

BOWIE, S. H. U. (1949), A prospector's handbook to radioactive mineral deposits. H. M. Geological Survey.

Butler, J. R. (1957), *Geochim. et Cosmochim. Acta* (in press).
Chernik, G. P. (1929), *J. Russ-Phys. Chem. Soc.*, **61**, 735–773.
Ellsworth, H. V. (1927), *Am. Mineral.*, **12**, 212–218.
Goldschmidt, V. M., and Thomassen (1924), *Videnskapsselskapets Skr. I. Mat. natur. Kl*, No. 5.
Gordon, Louis, Vanselow, C. H., and Willard, Hobart H. (1949), *Anal. Chem.*, **21**, 1323–1325.
Meyer, R. J., and Speter, M. (1910), *Chem. Zeit.*, **34**, 306.
Miller, Willet G. (1897). Ont. Bureau Mines 7th rept., Pt. III.
Murata, K. J., Rose, H. J., Jr., and Carron, M. K. (1953), *Geochim. et Cosmochim. Acta*, **4**, 292–300.
Wylie, A. W. (1950). *Australian J. Appl. Sci.*, **1**, 164–171.

THE AMERICAN MINERALOGIST, VOL. 42, SEPTEMBER–OCTOBER 1957

X-RAY POWDER DATA FOR ULEXITE AND HALOTRICHITE

Gretta S. Baur and L. B. Sand, *Department of Mineralogy, University of Utah, Salt Lake City, Utah.*

During a study, described elsewhere in this journal, on an optical property exhibited by fibrous minerals, routine *x*-ray diffraction analyses were made of the specimens. It was found that the three principal diffractions of ulexite had not been reported nor had any diffraction data on halotrichite.

The *x*-ray powder data for two ulexite samples and the ASTM data are presented in Table 1. Note the use of molybdenum radiation in the ASTM data, which probably accounts for the omission of the most prominent diffractions in the lower angle region. The chemical analysis for the ulexite specimen from Boron, California is given in Table 2.

The *x*-ray powder data and the chemical analysis for the halotrichite specimen studied are presented in Tables 3 and 4, respectively.

A General Electric XRD3 diffractometer unit with nickel filtered copper radiation was used. The samples were ground to pass 325 mesh and packed in a $3\frac{1}{2}'' \times 1''$ sample holder avoiding orientation as much as possible.

Acknowledgments

We are indebted to Messrs. John Harmon and Modesto Leonardi for providing the specimens of ulexite and Mr. Carl Austin for providing the halotrichite. Project G-2934 of the National Science Foundation and the University of Utah Research Fund gave financial support to the study.

TABLE 1. *X*-RAY DIFFRACTION POWDER DATA ON ULEXITE

Harmon's Specimen Boron, California CuKα		"Cottonball" Antofagasta, Chile CuKα		Ulexite ASTM Card 2-0914 MoKα	
d Å	rel. I	d Å	rel. I	d Å	rel. I
12.3	100	12.4	76		
7.89	71	7.89	100		
6.06	71	6.02	55		
4.62	19	4.62	9	4.70	20
4.37	34	4.35	26	4.39	30
4.19	64	4.17	54	4.18	40
		4.00	14		
3.60	18	3.60	9	3.64	20
3.34	15	3.31	10		
3.22	28	3.21	16	3.24	40
3.11	49	3.10	28	3.13	50
3.02	38	3.01	18	3.03	40
2.92	29	2.91	12		
2.85	49	2.85	35	2.84	60
2.77	23	2.77	30		
2.67	63	2.66	55	2.69	100
2.58	34	2.58	23	2.60	70
2.415	13	2.409	9	2.42	30
2.350	6				
2.279	10				
2.236	23	2.231	20	2.24	40
2.174	19	2.184	14	2.19	40
2.130	4	2.125	6		
2.088	18				
2.065	50	2.065	48	2.07	70
2.026	28	1.996	20	2.02	30
1.938	25	1.928	13	1.93	60
		1.897	6		
1.879	11	1.872	7	1.88	30
1.809	9	1.802	7		
1.789	12	1.783	8	1.79	30
1.751	15	1.748	9	1.75	50
1.714	11	1.708	8	1.71	20
1.697	7	1.691	6		
1.663	6	1.660	4		
1.643	6	1.641	5		
1.601	6	1.596	3		
1.572	6	1.569	5		
1.550	6	1.548	5		
1.470	6	1.470	4		
1.443	5	1.439	4		
1.420	3	1.420	2		
1.390	2	1.402	2		
1.367	3	1.363	2		
1.331	3	1.330	2		

TABLE 2. CHEMICAL ANALYSIS OF ULEXITE

Boron, California

Na_2O	7.8%
CaO	14.2
B_2O_3	43.7
H_2O	34.2
	99.9%

TABLE 3. *X*-RAY DIFFRACTION POWDER DATA ON HALOTRICHITE

White Mountains, California

d Å	rel. I	d Å	rel. I
10.4	17	2.96	18
9.50	13	2.86	27
7.82	11	2.76	20
6.02	28	2.67	23
5.24	16	2.61	18
4.77	100	2.55	18
4.62	31	2.447	10
4.29	55	2.390	6
4.09	45	2.279	12
3.95	33	2.231	6
3.75	40	2.009	14
3.48	100	1.947	7
3.30	18	1.868	20
3.16	17	1.776	6
3.05	17	1.663	6

TABLE 4. CHEMICAL ANALYSIS OF HALOTRICHITE

Pacific Coast Pyrophyllite Mine, White Mountains, California

FeO	6.8%
Al_2O_3	12.0
SO_3	37.1
H_2O	43.8
	99.7%

THE AMERICAN MINERALOGIST, VOL. 42, SEPTEMBER-OCTOBER 1957

STAGES IN THE OXIDATION OF MAGNETITE

HENRY LEPP, *University of Minnesota, Duluth Branch, Duluth, Minnesota.*

The oxidation of magnetite on heating has received considerable attention in the geologic literature largely because of the difference in behavior of natural and synthetic magnetite. Experimental work by a number of investigators (1, 2, 3, 4, 5) invariably showed synthetic magnetite to oxidize first to gamma-Fe_2O_3 (at temperatures below the inversion) whereas natural magnetite oxidized only to alpha-Fe_2O_3, usually at more elevated temperatures.

Schmidt and Vermaas (6) conducted the most recent study of the behavior of magnetite on heating. Their differential thermal curves for natural magnetite specimens showed two distinct exothermic peaks (360–375° C. and 580° C.), the earlier of which was most pronounced in fine specimens and varied proportionally with the fineness of the material. They concluded that magnetite goes through two stages of oxidation on being heated in air, the first stage being a surface oxidation to hematite and the second stage a complete oxidation also to hematite. They state that formation of gamma-Fe_2O_3 was not detected at any stage.

The writer (7) independently studied the oxidation of magnetite by DTA with near identical results. Magnetite was observed to pass through two distinct stages of oxidation on heating in air. The first stage was shown to be related to the specific surface of the specimens. The present interpretation, however, is sufficiently different to be worthy of record.

Gheith (5) studied the oxidation of synthetic magnetite by DTA and he obtained two exothermic peaks caused by an initial oxidation to gamma-Fe_2O_3 and subsequently by the inversion from gamma to alpha-Fe_2O_3. A comparison of his curves for synthetic magnetite with those obtained from fine grained natural magnetite specimens shows a correspondence between the exothermic peak for the oxidation to gamma-Fe_2O_3 in the synthetic specimens and the first exothermic peak in the DTA curves of fine grained natural magnetite specimens. This suggests to the writer that the first peak in the DTA curves for natural magnetite may also represent oxidation to gamma-Fe_2O_3.

To investigate the nature of the first exothermic peak obtained from natural magnetite, specimens of finely ground (−250 mesh), clean magnetite from Minneville, N.Y. were heated to 430° C. and 500° C. in a differential thermal analysis unit. Both temperatures are above the first peak and below the range of the second peak for natural magnetite. The specimens after heating were brownish black and intensely magnetic. *X*-ray powder photographs of the products showed strong magnetite patterns with only a few of the strongest hematite lines.

The distribution and relative intensities of the lines in the *x*-ray photographs of these products suggested that only a very minor quantity of magnetite had become oxidized in each trial, as found by Schmidt and Vermaas (6). Chemical analysis of the ferrous iron content, however, revealed a much different situation. Whereas the original material came from a single crystal and closely approached the theoretical composition of magnetite, the specimens heated to 430° C. and 500° C. showed Fe_2O_3:Fe_3O_4 ratios of 34:66 and 45:55 respectively. This suggests that the few poorly developed hematite lines in the *x*-ray photographs of the heat treated specimens did not represent all the oxidation; that most of the oxidation below 500° C. must actually have involved a change to gamma-Fe_2O_3.

This conclusion is supported by the fact that the *x*-ray photographs of the heat treated specimens showed a distinct line broadening at high values of θ, a broadening not present in the untreated magnetite. The fact that gamma-Fe_2O_3 has slightly different cell dimensions than magnetite probably accounts for the broadening.

As a result of this differential thermal study the writer proposes that magnetite goes through the following stages during rapid oxidation:

(1) $4Fe_3O_4+O_2 \rightarrow 6$ gamma-Fe_2O_3; commencing at approximately 200° C. and culminating at about 375–400° C.

(2) Gamma-$Fe_2O_3 \rightarrow$ alpha-Fe_2O_3; starting at about 375° C. and probably terminating at from 525 to 550° C. Gheith (5) found experimentally that this transition temperature is related to the temperature of formation of the gamma-Fe_2O_3.

(3) $4Fe_3O_4+O_2 \rightarrow 6$ alpha-Fe_2O_3; starting at from 550 to 575° C. The culmination and point of completion of this reaction are dependent upon the extent of reaction 1.

Reaction 1 is clearly shown by DTA studies to be related to the specific surface of the specimen. It is believed to represent a nucleation process wherein gamma-Fe_2O_3 forms on the surface of magnetite grains according to the underlying pattern. All magnetite probably becomes oxidized on the surface to gamma-Fe_2O_3 on heating, but this reaction is quantitatively unimportant in sizes coarser than 60 mesh and hence it has escaped detection in oxidation studies of natural magnetite.

Rate of oxidation appears to be an important factor in the formation of gamma-Fe_2O_3 on magnetite. Experiments conducted by the writer (7) on the oxidation of siderite illustrate the importance of reaction rates. Siderite first becomes oxidized to magnetite. Rapid oxidation of finely divided siderite at moderate temperatures in hydrothermal or dry environments resulted in the formation of gamma-Fe_2O_3. In experiments with the same materials and at the same temperatures alpha-Fe_2O_3 was the final product when the oxidation rate was retarded by CO_2 in the system. Apparently rapid oxidation favors the type of mimicry which results in the magnetite structure being preserved in the ferric oxide.

The rate of oxidation of magnetite at a given temperature and oxygen pressure is a function of the specific surface of the material and of the degree of perfection of the crystal lattice. The most pronounced difference in natural and synthetic magnetite is grain size. This alone could easily account for the differences that have been found in the behavior of the two materials during rapid oxidation. Minor structural irregularities of synthetic magnetite proposed by Starke (8) have been invoked to account for the fact that it oxidizes to gamma-Fe_2O_3, but these irregularities are probably only of secondary importance.

REFERENCES

(1) Sossman, R. B., and Hostetter, J. C. (1917), The ferrous iron content and magnetic susceptibility of some artificial and natural oxides of iron. *Trans. Am. Inst. Min. Eng.*, **58,** 409–433.

(2) Welo, L. A., and Baudisch, O. (1925), The two stage transformation of magnetite into hematite. *Phil. Mag.*, **50,** 399–408.

(3) Gruner, J. W. (1926), Magnetite—martite—hematite. *Econ. Geol.*, **21,** 325–393.

(4) Twenhofel, L. H. (1927), Changes in the oxidation of iron in magnetite. *Econ. Geol.*, **22,** 180–188.

(5) Gheith, M. A. (1952), Differential thermal analysis of certain iron oxides and their hydrates. *Am. Jour. Sci.*, **250,** 677–695.

(6) Schmidt, E. R., and Vermaas, F. H. S. (1955), Differential thermal analysis and cell dimensions of some natural magnetites. *Ann. Mineral.* **40,** 422–431.

(7) Lepp, H. (1954), An experimental study of interconversions among iron carbonates, oxides and sulfides. Unpublished Ph.D. Thesis, Univ. of Minn.

(8) Starke, K. (1939), Zur Struktur kunstlicher Magnetit. *Zeit. Phys. Chem.*, **B42,** 159–172.

THE AMERICAN MINERALOGIST, VOL. 42, SEPTEMBER-OCTOBER 1957

THE SEPARATION OF CLAY MINERALS FROM CARBONATE ROCKS

Satyabrata Ray, H. R. Gault and Charles G. Dodd,[1]
Lehigh University, Bethlehem, Pennsylvania.

The separation of the clay mineral fraction of a carbonate rock is accomplished ordinarily by acid digestion. Hydrochloric acid often is preferred because it is a strong acid, forms soluble compounds and facilitates rapid solution. When insoluble silica residues are not the primary objectives of carbonate rock solution, the extent of acid reaction with the minerals of interest, i.e. the clays, must be considered. Grim, Lamar and Bradley (1937) suggested placing the ground rock sample in two liters of distilled water and adding a few drops at a time of concentrated HCl, in order to keep a low concentration of acid and not destroy the clay minerals. The pH of such a solution is very low, however; and the present authors have observed that in such a procedure the reaction will start in a very low strength acid, but it is necessary to increase the acid concentration considerably toward the end of the process in order to dissolve all of the sample. During a study of the mineralogy of the Ordovician Jacksonburg cement rock formation of eastern Pennsylvania (a fine-grained, argillaceous, black limestone) the problem of destruction of clay minerals by acid was avoided by using cation exchange resins to effect solution of the carbonate in a very weakly acidic solution of relatively high pH.

---

[1] Now at the University of Oklahoma.

Acid-insoluble residues from carbonate rocks contain clay minerals and quartz, chert, and other insoluble minerals. Strong acids are capable of dissolving some clay minerals such as ferri-ferrous chlorites, various members of the montmorillonite family such as hectorite, probably some of the hydrated micas and possibly others. Few quantitative data are available on rates of solution of identified clay minerals in acids. In order to minimize the probability of losing significant minerals from the Jacksonburg clay mineral suite by acid decomposition, a method was developed that did not decompose or dissolve a highly acid reactive clay mineral, hectorite, while completely dissolving the carbonate fraction.

Various mechanical mixtures of quartz, calcite, dolomite, and hectorite were prepared to simulate impure calcitic and dolomitic limestones. These mixtures were treated with solutions of hydrochloric, formic and acetic acids and with the cation-exchange resins, Amberlite IRC-50 and IR-120. IRC-50 derives its exchange activity from carboxylic acid groups, the IR-120 from sulfonic acid groups. A slurry in distilled water of the hydrogen form of the IRC-50 resin has a pH of about 6 or a hydronium ion concentration of about 10^{-6} molar. This compares with a hydronium ion concentration of about 9×10^{-3} molar for a 4.4 molar solution of acetic acid (1:3 by volume); about 3.3×10^{-2} molar for a 6 molar solution of formic acid (1:3 by volume); and about 3 molar for a 1:3 solution of hydrochloric acid, all at room temperature. The significant variable controlling the rates of reaction of the various acid solutions with the clay minerals, the hydronium ion concentration, is, therefore, of the order of a million times smaller in the case of the resin than in the hydrochloric acid solutions. If the reaction of clay minerals with acids were a first-order reaction, the clay would be decomposed by the resin at one-millionth the rate of decomposition in hydrochloric acid solutions.

In the cases of acetic and formic acids the corresponding rates would be several thousand times slower. Although the pH of the resin slurry decreases with increasing temperature (pH 5.9 at 28° C. vs. pH 5.3 at 70° C.) the slurry hydronium ion concentration is still markedly lower than those of the acids.

The clay mineral hectorite, a magnesium end-member of the montmorillonite family, was used in the simulated limestone mixtures because it reacts more rapidly with acids than other clay minerals. If it could be shown that detectable amounts of hectorite were not lost from the sample mixtures while the calcite was consistently dissolved at a controlled pH, this would serve as an acceptable criterion for an improved clay mineral separation procedure. If only negligible amounts of hectorite were decomposed by the solution procedure under test, this procedure could be relied upon for separations of all clay minerals in any carbonate rock. *X*-ray diffraction analysis was used to determine the amount of hectorite in the dried residues of the mineral mixtures after digestion. Quartz in the original sample mixtures and in the residues served as an internal standard for assignment of "*d*" spacings. Only semiquantitative estimates of the amount of clay mineral were made with respect to the amount of quartz, because of the possibility that colloidal silica released in the breakdown of hectorite, would coat the quartz grains and decrease quartz line intensities.

Four different mineral mixtures were prepared: Mix 1: 50% quartz, 50% hectorite; Mix 2: 20% quartz, 20% hectorite, 60% calcite; Mix 3: $2\frac{1}{2}$% quartz, $2\frac{1}{2}$% hectorite, 95% calcite; and Mix 4: $2\frac{1}{2}$% quartz, $2\frac{1}{2}$% hectorite, 95% dolomite. The proportion of quartz to hectorite was the same in each mix. All materials were ground to pass a 270-mesh sieve. A powder pattern of Mix 1 showed, among many lines, a diffuse but strong line at 14.5 Å representing hectorite.

Mix 2 was split into four fractions. Three were treated respectively with 3 molar hydrochloric acid, 4.4 molar acetic acid (pH 1.9) and 6 molar formic acid (pH 1.5). Excess of acid was added in each case. The three samples were heated during digestion over a low gas flame at about 80–85° C. for about $1\frac{1}{2}$ hours. The *x*-ray powder patterns of the hydrochloric and formic acid residues showed no trace of the 14 Å line but did show faint diffuse zones from about 12 Å to about 6.7 Å. Apparently the hectorite was destroyed. The acetic acid residue showed a strong line at 16.2 Å indicating that hectorite was not destroyed by acetic acid.

The fourth fraction of Mix 2 was treated with Amberlite IRC-50 by the batch technique. Theoretically $2\frac{1}{2}$ grams of calcite in the mix would require 15 cc. of resin for dissolution but an excess was used (70 cc.). Sufficient water was added for the reaction to proceed. The resin-water-sample slurry was heated on a water bath (70° C.) and stirred intermittently. The bulk of the calcite was dissolved in two hours. Resin and residue were separated by screening on 116-mesh cloth screen. The resin was regenerated with 10% solution of hydrochloric acid and the residue put through a second cycle. All effervescence ceased during the second cycle. An *x*-ray pattern of the dried residue showed a sharp, strong line at 16.2 Å, which was assigned to hectorite.

The increase in the "*d*" value from 14.5 Å to 16.2 Å is attributed to a total conversion of the hectorite to the H^+ form with partial dehydration as a result of drying the residue. This "*d*" value lies within the range of 19.3 Å to 14.5 Å given by Barshad (1950) as characteristic of an "immersed in water" and a "dry" condition of H^+ montmorillonite. The sharpness of the line of the resin residue compared with the broad diffuse line of Mix 1 is considered to be due to (1) conversion of the hectorite to an all H^+ form from a largely Ca^{++} form, (2) partial but uniform dehydration of the individual layers and (3) a similar arrangement of the water molecules in the layers. The 16.2 Å value obtained here is closest to one given by Barshad (1949) for montmorillonite with three monomolecular layers of water with the water molecules forming tetrahedra at the water-oxygen interfaces and octahedra at the water-water interfaces.

To test if hectorite could be recovered from a mixture containing a minor amount of the mineral, several fractions of Mix 3 were treated with acids and resin. A four gram sample was digested with Amberlite IRC-50 following the procedure for Mix 2, except that the first cycle was four hours long and the second cycle was three hours. The bulk of the calcite was digested in the first cycle. The *x*-ray powder pattern showed the hectorite line at 14.6 Å.

Other fractions of Mix 3 were treated with acids but at lower concentrations than those used for Mix 2. A six gram sample was treated with 850 cc. of .2 molar hydrochloric acid (pH=.9) for four hours at room temperature (20° C.). The powder pattern of the residue showed the hectorite line. However, a five gram sample treated with 700 cc. of .2 molar hydrochloric acid on a water bath for four hours showed only a very faint line in the vicinity of 14 Å, indicating almost complete destruction of the hectorite.

A six gram sample of Mix 3 was treated with 500 cc. of one molar formic acid (pH 1.95) for nine hours and an eight gram sample was treated with 170 cc. of 4.4 molar acetic acid (pH 1.9) for $6\frac{1}{2}$ hours, both at room temperature. Powder patterns of these two residues showed strong lines at 14.9 Å. No calcite lines were present. Treatment of the formic acid residue with fresh one molar formic acid for four hours over a low flame destroyed almost all of the hectorite. The acetic acid residue was treated with 100 cc. of fresh 4.4 molar acetic acid but heated on a water bath for $3\frac{1}{2}$ hours. The powder pattern showed a strong hectorite line.

The solution of dolomite (Mix 4) with the IRC-50 resin was a slower process than that of calcite, but it was accomplished by heating the resin-sample-water slurry gently over a flame and continuing through four two-hour cycles. Some hectorite may have been destroyed because of the length of the treatment at elevated temperatures (80–85° C.), but the characteristic lines for hectorite were definitely present in the diffraction patterns of the residue.

These experiments indicate that the use of hydrochloric and formic acids for extraction of acid-sensitive clay minerals from limestone and dolomite is restricted to solutions at room temperature with a pH no lower than 2. Under these conditions digestion is slow, particularly for dolomite. Amberlite IRC-50, however, can be used at elevated temperatures and despite the lower concentration of hydronium ions in its slurry, the reaction times are about comparable for limestone and apparently faster for dolomite. Acetic acid seems to be as effective as the resin for calcite but less so for dolomite. Gault and Weiler (1955) report that an excess of 4.4 molar acetic acid dissolves only about 10% of a sample of dolomite in 30 hours compared with 60% of a limestone sample in five hours and 80% in 30 hours.

Amberlite IR-120 in its NH_4^+ form has also been tried with Jacksonburg limestone samples.[2] The reaction in this case leads to the formation of $(NH_4)_2CO_3$ which is soluble and passes through the cloth screen with the residue. Heating on a water bath decomposes the $(NH_4)_2CO_3$ and the dried residue is free of it. The reaction with the IR-120 resin takes place at a pH of about 6.1. The chlorite and illite lines are well preserved in the *x*-ray diffraction patterns.

The IR-120 in the NH_4^+ form is less desirable than the IRC-50 in the H^+ form because of the slower reaction. Even after four two-hour cycles of treatment, the residue showed calcite lines. Dolomite would require even more cycles for dissolution.

The authors are indebted to Dr. G. T. Kerr of Aircraft Marine Products for some helpful suggestions. The work was done as a part of projects supported by the National Science Foundation and the Research Committee of the American Association of Petroleum Geologists.

References

Barshad, I. (1949), The nature of lattice expansion and its relation to hydration in montmorillonite and vermiculite, *Am. Mineral.*, **34,** 675–684.

---

[2] Lloyd (1954) has described a technique using IR-120 in the H^+ form, but he did not make a systematic check of the method.

Barshad, I. (1950), The effect of interlayer cations on the expansion of the mica type of crystal lattice, *Am. Mineral.*, **35**, 225–238.

Gault, H. R., and Kenneth A. Weiler (1955), Studies of carbonate rocks. III, Acetic acid for insoluble residues, *Proc. of Pennsylvania Acad. of Science*, **29**, 181–185.

Grim, R. E., Lamar, J. E. and Bradley, W. F. (1937), The clay minerals in Illinois limestones and dolomites, *Jour. Geol.*, **45**, 829–843.

Lloyd, R. M. (1954), A technique for separating clay minerals from limestones, *Jour. Sed. Pet.*, **24**, 218.

THE AMERICAN MINERALOGIST, VOL. 42, SEPTEMBER-OCTOBER 1957

TITANCLINOHUMITE FROM THE WICHITA MOUNTAINS, OKLAHOMA

W. T. Huang, *Geology Department, Hardin-Simmons University, Abilene, Texas.*

Significant megascopic quantities of titanclinohumite have been identified in two rock specimens presented by J. V. Smith, a local ranger, found near the U.S. Post Office at Meers in 1950, when the writer first visited the gabbro-granophyre complex of Precambrian age in the Wichita Mountains of southwestern Oklahoma. Later, in 1952, titanclinohumite was again found in magnetite gabbro and troctolite at Iron Mountain, Sec. 28, T.4N., R.16W, and a diallagite exposure six miles northwest of Meers, NW$\frac{1}{4}$, Sec. 30, T.4N., R.14W., while the writer undertook the investigation of the Wichita Mountains igneous complex.

The gabbroic rocks at Iron Mountain and diallagite in the area six miles northwest of Meers are contaminated with granitic materials and veined with pegmatites, as both localities lie in the contact zone between gabbro and granophyre of the igneous complex. The ramifying quartzofeldspathic veinlets, stringers, and pegmatite patches are flecked by small black titanclinohumite grains. Many blackish brown titanclinohumite grains are sparsely distributed in the diallagite, and at Iron Mountain brown titanclinohumite is admixed with olivine crystals both in magnetite gabbro and troctolite.

Alteration is pronounced in the gabbroic rocks, and the severe alteration could not be attributed to atmospheric weathering alone. The distribution of alteration products is patchy and irregular, as if caused by a granophyric melt and volatiles which migrated through the rocks and altered the minerals in their paths. Olivine is altered to iron minerals. Plagioclase has been partly replaced by aggregates of prehnite. The aggregates form irregular patches and are associated with chlorite, zeolite, and iron ores. Alteration of augite indicates a tendency to form pale-green tremolite, prehnite, biotite, and chlorite. From the foregoing description it is likely that formation of the titanclinohumite is due to contact action of granophyric melt containing fluorine upon gabbroic rocks. The mineralogy of the two specimens collected by Smith is significant and support the view just set forth.

The first specimen, 3″×5.5″ in size, is gabbroic in composition, medium-grained, brecciated, and altered. Titanclinohumite grains ranging from 4.5 mm. to about 1 mm. in diameter, are irregularly distributed in the rock, and make up about 18 per cent. They are associated with such contact metamorphic minerals as phlogopite, spinel, garnet (grossularite) diopside, and epidote. Undoubtedly these minerals have been developed by contact action of granophyric melt upon the gabbroic rocks.

The second specimen, 2″×4.5″ in size, is a medium-grained mixed rock, probably granogabbro, and exhibits peculiar pseudodiabasic texture. Separate crystals of calcic feldspar and pyroxene are associated with such magmatically incongrous minerals as quartz and alkalic feldspar. Both textural and mineralogical characters of the specimen strongly point to the striking resemblance of the "intermediate rock," which occurs as a narrow zone between gabbro and granophyre in the Wichita Mountains (Huang, 1955). Only a few titanclinohumite grains ranging from 2 mm. to 2.8 mm. in diameter, were found in this specimen. But they are associated with a few small euhedral cassiterite, grossularite, and diopside crystals. Thus, the titanclinohumite grains are accompanied by minerals commonly found in contact zone of intruded igneous rocks.

All the titanclinohumite grains identified are anhedral, without twinning; some have imperfect cleavage. Hardness ranges from 6 to 6.5; it is somewhat brittle. Fracture is subconchoidal to uneven. The specific gravity is 3.34. The mineral is commonly black in color, but due to alteration it may be blackish, black brown, passing into brown. The luster is subvitreous and slightly resinous.

X-ray studies both by Laue and rotation methods showed this titanclinohumite to be monoclinic, with $\beta=101°44'$. The unit cell dimensions are: $a_0=13.63$ Å, $b_0=4.80$ Å, $c_0=10.12$ Å.

Optically this mineral is biaxial with $(+)2V_D=52°–57°$. Indices of refraction for D light at 25° C. are: $\alpha=1.702$, $\beta=1.709$, $\gamma=1.728$. Inclined dispersion is weak to distinct. Pleochroism is imperceptible.

Partial data of chemical analysis from titanclinohumite specimen collected at Iron Mountain are: TiO_2 2.45%, Fe_2O_3 1.20%, FeO 11.25%, F 1.02%, H_2O^+ 1.05%. Table 1 shows the spectrographic results. Sr, Ni, Cr, and Co were determined by mixing one part of sample with two parts of graphite buffer and arcing 10 mgs. of the mixture to completion in a platform electrode at 16 amperes. Cu, Pu, and Ga were measured with centerpost electrodes at 8 amperes (DC arc). Arcing was terminated after the sodium burning was completed, usually 60–62 seconds for a 10 mg. sample.

TABLE 1. SPECTROGRAPHIC ANALYSES

Locality	Specimen	Sr	Cu	Cr	Ni	Co	Pb	Ga
IM	Titanclinohumite*	0.10%	0.01%	—	~0.008%	—	—	—
6NW	Titanclinohumite	.07	.01	—	—	—	—	—
6NW	Titanclinohumite	.03	.005	0.01%	.1	—	—	—
IM	Olivine	.07	.005	—	—	—	—	—
6NW	Olivine	.01	.0005	—	.1	—	—	—

IM—Iron Mountain; 6NW—6 miles northwest of Meers.

Dashes indicate amounts near or below limits of detection but without marked variation, as follows: Ni 0.008%, Cr 0.01, Co 0.0036, Pb 0.0025, Ga 0.002.

* Chemically analyzed titanclinohumite.

Although the spectrographic analyses indicate clearly that the same trace elements are present in the titanclinohumite and the associated olivine crystals, and the mineral is found in mafic, ultramafic, and mixed rocks, there is no evidence that this titanclinohumite was derived from olivine by deuteric alteration. Absence of residual grains of olivine surrounded by or related to titanclinohumite and the fact that the alteration of olivine in the area studied commonly has led either to the formation of coronas or to the selective replacement by late iron minerals (Huang, 1954), argue against the genetic relationship between olivine and titanclinohumite. In view of the mineralogy, lithology, and textural features found in the specimens collected by Smith and the field occurrence of the titanclinohumite in the Wichita Mountains already described, it is believed that this titanclinohumite may have been developed by contact action on gabbroic rocks of a granophyric melt containing fluorine.

The writer wishes to express his appreciation to Mr. J. V. Smith for the specimens that he contributed to this investigation, and to Mr. Earl Smith, graduate student at the University of Oklahoma, who assisted the spectrographic analysis of the titanclinohumite in the magnetite gabbro collected at Iron Mountain.

REFERENCES

HUANG, W. T. (1954), Petrography of the troctolite of the Wichita Mountains, Oklahoma: *Am. Mineral.*, **39,** 549–565.

——— (1955), Occurrences of leucogranogabbro and asssociated igneous rocks in the Wichita Mountains, Oklahoma: *Am. Jour. Sci.*, **253,** 341–357.

THE AMERICAN MINERALOGIST, VOL. 42, SEPTEMBER-OCTOBER 1957

TECHNIQUE FOR THINNED POLISHED SECTIONS*

Alan G. King,† *U. S. Geological Survey, Washington, D. C.*

Techniques that have been developed to make thinned polished sections simplify some of the problems concerned with their manufacture. In contrast to polishing a thin section, thinning a polished section is independent of the polishing operation. Any polishing method can be used on the sample, and a laboratory's established techniques need not be changed to adapt to this application.

Thinned polish sections have one primary use—to study the relationship between transparent and opaque materials. Neither thin sections nor polished sections by themselves are satisfactory for this type of study. For certain problems or materials the use of all three techniques would be required.

Technique

The methods used in the laboratory comprise three basic operations: polishing, thinning, and transfer of the section.

Polishing

As the polishing step is independent of thinning, it will be briefly summarized. Basically the process is done in five steps: (1) sawing, (2) embedding, (3) impregnating with plastic, (4) prepolish surfacing, and (5) polishing.

The area of the rock specimen, selected for the desired exposure of textures of minerals, is sawed to form a wafer about $\frac{1}{4}\times 1\times\frac{3}{4}$ inch. Sawing is done with a 12-inch water-cooled glass-cutting saw blade made from loosely bonded silicon carbide.

The chip is embedded in phenol-formaldehyde resin, and the surface ground with size $303\frac{1}{2}$ emery in water. Next the briquette is dried with infrared lamps and then impregnated with an epoxy resin.[1] This impregnation is done either by flooding the surface with a few drops of plastic and allowing the chip to absorb as much plastic as possible or by forcing the plastic into the chip with air pressure. The sample is surfaced before polishing by grinding with sizes $303\frac{1}{2}$ and 305 emery on brass laps.

The actual polishing is a technique developed by Professor Edward

---

* Publication authorized by the Director, U. S. Geological Survey.

† Present address: 2-B Boyd St., Worcester, Mass.

[1] Bonding agent R-313 plus hardener, Carl H. Biggs Co., 2255 Barry Ave., Los Angeles, Calif., or AL-105, LV, AL-107, Acme Wire Co., New Haven, Conn.

Sampson, Princeton University (personal communication). He uses silk-covered laps, diamond abrasive in oil, and pressure against the specimen as it is being polished.

The polishing step is independent of later thinning, and any adequate method can be used. The only requirement of the polishing method is that it should produce sections having little relief.

Thinning

The briquette is sawed with a cut parallel to and about $\frac{1}{8}$ inch below the polished surface. A gentle sawing action is recommended to prevent shattering in the soft brittle minerals. Either a saw blade composed of small diamond fragments sintered into bronze around the entire periphery or a silicon carbide blade has proved satisfactory. The edges are trimmed on the embedding plastic to fit a standard petrographic slide. The sample is washed in perchlorethylene to remove any oil that might remain from polishing and then dried on a hot plate at about 150° C.

The polished surface is temporarily mounted against a petrographic slide with Lakeside 70-C cement. The entire top surface of the slide is covered with a smear of the cement.

When cooled, the temporarily mounted chip is reduced to standard petrographic thickness by a modified thin-section grinding method. This grinding is accomplished in three stages: (1) size 600 silicon carbide in water on an 8-inch 600-rpm. lap, (2) size 303½ emery[2] in water on an 8-inch 600-rpm. lap, and (3) size 305 emery in water on an 8-inch 170-rpm. lap.

Rough grinding during the thinning operation causes the polished surface to be damaged. Accordingly the section is left extrathick (compared to usual thin sections) after the 600 silicon carbide and 303½ emery grinding stages to prevent this damage. The 600 silicon carbide grinding should reduce the section to a thickness of about 0.25 mm. After grinding with 303½ emery the section should be about 60 or 70 microns thick.

All the grinding should be done in water that is about 20° to 30° C. If the water is below 20° C. the thermoplastic cement becomes too brittle and the section will pluck. If the water is above 30° C. the cement becomes too soft and the section may warp. The temperature can be controlled either by using large reservoirs in which the water has come in equilibrium with room temperature or by adding a mixing valve between the hot and cold water supply to the lap table. Speeds faster than about 170 rpm. at the 305 emery grinding stage will damage the sections.

During the last stages of thinning with the 305 emery, the sample may pluck and thus become badly scratched. This effect is more pronounced when thinning a polished section than when making the usual thin section. The Lakeside bond is weaker between a polished surface and the temporary slide than between a slide and a ground surface; thus more plucking can be expected. Certain materials, such as sandstones, galena, and sphalerite, have a tendency to pluck at the thin edges of a specimen. If the section can be ground uniformly flat and thin, this tendency is minimized. Such a grinding skill is acquired only with practice. Plucking can best be controlled by starting with a polished surface that is well impregnated with epoxy resin. This kind of resin will bond the surface material together and thus may prevent fragments from plucklng A slight increase in the temperature of the grinding media will also minimize plucking.

---

[2] Sizes 303½ and 305 emery, American Optical Co.

As the section is being ground and approaches 30-micron thickness, soft minerals such as galena or sphalerite may warp and wrinkle. This particular damage is caused by shear against the minerals as they drag on the lap surface and can be prevented by slower lap speeds and smaller abrasive particle sizes. The combination of a 170-rpm. 8-inch lap and 305 emery is satisfactory. Unfortunately 305 emery from different manufacturers can vary considerably in its average particle size. Some batches that were tried were completely unsatisfactory and the polished surfaces were ruined.

Transfer

When the thinning with 305 emery is completed, the thinned polished section is essentially finished. The rock section has the polish on one surface and has been ground to standard petrographic thickness. However, it is mounted in reverse and accordingly must be transferred so as to expose the polished surface. This transfer is accomplished by cementing the permanent petrographic glass slide to the ground surface of the rock with the epoxy plastic bonding agent, R-313, and then removing the temporary slide. Any exposed glass on the temporary slide should first be coated with a silicone stopcock grease to prevent the two glass slides from bonding to each other. A minimum amount of plastic should be used, one drop or less. After the R-313 has polymerized overnight the sandwich of slides and thinned section is chilled. The two slides can then be separated by wedging a razor blade between them. As the R-313 forms a better bond to the rock and is less brittle than Lakeside 70-C, especially when chilled, the rock slide adheres to the new slide and is transferred from its former position. The polished surface is washed with 2-ethoxyethanol solvent which removes the Lakeside. The section is thus completed.

Different kinds of materials have been prepared with this technique. The photographs show some of the results that can be expected.

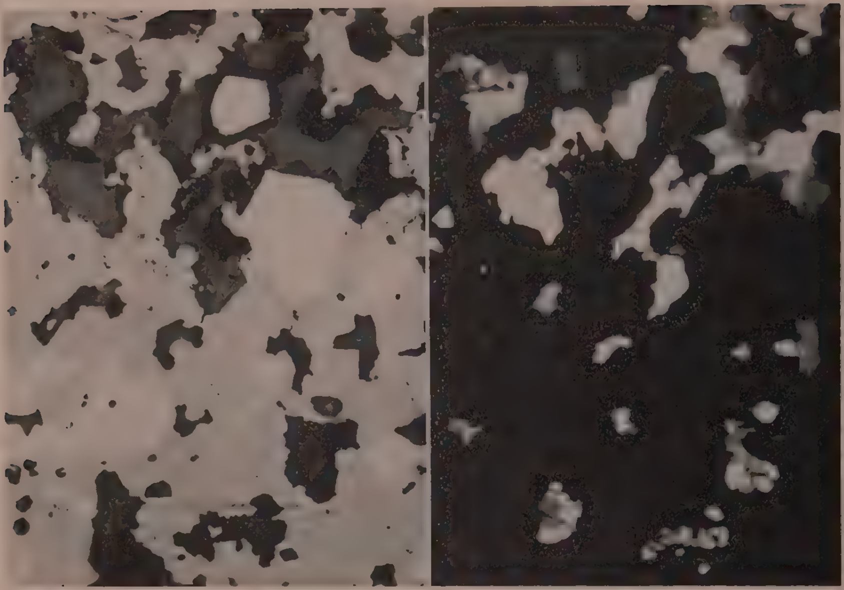

FIG. 1. Enargite, pyrite and quartz. (left) Vertical illumination; (right) Transmitted light, crossed nicols. Magnification 150×.

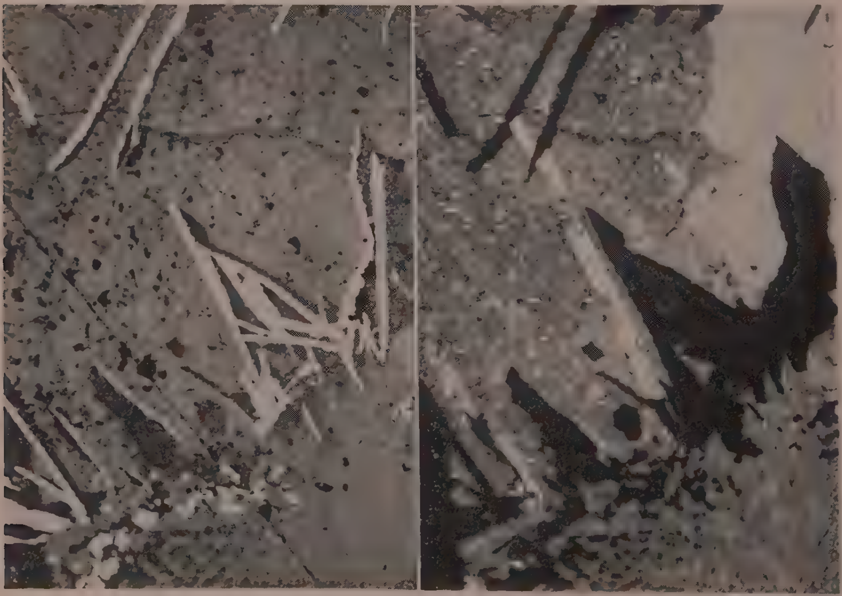

FIG. 2. Marcasite and calcite. (left) Vertical illumination; (right) Transmitted light, crossed nicols. Magnification 150×.

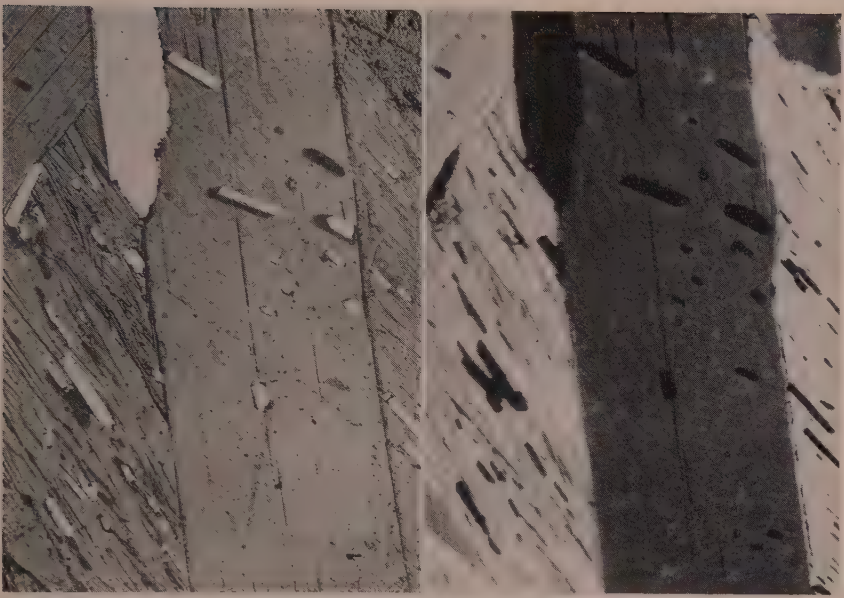

FIG. 3. Magnetite and muscovite. (left) Vertical illumination; (right) Transmitted light, crossed nicols. Magnification 150×.

SUMMARY

The technique described above produces high quality thinned polished sections. As the thinning technique is independent of the polishing process and does not require special equipment—with the exception of a slow lap, the technique is readily adaptable in different laboratories. Two difficulties of this method are (1) plucking and (2) damage to the polished surface. The former can be controlled by plastic impregnations and temperature regulation of the grinding media. The latter can be controlled by using slow lap speeds, fine abrasive sizes, and gentle grinding technique.

The author wishes to express his appreciation to the following people for suggestions and material aid in carrying out this investigation: Rudolf Von Huene, California Institute of Technology; Manning M. Cochran, Ross Jensen, and Leonard B. Riley of the U. S. Geological Survey; and Robert A. Laverty of the U. S. Atomic Energy Commission.

SELECTED BIBLIOGRAPHY

BRISON, R. J. (1951), A method for the preparation of polished thin sections of mineral grains: *Am. Mineral.*, **36**, 731–735.

DONNAY, J. D. H. (1930), Thinned polished sections: *Econ. Geology*, **25**, 270–274.

GRONDIJS, H. F., AND SCHOUTEN, C., 1931, Polished thin sections of ore and rock: *Econ. Geology*, **26**, 343–345.

Kennedy, G. C. (1945), The preparation of polished thin sections: *Econ. Geology*, **40**, 353–360.

Meyer, Charles (1946), Notes on the cutting and polishing of thin sections: *Econ. Geology*, **41**, 166–172.

Rankama, Kalervo (1941), An improved technique for the making of thinned polished sections: *Econ. Geology*, **36**, 561–563.

THE AMERICAN MINERALOGIST, VOL. 42, SEPTEMBER–OCTOBER 1957

AN APPARATUS FOR HAND-PICKING MINERAL GRAINS

M. V. N. Murthy,* *Geological Survey of India, Calcutta-13, India.*

Separation of pure samples of finely powdered (−50 to +200 mesh, A.S.T.M.) minerals from a mixture involves the tedious process of hand-picking under a binocular microscope. The apparatus described below (Fig. 1) makes use of a soft plastic water-pistol as a suction device for collecting grains through an intravenous needle and polyethylene tubing into a glass vial. Both hands are used in the operation, which consists of segregating grains with a needle held in one hand and collecting them with the apparatus held in the other. This speeds up the process and lessens the strain inevitable in conventional hand-picking procedures.

Making the Apparatus

The following components, all of which are readily available, are required to make up the apparatus: (1) a soft plastic toy water-pistol, or alternatively a polyethylene bottle used for nasal sprays, (2) an intravenous needle, 18 or 19 gauge and two inches long, (3) a 3-inch length of polyethylene tubing with a 0.1 inch bore, commonly found in polyethylene wash bottles, (4) a small glass vial with hard plastic cap, and (5) a hard rubber check valve of the type used in rubber pressure or vacuum bulbs.

Two holes with diameters slightly less than those of the rubber valve at A and the plastic cap of the vial at B (Fig. 1) are punched into the water-pistol. The holes can easily be made with the tip of a glass rod of suitable diameter. Two holes are drilled into the plastic cap of the vial (C); the larger to take the polyethylene tubing, and the smaller to allow for the evacuation of air from the vial when using the apparatus. The hub of the intravenous needle is cut off, and the pointed end ground to a 45° angle with a narrow sharp tip.

---

* Postdoctorate Fellow of National Research Council of Canada at the Mineralogy Division, Geological Survey of Canada, Ottawa, Department of Mines and Technical Surveys.

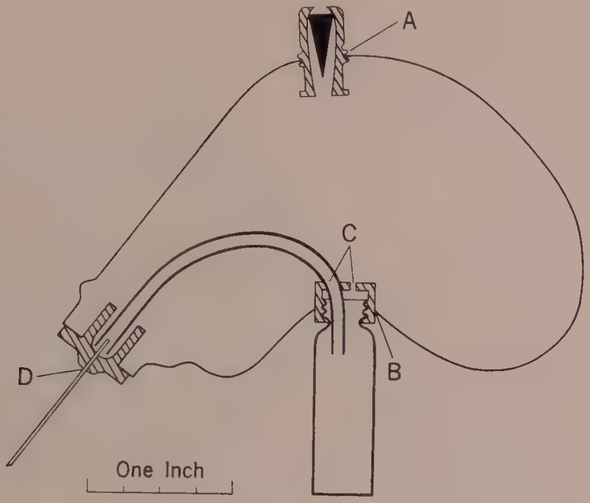

Fig. 1. Mineral-picking apparatus.

The cut end of the intravenous needle is inserted into the fine bore in the cap of the water-pistol at D, and the plastic tube supplied with the pistol replaced by polyethylene tubing, which has proved more satisfactory. Adhesive tape should be wound around the polyethylene tubing to ensure the necessary tight fit. The other end of the tubing is inserted tightly into the larger hole in the plastic cap of the vial, which is then mounted in the hole in the pistol at B. The valve is inserted into the hole at A.

Procedure for Using the Apparatus

Mineral grains are spread on a glass plate under a binocular microscope. A few grains are segregated with a needle held in one hand. Instead of the conventional straight-tipped needle, the writer prefers one with a hooked tip, easily made by grinding a needle of soft metal that will bend without breaking. The mineral-picking apparatus is held with the other hand (Fig. 2), and pressed with the thumb to expel air through the valve. The grains may then be sucked in by releasing the thumb pressure.

If a check valve is not available, a glass tube can be used instead, but to create the vacuum necessary to suck in the grains, the tube must be closed with the index finger after expelling air, and the thumb pressure released slowly. The co-ordination of the finger and thumb can be acquired easily with some practice.

The water-pistol is available in several colors and in picking two or more minerals from a mixture, different colored pistols may be used. The

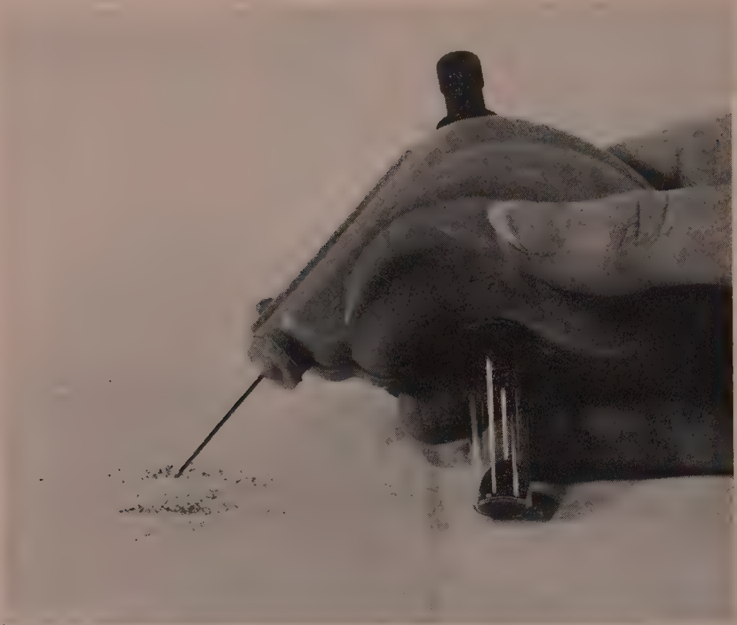

FIG. 2. Mineral-picking apparatus in use.

apparatus is inexpensive, easy to make, and has proved very useful in separating pure concentrates of zircons for age determinations.

ACKNOWLEDGMENTS

The writer wishes to thank Dr. J. A. Maxwell, Geological Survey of Canada, for suggesting the use of an intravenous needle. Suggestions from Dr. R. J. Traill, Geological Survey of Canada, and my wife, Mrs. Syamala Murthy, were very helpful in designing the apparatus The staff of the Royal Canadian Army Dental School very kindly assisted the writer in grinding the needles.

THE AMERICAN MINERALOGIST, VOL. 42, SEPTEMBER-OCTOBER 1957

IMAGE PROJECTION BY FIBROUS MINERALS

Gretta S. Baur, Willard N. Larsen, and L. B. Sand, *Department of Mineralogy, University of Utah, Salt Lake City, Utah.*

An optical property of ulexite, $NaCaB_5O_9 \cdot 8H_2O$, was brought to the writers' attention by Mr. John Harmon in the summer of 1956. Transverse sections of parallel fibrous aggregates of ulexite project an image of an object against one surface to the opposite surface. This effect is shown in Fig. 1. Since we could find no reference in the mineralogical literature to this phenomenon, although known for synthetic fibers, it was thought desirable to report on this optical property.

Microscopic studies of the images made it evident that the optical effect was due to the reflections along the twinned fiber interfaces. The most prominent twinning plane in ulexite is (010) with its poles intersecting at an angle of 35°. Narrower and more closely spaced twins may be superimposed on the former and are possibly twinned on (100). Width of the twins ranges from 0.06 mm. for the widest to 0.005 mm. for the narrowest. A thin-section cut perpendicular to the fibers shows the fibers to have an irregular serrated outline giving a mosaic texture. The areas of the fiber cross-sections vary from 0.06 $mm.^2$ to 0.75 $mm.^2$ The interfaces act as reflecting surfaces due to the different indices of refraction that exist across them. The light rays which impinge on the interface well below the critical angle, emerge from the side of the crystal aggregate; so when viewed from the side near the transverse surface, the aggregate is translucent.

The image is projected (*a*) whether the light comes from above only with the object on an opaque surface and with the sides of the crystal aggregate covered, (*b*) whether the light comes only from below through a partly transparent object, or (*c*) whether the light is reflected off the surface and to the transverse surface of the tilted section. In cases (*a*) and (*b*) the image is not changed in size; in case (*c*) the height of the image is reduced as a function of the angle of inclination. If the object is colored, all colors are reproduced in the image. The surfaces do not have to be parallel, but if they are not, a distortion in size of the image will result. Parallel surfaces cut perpendicular to the fibers will produce the best image, but a rough image can be seen even on the as-found mineral specimen.

Once it was noted that the image resulted from reflections along the fiber interfaces, other fibrous minerals were sought which exhibited the same optical effect. Such minerals were found in trona, $Na_2CO_3 \cdot HNaCO_3 \cdot 2H_2O$, and halotrichite, $FeSO_4 \cdot Al_2(SO_4)_3 \cdot 22H_2O$, and undoubtedly there are many others. The mosaic texture of the compact fiber aggregates of trona was very similar to that of the ulexite. The width of the twins and the areas of the fiber cross-sections in the trona specimen cover the same range as the ulexite, and the image produced was identical.

The image projected by the halotrichite was much sharper and darker than those of the ulexite and trona. However, the fiber aggregate was very friable and only small transverse sections were obtained for examination. The twins in the halotrichite range in width from 0.001 mm. to 0.005 mm., and the areas of the cross-sections of the fibers ranged up to only 0.007 mm.^2 maximum.

Discussion

It seems unusual that this optical phenomenon of fibrous mineral aggregates had not been noted and described previously, but such seems to be the case. It is unlikely that these three fibrous minerals are the only ones that will project an image. Satin spar gypsum crudely exhibits the effect, but in the specimen at hand the fibers were too coarse to transmit a good image. The sharpness of the image will be a function of the thickness of the fibers, and the best images will be projected by those aggregates with fibers of small cross-sectional area. The halotrichite with very fine fibers showed a much better image than the trona and ulexite with coarser fibers. This also can be noticed in different areas of a crystal aggregate where there are patches of fine and coarse fibers. The sharpest image is observed when looking directly down the fibers. The image becomes progressively more diffuse, and finally disappears to the eye, as the angle from the vertical is increased.

The effect of transmitting light along a bundle of synthetic fibers is by the same mechanism. If the end of a glass rod is placed on an object, a badly distorted image can be noticed on the opposite end. The essential factors are the existence of different indices of refraction at the fiber interfaces to produce reflection of the majority of the light rays; and that the fibers are of small enough diameter to produce a good image, since the resulting image is the sum total of images produced by each fiber.

Acknowledgments

We gratefully acknowledge the persons who generously gave of their specimens, M. E. Blessing, U.S.G.S., Salt Lake City, Mr. Carl Austin, Mr. M. Leonardi, American Potash Corp., Trona, Calif., Mr. G. Dub, California Borate Co., Boron, Calif., and especially Mr. Harmon, who made us aware of this phenomenon in minerals. Mr. D. A. Buckner, graduate student in the Department of Mineralogy, assisted in the field collections. The photographic work was done by Mr. J. Nelson. Project

G-2934 of the National Science Foundation and the University of Utah Research Fund provided financial support for the study.

Addendum

Since this manuscript was submitted, an article describing and illustrating this effect has appeared, as follows:

Dietz, Ralph W. (1957), Television ulexite: Gems and Minerals, No. 232, 16–17.

THE AMERICAN MINERALOGIST, VOL. 42, SEPTEMBER–OCTOBER 1957

THE HYDRATION OF KERNITE ($Na_2B_4O_7 \cdot 4H_2O$)[1]

SIEGFRIED MUESSIG AND ROBERT D. ALLEN,[2] *U. S. Geological Survey, Spokane, Washington, and Claremont, California.*

New observations and other data from the literature have led us to conclude that kernite ($Na_2B_4O_7 \cdot 4H_2O$) hydrates directly to borax ($Na_2B_4O_7 \cdot 10H_2O$) without going through the tincalconite ($Na_2B_4O_7 \cdot 5H_2O$) phase, and that the many specimens of kernite that seem to have altered directly to tincalconite all once contained borax, which itself has dehydrated to tincalconite. Our evidence for these conclusions is presented below.

In their study of the system $Na_2B_4O_7$—H_2O, Menzel, Schulz, and others (summarized by Menzel and Schulz (1940)), showed that kernite hydrates to borax without going through the tincalconite phase, which is metastable. Gale (1946), in his work in the Kramer district, where kernite occurs, noted that kernite "is . . . altered to a later regeneration of tincal [sic] in places, especially as seen in zonal envelopes surrounding and retaining the outer forms of individual kernite crystals." Gale's observation serves as a starting point for our work.

In the mines at Kramer, most of the kernite crystals have a crystalline shell (Gale's envelope) around them. In the older workings, these shells, as seen in cross section on mine walls, are nearly all tincalconite that is white and easily distinguished from the clear cores of kernite. In more recent workings and in fresh cuts made into older mine walls, however, the shells are clear borax. We dug into the walls where kernite was rimmed with tincalconite and found that these shells gradually passed into massive clear borax farther away from the mine walls. All this suggests that: (1) the tincalconite seen in the older workings dates from the opening of the mine; (2) the tincalconite is a dehydration product of the borax rather than a hydration product of the kernite; and (3) the kernite has altered directly to borax.

---

[1] Publication authorized by the Director, U. S. Geological Survey.

[2] Present address: Jet Propulsion Laboratory, California Institute of Technology, Pasadena, California.

Several large kernite fragments having clear borax attached to them (parts of the shells) were collected by Muessig in early 1953. Within a month the borax was covered with a coating of tincalconite and by 1956 the borax had dehydrated completely to tincalconite; however, the kernite is still clear (Feb. 1957). Again, it is the borax, not the kernite, that has gone to tincalconite.

In 1954 we noted that one of the clear pieces of kernite, with borax attached at one end, started to split along its cleavages—a phenomenon also noted by Schaller (1930). Tincalconite and a small amount of borax occurred as a thin film along the cleavage planes. To see if such tincalconite is an alteration product of kernite, or of borax as we suspected, we cut a large thin section from a piece of kernite, which had part of a borax shell attached; the borax had altered superficially to tincalconite. As seen in the thin section, most of the attached borax had altered to tincalconite. The kernite within the borax shell is clear, but is cut by many linear, thin veins of borax-tincalconite. In places the veins are nearly all tincalconite; borax occurs only as irregularly shaped remnants within the finely crystalline tincalconite. Such veins grade into those that are mostly borax clouded by minute euhedral crystals of tincalconite. All contacts between the veins and the kernite are sharp and straight; the contact between the shell of borax-tincalconite and kernite is sharp but irregular, and the veins are apophyses from the shell. From these observations, and that of Gale that the borax shells are pseudomorphous after kernite, we deduce that: (1) the kernite hydrated along its edges to borax; (2) at the same time, water-borate solutions moved along the kernite cleavage planes and formed film-like borax veins (some of these veins may be nothing more than hydration products of the contiguous kernite); and (3) the tincalconite, which caused the kernite to fall apart along cleavage planes, formed from the borax of the veins, not from the kernite.

Lastly, we put into bottles two small cleavage fragments of clear kernite, one of which had a small piece of borax attached to it; the other was borax-free. Within the bottles, and attached to the caps, we put tissue paper soaked with water and then capped the bottles tightly. The air within the bottles was probably saturated with water vapor. After two months we took the fragments out of the bottles and powdered them. Immediate microscopic and *x*-ray study of the powders revealed only borax. We conclude that all the kernite, both with and without attached borax, hydrated to borax.

The chemical and mineralogical work of Menzel, and others, the mine observations of Gale, and our own observations and experiments lead to the following conclusions: (1) kernite hydrates under unknown geologic conditions directly to borax; (2) kernite hydrates at room temperatures in water-saturated air directly to borax; (3) specimens of kernite that are altered probably contained undetected borax, which is really what dehydrated to form tincalconite; and (4) so far as we are aware kernite never hydrates directly to tincalconite.

Our findings differ from those of Schaller (1930), who reported that kernite hydrates to tincalconite "if any borax is attached to the kernite," rather than to borax, and that kernite without associated borax does not alter to tincalconite. Schaller made his observations in humid air in Washington, D. C., yet other writers—for example, Palache, Berman, and Frondel (1951)—have cited him and inferred that kernite in contact with borax normally alters to tincalconite. Schaller would probably have reached the same conclusions as we have, had he had the data available at the time of our study.

REFERENCES

PALACHE, C., BERMAN, H., AND FRONDEL, C. (1951), Dana's system of mineralogy, vol. II, 7th ed., 336.

GALE, H. S. (1946), Geology of the Kramer borate district, Kern County, California: *Calif. Journ. Mines & Geol.*, **42**, 325–378.

MENZEL, H., AND SCHULZ, H. (1940), Der Kernit (Rasorit) $Na_2B_4O_7 \cdot 4H_2O$; Zur Kenntnis der Borsäuren und borsauren Alkalisalze. X: *Zeit. anorg. allge. Chemie*, **245**, 167–182.

SCHALLER, W. T. (1930), Borate minerals from the Kramer district, Mohave Desert, California: *U. S. Geol. Survey Prof. Paper* **158-I**, 162–163.

BOOK REVIEWS

INSTRUMENTAL ANALYSIS, by PAUL DELAHAY, xi and 384 pages, The Macmillan Company, 61 Fifth Ave., New York 11, New York, 1957, $7.90.

The volume covers Electrode Potentials, Potentiometry, Voltammetry, Voltammetric Titrations, Electrogravimetry, Coulometry, Conductometry and High-Frequency methods, Emission Spectroscopy, Absorption Spectrometry, Fluorometry, Raman Spectroscopy, *X*-ray Spectroscopy including absorption, diffraction, and fluorescence methods, Mass Spectrometry, and Nuclear Radiation methods such as tracer methods and activation analysis.

The author attempts neither to discuss instrumentation from the design standpoint nor to give details of commercially available instruments; nor is his aim to present the application of instrumental techniques to specific analytical problems. Emphasis is placed on fundamental theory. The author makes good use of schematic electrical and optical diagrams. His discussions of the limitations and applications of the various methods are excellent.

About fifty experiments are presented as laboratory exercises and many problems are provided for study purposes. Here again the experiments and problems are designed to illustrate points of theory.

The book is intended for both undergraduate and graduate students. However, students without some background in physical chemistry may find the presentation of electrochemical theory too concise and a little heavy. The extensive references to original literature and the comprehensive up-to-date bibliographies which include key research papers, review articles, reference books, and monographs are extremely valuable to the research chemist.

ERRATA AND POINTS THAT CAN BE CLARIFIED

p. 23. Table IV, last column. Heading should be: E^0 for $M^{+n}+ne=M$.

p. 44. $\frac{AB}{A'B'}\ \frac{BC}{B'C'}$ should be $\frac{AB}{A'B'}=\frac{BC}{B'C}$

p. 44. $B'C'=q-v$ should be $B'C=q-v$.

p. 47. 2nd paragraph: $C_H{}^+$ should be $C_{OH}{}^-$

p. 76. Fig. 30: Ordinate $\bar{i}/\bar{i}_d$ difficult to read because of small size of print.

p. 82. 3rd paragraph, last sentence: *if* should be *is*.

p. 87. 4th line from bottom: Fig. 33 should be Fig. 34.

p. 96. Paragraph 4 can be misinterpreted. Author should specify that E_1 should be less than the decomposition potential and that E_2 should be a potential where the diffusion current is observed.

p. 131. Line 23: *iodine* should be *iodide*.

p. 164. Last paragraph can be clarified by indicating on Fig. 58 what the angle θ is.

p. 167. Line 11 from bottom: Instead of "the effect of birefringence thus cancels" it would perhaps be better to say: this compensates for any optical rotation produced in the initial passage.

p. 169. Paragraph 5: *Conversely* should be *Similarly*.

p. 174. 2nd paragraph: A diagram of the circuit would help to clarify. 4th paragraph 3rd line: *Spark* Spectra are due to excited ions and not atoms.

p. 213. 2nd line: *fibers* should be *filters*.

p. 225. Discussion of Fig. 96 would be more understandable if author stated that no monochromator is used.

p. 246. 3rd line from bottom: the statement "Some of these elements (boron, for instance) cannot be conveniently analyzed by filter photometry because of lack of a suitable reagent" is not true. There are several excellent reagents for boron, for example, 1,1 dianthrimide. Similarly for the other elements quoted.

p. 265. 2nd paragraph: *without* should be *with*.

p. 281. 1st paragraph: *electic* should be *electric*.

p. 292. Footnote 41: *Burea* should be *Bureau*.

p. 312. $\dfrac{1-e^{-0.40\times 1.5}}{0.40\times 0.15}$ should be $\dfrac{1-e^{-0.40\times 1.5}}{0.40\times 1.5}$

p. 316. Line 22 and 25: (4–22) should be (14–22).

p. 321. Line 17 and Table XXII: Radionuclides do not (usually) disintegrate with independent gamma ray emission. Gamma ray emission is usually an accompaniment of beta or alpha emission. This should be made clear for line 17 and footnote C Table XXII.

Line 2 from bottom: *smaller* should be *larger*.

p. 328. P and R in reference to Fig. 131 are not shown on Fig. 131.

F. S. GRIMALDI

The second edition of the DIRECTORY OF GEOLOGICAL MATERIAL IN NORTH AMERICA by R. H. Dott, J. V. Howell, A. I. Levorsen and J. Weaver, is now available.

It contains the names and addresses of societies, governmental agencies, journals, museums, and universities publishing geological material. It lists sources of maps, air photographs, cross-sections, well elevations, well cuttings and cores, production data, and scouting and drilling reports. It gives locations of libraries, book dealers, museums, and paleontological and mineral collections.

Send orders and remittances to:

The American Association of Petroleum Geologists
Box 979, Tulsa 1, Oklahoma
Prices: Members AAPG $3.00; non-members $3.50

THE WORLD DIRECTORY OF CRYSTALLOGRAPHERS, compiled by William Parrish (Philips Laboratories, Contribution No. 115), is available at $1.50 postpaid from Polycrystal Book Service, 84 Livingston St., Brooklyn 1, New York.

The directory is arranged by countries, and gives names, addresses and fields of specialization.

NEW MINERAL NAMES

Preobrazhenskite

Ya. Ya. Yarzhemskii. Preobrazhenskite, a new borate of the saliferous strata of the Inder uplift. *Doklady Akad. Nauk S.S.S.R.*, **111**, 1087–1090 (1956) (in Russian).

The mineral is wide-spread in small amounts in several parts of the area. It occurs in colorless, lemon-yellow, and dark gray nodules in fine-grained halite-polyhalite rock and encloses kaliborite and boracite. In places it has been partially replaced by inyoite.

Chemical analysis by E. M. Petrov and V. P. Erekhovich gave B_2O_3 60.91, MgO 20.82, CaO 0.01, K 0.25, Na 0.38, Cl 0.82, Br 0.008, SO_3 not found, R_2O_3 0.11, SiO_2 0.13, insol. 0.06, H_2O^- 0.20, H_2O^+ 14.30, sum 98.00%. This corresponds to $3\,MgO\cdot 5B_2O_3\cdot 4.5H_2O$.

Hardness $4\frac{1}{2}$–5. G. not given. Optically nearly uniaxial, positive, with *ns* γ 1.594–1.596, $\beta \simeq \alpha$ 1.573–1.576. *X*-ray study by V. I. Appolonov indicated low symmetry; the powder data (not given M.F.) differ from those of other borates. A D.T.A. curve by V. P. Ivanov shows a large endothermic break at 540–600°, a sharp exothermic break at 730–750, and a moderate endothermic break at 900–950°.

The name is for Pavla Ivanovich Preobrazhensk (1874–1944), "tireless investigator of salt deposits of the U.S.S.R."

Michael Fleischer

Mauritzite

L. Tokody, T. Mándy, and S. Nemes-Varga. Mauritzit, ein neues Mineral von Erdobenye (Ungarn). *Neues Jahrb. Mineral.*, **1957**, No. 2, 33–39.

The mineral occurs in a quarry in hydrothermally altered pyroxene-andesite at Mulatóhegy near Erdöbénye, Hungary, with quartz, tridymite, opal, barite, halotrichite, calcite, siderite, and ilmenite. It is in mammillary forms, intimately mixed with chalcedony ("quartzin"). It is bluish-black, dull, streak and powder yellowish-brown with a greenish tinge. Sp. gr. and hardness not determined. Under the microscope straw-yellow, transparent, apparently isotropic with mean *n* 1.6035.

Analysis gave SiO_2 38.62, TiO tr., Al_2O_3 6.29, Fe_2O_3 19.90, FeO 6.29, MnO 0.12, MgO 9.83, CaO 1.42, K_2O, Na_2O, and P_2O_5 tr., H_2O^- 12.90, H_2O^+ 4.99, CO_2 0.18, sum 100.54%. This corresponds, after deducting all SiO_2 as quartz and CO_2 as $CaCO_3$ to $2\,(Mg,Fe)\,O\cdot(Fe,Al)_2O_3\cdot 5H_2O$. The water is all lost at 150° and the dehydration is reversible for material heated up to 200°. The D.T.A. curve shows a single large endothermic break at 150°. The mineral dissolves in cold (1+1) HCl, leaving a residue of chalcedony.

The *x*-ray pattern shows lines of following spacings (Å) and intensities: 14.5 5, 4.54 4, 2.619 4 (broad), 1.735 2, 1.531 5, 1.318 3 (broad). This is shown to correspond closely to the pattern of a member of the montmorillonite group with a_0 5.31, b_0 9.19A.

The mineral is interpreted as being a silica-free montmorillonite of formula

$$(Al_{1.52}Fe_{1.48}{}^{+3}H_{20})(Fe_{1.58}{}^{+3}Fe_{1.07}{}^{+2}Mg_{3.03}Ca_{0.31})O_{20}(OH)_4.$$

The name is for Bela Mauritz, 1881—, Hungarian mineralogist.

Discussion.—I find it very difficult to accept the authors' interpretation. The mineral corresponds very well with a montmorillonite intermediate between nontronite and griffithite (compare Faust, J., Wash. Acad. Sci. 45, 66–70 (1955)), if most of the SiO_2 found belongs to the mineral. The powder pattern shows no quartz lines and the authors' interpretation means that 38.6% quartz, even though present as chalcedony, gave no pattern. It is also hard to believe that a hydrous oxide with the formula calculated could be dehydrated and rehydrated reversibly when heated to temperatures up to 200°. Further work is obviously necessary.

M. F.